RAMAN FIBRE LASER BASED AMPLIFICATION IN COHERENT TRANSMISSION SYSTEMS

MINGMIN TAN

Doctor of Philosophy

ASTON UNIVERSITY

December 2015

Aston University

Raman Fibre Laser Based Amplification in Coherent Transmission Systems

Mingming Tan

Doctor of Philosophy

2015

Summary

The thesis presents a detailed study of different Raman fibre laser (RFL) based amplification techniques and their applications in long-haul/unrepeatered coherent transmission systems.

RFL based amplifications techniques were characterised from different aspects, including signal/noise power distributions, relative intensity noise (RIN), mode structures of induced Raman fibre lasers, and so on. It was found for the first time that RFL based amplification techniques could be divided into three categories in terms of the fibre laser regime, which were Fabry-Perot fibre laser with two FBGs, weak Fabry-Perot fibre laser with one FBG and very low reflection near the input, and random distributed feedback (DFB) fibre laser with one FBG. It was also found that lowering the reflection near the input could mitigate the RIN of the signal significantly, thanks to the reduced efficiency of the Stokes shift from the FW-propagated pump.

In order to evaluate the transmission performance, different RFL based amplifiers were evaluated and optimised in long-haul coherent transmission systems. The results showed that Fabry-Perot fibre laser based amplifier with two FBGs gave >4.15 dB Q factor penalty using symmetrical bidirectional pumping, as the RIN of the signal was increased significantly. However, random distributed feedback fibre laser based amplifier with one FBG could mitigate the RIN of the signal, which enabled the use of bidirectional second order pumping and consequently give the best transmission performance up to 7915 km. Furthermore, using random DFB fibre laser based amplifier was proved to be effective to combat the nonlinear impairment, and the maximum reach was enhanced by >28% in mid-link single/dual band optical phase conjugator (OPC) transmission systems. In addition, unrepeatered transmission over >350 km fibre length using RFL based amplification technique were presented experimentally using DP-QPSK and DP-16QAM transmitter.

Keywords: Raman amplification, fibre amplifiers, coherent communications

Acknowledgement

The thesis and related research work can be completed thanks to the support and help from many people.

First, I would like to thank my supervisor Dr Paul Harper for patient guidance in the lab and inspiring ideas. It has been a precious and valuable experience under the supervision of Dr Paul Harper.

Second, I would like to thank all the collaborators of the research work, particularly to Prof. Sergei Turitsyn and Prof. Andrew Ellis for providing the guidance and support, and to Dr Ian Phillips for the numerous help in the lab. I would like to specially thank Dr Pawel Rosa for collaboration and help in both experimental work and simulations. I also would like thank Dr Marc Stephens, Dr Son Thai Le, and Dr Juan Diego Ania-Castanon for the collaboration work and I have learnt and benefited so much. Other colleagues from optics communication group of AiPT also provided constant support, and I really appreciate it.

Third, I acknowledge the EPSRC programme grant UNLOC and Aston University studentship for the financial support. I also would like to thank Dr. Zhongyuan Sun, Changle Wang, and Prof. Lin Zhang for the high quality FBGs.

In the end, I would like to particularly thank my wife Yang Zhao for her support from all the aspects and my parents who have provided constant support during the period of my PhD.

Contents

SUMMARY **2**

ACKNOWLEDGEMENT **3**

CONTENTS **4**

ABBREVIATIONS **8**

LIST OF TABLES **10**

LIST OF FIGURES **11**

1. INTRODUCTION **17**

1.1 Contents summary and collaboration acknowledgement **18**

1.2 Publications **22**

2. OPTICAL AMPLIFICATION **26**

2.1 Erbium-doped fibre amplification **29**

2.2 Raman amplification **30**

2.2.1 Raman amplification in optical fibres 31

2.2.2 Distributed Raman amplification and its benefits 33

2.2.2.1 Improved noise performance of distributed Raman amplifications 35

2.2.3 Performance limitation factors of distributed Raman amplifications 39

2.2.3.1 Multiple path interference 39

2.2.3.2 Relative Intensity Noise 41

2.3 Advanced Raman amplification techniques **43**

2.3.1 Bi-directionally pumped distributed Raman amplifications 43

2.3.2 High order distributed Raman amplifications 45

2.4 Summary **50**

3. TRANSMISSION SUBSYSTEMS **52**

3.1 Modulation schemes and optical modulators **52**

3.1.1 Modulation schemes 52
3.1.2 Mach-Zehnder modulator (MZM) and its functionality 56

3.2 Recirculating loop 58

3.3 Coherent receiver 61

3.4 Transmission impairments 64

3.5 Bit error rate and Q factor 67

3.5 Summary 68

4. RAMAN FIBRE LASER BASED AMPLIFICATION.....69

4.1 Fabry-Perot fibre laser based amplification with two FBGs 70
4.1.1 Experimental setup 70
4.1.2 Signal/noise power distribution along the fibre 71
4.1.3 Relative intensity noise 73
4.1.4 Electrical/optical spectra of induced Raman fibre laser 76
4.1.5 Raman gain profile 78

4.2 Fabry-Perot fibre laser based amplification with one FBG 80
4.2.1 Experimental setup 80
4.2.2 Signal/noise power distribution along the fibre 81
4.2.3 Relative intensity noise 81
4.2.4 Electrical spectra of induced Raman fibre laser 82

4.3 Random DFB fibre laser based amplification with one FBG 83
4.3.1 Experimental setup 83
4.3.2 Signal/noise power distribution along the fibre 84
4.3.3 Relative intensity noise 85
4.3.4 Electrical spectra of induced Raman fibre laser 85

4.4 Comparisons of Fabry-Perot fibre laser based amplification and random DFB fibre laser based amplification 86
4.4.1 Experimental setup 87
4.4.2 Results and discussions 88
4.4.3 Summary 92

4.5 Summary and conclusion 92

5. LONG-HAUL COHERENT TRANSMISSION USING RAMAN FIBRE LASER BASED AMPLIFICATION 94

5.1 Evaluation of 100G WDM-QPSK long-haul transmission system using Fabry-Perot fibre laser based amplification with two FBGs 94

5.1.1 Experimental setup 95

5.1.2 Transmission Results and discussions 97

5.1.3 RIN and mode structures of Raman fibre laser 100

5.1.4 Summary 102

5.2 Transmission performance enhancement using random DFB fibre laser based amplification with bidirectional pumping 102

5.2.1 Experimental setup and characterisations of different Raman amplification schemes 103

5.2.2 Transmission results and discussions 107

5.2.3 Summary 109

5.3 Long-haul coherent transmission using Raman fibre laser based amplification and optical phase conjugation 110

5.3.1 Optical phase conjugation 110

5.3.1.1 Experimental setup of optical phase conjugator characterisations 111

5.3.1.2 Experiments results of OPC characterisations 113

5.3.2 Long-haul transmissions with single band OPC 116

5.3.2.1 Experimental setup 117

5.3.2.2 EDFA only system without and with OPC 119

5.3.2.3 BW-pumped RFL based amplification without and with OPC 120

5.3.2.4 Bidirectional pumped RFL based amplification without and with OPC 122

5.3.2.5 Summary 123

5.3.3 Long-haul transmission using dual band OPC 124

5.3.3.1 Experimental setup 124

5.3.3.2 Transmission results and discussions 127

5.3.3.3 Summary 131

5.4 Summary and conclusions 131

6. UNREPEATERED COHERENT TRANSMISSION USING RAMAN FIBRE LASER BASED AMPLIFICATION 133

6.1 Review of unrepeatered transmission in recent years 133

6.2 Unrepeatered DP-QPSK transmission using random DFB fibre laser based amplification 137

6.2.1 Experimental setup 137
6.2.2 Transmission results and discussions 139
6.2.3 Summary 142

6.3 Unrepeatered Nyquist DP-16QAM transmission using random DFB fibre laser based amplification and DBP 142
6.3.1 Experiment setup 143
6.3.2 Transmission results and discussions 144
6.3.3 Summary 146

6.4 Summary and conclusion 146

7. CONCLUSION AND FUTURE WORK 148

7.1 Conclusion 148

7.2 Future work 151

REFERENCES 152

Abbreviations

ADC	Analogue-to-Digital Convertor
AOM	Acousto-Optic Modulator
ASK	Amplitude-shift-keying
AWG	Array Waveguide Grating
AWG	Arbitrary Waveform Generator
BPSK	Binary-Phase-Shift-Keying
DAC	Digital-to-Analogue Convertor
DBP	Digital Back Propagation
DDG	Digital Delay Generator
DFB	Distributed Feedback
DPSK	Differential-Phase-Shift-Keying
DSP	Digital Signal Processing
DWDM	Dense Wavelength Division Multiplexing
EAM	Electro-Absorption Modulator
ECL	External Cavity Laser
EDFA	Erbium-Doped Fibre Amplifier
ESA	Electrical Spectrum Analyser
F-P	Fabry-Perot
FBG	Fibre Bragg Grating
FOPA	Fibre Optical Parametric Amplifier
FSK	Frequency-Shift-Keying
FWM	Four Wave Mixing
GFF	Gain Flattening Filter
GVD	Group Velocity Dispersion
HNLF	Highly Nonlinear Fibre
LO	Local Oscillator

MZM	Mach-Zehnder Modulator
MPI	Multi-Path Interference
NF	Noise Figure
NFT	Nonlinear Fourier Transform
NLSE	Nonlinear Schrodinger Equation
OOK	On-Off Keying
OPC	Optical Phase Conjugation
OSNR	Optical Signal-to-Noise Ratio
OTDR	Optical Time Domain Reflectometer
PBS	Polarisation Beam Splitter
PDM	Polarisation Division Multiplexing
PMD	Polarisation Mode Dispersion
PSCF	Pure Silica Core Fibre
QAM	Quadrature-Amplitude-Modulation
QPSK	Quadrature-Phase-Shift-Keying
RFL	Raman Fibre Laser
RIN	Relative Intensity Noise
ROPA	Remote Optically Pumped Amplifier
RS	Rayleigh Scattering
SBS	Stimulated Brillion Scattering
SE	Spectral Efficiency
SSMF	Standard Single Mode Fibre
SOA	Semiconductor Optical Amplifier
SPM	Self-Phase Modulation
SPV	Signal Power Variation
SRS	Stimulated Raman Scattering
WSS	Wavelength Selective Switch
XPM	Cross Phase Modulation

List of Tables

Table 1.1. Collaboration work 20

Table 2.1. Simulation parameters [5] 49

Table 4.1. Second order FW-pump power, BW-pump power, and FW-pump power ratio 70

Table 4.2. Second order FW-pump power, BW-pump power, and FW-pump power ratio 80

Table 4.3. Second order FW-pump power, BW-pump power, and FW-pump power ratio 84

Table 6.1. Summary of recent unrepeatered transmission work with advanced modulation. 136

Table 6.2. FW-pump power and BW-pump powers in the experiments 139

Table 7.1. Different Raman fibre laser based amplification techniques 148

List of Figures

Figure 2.1. Experimental measurement of the attenuation versus wavelength on the standard single mode fibre (OFS MC-SM) [9] 26

Figure 2.2. Schematic diagram of bi-directionally pumped EDFA 29

Figure 2.3. Schematic diagram of dual-stage EDFA [4] 30

Figure 2.4. Schematic diagram of Raman amplification [20] 31

Figure 2.5. Raman gain efficiency versus wavelength using three different fibres. (OFS-MC complies with ITU G. 652 standard, Truewave fibre, and LEAF fibre complies with ITU G.655 standards [9,22,23]. 31

Figure 2.6. Schematic diagram of first order Raman amplification with bidirectional pumping 34

Figure 2.7. Schematic diagram of signal power profiles comparisons using distributed Raman amplification (section 2.3.2 Raman fibre laser based amplification with backward pumping only) and discrete amplification (EDFA) [20,29]. 34

Figure 2.8. Raman gain profile using six backward-propagated pumps [31] 35

Figure 2.9. Signal power profiles using distributed Raman amplifier and discrete amplifier 38

Figure 2.10. Schematic of double Rayleigh scattering mechanism in the fibre [1] 40

Figure 2.11. Measured RIN of the signal at the output end using URFL based amplifier [42] 42

Figure 2.12. Schematic of dual order pumping configuration [50] 44

Figure 2.13. Signal power profiles using bidirectional pumping and backward pumping only 45

Figure 2.14. Schematic diagram and the pump powers of dual order pumping scheme 46

Figure 2.15. Signal power profiles using dual order and first order Raman amplifier with BW-pumping only 46

Figure 2.16. Schematic diagram of Raman fibre laser based amplification 47

Figure 2.17. Simulation of Rama fibre laser based amplifier with bidirectional pumping and two FBGs [5] 48

Figure 3.1. Constellation diagrams of OOK, BPSK, and QPSK 54

Figure 3.2. Constellation diagrams of (a) 8-PSK; (b)16QAM 55

Figure 3.3. The schematic diagram of MZM [2] 56

Figure 3.4. Schematic diagram of QPSK modulator nesting three MZMs [2,58] 57

Figure 3.5. Schematic diagram of straight in-line system 58

Figure 3.6. A recirculating loop schematic diagram (Solid line: optical signal transmission; dotted line: electrical signal) 59

Figure 3.7. Timing controls of recirculating loop [64,65] 60

Figure 3.8. Schematic diagram of coherent detection mechanism [2] 62

Figure 3.9. A schematic diagram of coherent detector on the PDM signal 63

Figure 3.10. A schematic diagram of a 90 degree optical hybrid [57] 64

Figure 4.1. Schematic diagram of F-P fibre laser based amplification with two FBGs 70

Figure 4.2. Schematic diagram of modified OTDR setup [30] 71

Figure 4.3. Experimental data (solid line) and simulations (dotted line) of signal power distributions with different pump powers [42]. 72

Figure 4.4. Simulated noise power distributions with different pump powers [42]. 72

Figure 4.5. Schematic diagrams of RIN measurement setup 74

Figure 4.6. Measured RIN of second order pump at 1366 nm 74

Figure 4.7. Schematic diagrams of RIN measurement on the signal and induced fibre laser 75

Figure 4.8. Measured RIN of the signal at the output end 75

Figure 4.9. Measured RIN of the FW-propagated induced fibre laser 75

Figure 4.10. Measured electrical spectra of the FW-propagated induced fibre laser 76

Figure 4.11. Measured optical spectra of the FW-propagated induced fibre laser 78

Figure 4.12. Measured Raman profiles for different pump power combinations 79

Figure 4.13. Measured Raman profiles for Fabry-Perot fibre laser based amplification technique with FBGs at different wavelengths 79

Figure 4.14. Schematic diagram of F-P fibre laser based amplification with one FBG 80

Figure 4.15(a). Experimental data (solid line) and simulations (dotted line) of signal power distributions with different FW-pump power. (b). Simulated noise distributions (dotted line) with different FW-pump powers [48]. 81

Figure 4.16. Measured RIN of the signal at the output end 82

Figure 4.17. Measured electrical spectra of the FW-propagated fibre laser 83

Figure 4.18. Schematic diagram of random DFB fibre laser based amplification with one FBG 83

Figure 4.19(a). Experimental data (solid line) and simulations (dotted line) of signal power

distributions with different FW-pump power. (b). Simulated noise distributions (dotted line) with different FW-pump powers [48]. 84
Figure 4.20. Measured RIN of the signal at the output end 85
Figure 4.21. Measured electrical spectra of the FW-propagated fibre laser 86
Figure 4.22. Schematic diagrams and pump powers of amplification schemes R1, R2, and R3. 87
Figure 4.23. Experimental (solid) and simulated (dashed) signal power profiles using the schemes (a). R1, (b) R2, and (c) R3. [48] 88
Figure 4.24. RIN of the output signal using pumping schemes (a). R1, (b). R2, and (c). R3. 90
Figure 4.25. Intra-cavity forward-propagated laser mode structures (a) R1, (b). R2, and (c).R3. 92
Figure 5.1. Experimental setup of DP-QPSK WDM transmitter, recirculating loop using Raman fibre laser based amplification technique, and coherent receiver. 95
Figure 5.2(a).Second order FW-pump, BW-pump power, and FW-pump power ratio used in the experiments; (b). Raman gain spectra using different pump power ratios. 96
Figure 5.3(a). Experimental data (solid line) and simulations (dotted line) of signal power distributions with different FW-pump power. (b). Simulated noise distributions (dotted line) with different FW-pump powers [42]. 97
Figure 5.4(a). Simulated Q factors versus launch power per channel at 1666 km using 1545.32 nm channel assuming that the system performance is limited by ASE noise and fibre nonlinearity only. (b). Measured Q factors versus launch power per channel at 1666 km using 1545.32 nm channel. (c). Signal power variations and Q factor penalties (based on experimental results using BW-pump only) versus FW-pump power ratios. (d). Q factor penalties (based on the simulation data of each corresponding scheme) versus FW-pump power ratios [42]. 98
Figure 5.5(a). Q factors of the central channel at 1545.32 nm versus transmission distances using different pump powers. (b). Q factors for all ten channels and received spectra measured at 7082 km with BW-pump only. (c). Q factors for all ten channels and received spectra measured at 5832 km with 27.6% FW-pump power ratio. 100
Figure 5.6(a). Measured RIN of the Raman fibre laser and the output signal after 83 km span. (b). Measured mode spacing of the Raman fibre laser. 101
Figure 5.7. Experimental set-up of transmitter, recirculating loop, and coherent receiver. 104

Figure 5.8. Back to back Q factors versus OSNR of the central channel at 1545.32 nm 104

Figure 5.9(a). Schematic diagrams and pump powers of different Raman configurations; (b). Experimental data (solid lines) and simulations (dotted lines) of signal power distributions using different Raman configurations. (c). Simulations of noise power distributions (dotted lines) using different Raman configurations [97]. 105

Figure 5.10(a).RIN of output signal using three random fibre laser based scheme. (b). Mode structures of forward-propagated random fibre lasers 106

Figure 5.11(a). Experimental (solid points) and simulated (dashed lines) Q factors versus launch power per channel at 3333km [97]. (b). Q factors versus transmission distances. 108

Figure 5.12. OSNRs, Q factors, and received spectra measured at its maximum reach: (a). Bi-directionally pumped random laser scheme R2 (symmetrical pumping) at 7082km; (b). Bi-directionally pumped random laser scheme R3 (BW-biased pumping) at 7915km; (c).BW-pumped random laser scheme R4 at 7082km; (d). BW-pumped first order scheme R6 at 4999km. 109

Figure 5.13. The schematic diagrams of OPC and the characterisations system [103] 112

Figure 5.14. A sample spectrum measured at the output of PBS [103] 112

Figure 5.15. Q factor versus OSNR (dB/0.1nm) of DP-QPSK transmitter (a) and conjugated signals (b) 114

Figure 5.16. Comparisons of Q factor versus OSNR between original and conjugated signals after averaged over 10 channels 114

Figure 5.17. Output OSNR versus Input OSNR 115

Figure 5.18. OSNR penalty versus input OSNR 115

Figure 5.19. Schematic diagram of the experimental setup 118

Figure 5.20(a). Schematic diagrams of three amplification schemes. (b). Signal power profiles along the fibre with different amplification schemes. 118

Figure 5.21(a). Q factor versus launch power without and with OPC. (b). Q factor versus transmission distance without and with OPC. 120

Figure 5.22(a). Received spectrum at maximum transmission distance. (b). Q factors for all the channels without and with OPC using EDFA 120

Figure 5.23(a). Q factor versus launch power without and with OPC. (b). Q factor versus

transmission distance without and with OPC. 121

Figure 5.24(a). Received spectrum at 65 recirculations. (b). Q factors for all the channels without and with OPC using BW-pumped RFL based amplification 122

Figure 5.25(a). Q factor versus launch power without and with OPC. (b). Q factor versus transmission distance without and with OPC 122

Figure 5.26(a). Received spectrum at 62 recirculations. (b). Q factors for all the channels without and with OPC using bidirectional-pumped RFL based amplification 123

Figure 5.27. Schematic of Nyquist DP-16QAM WDM transmitter [111] 125

Figure 5.28. Signal power profiles of random DFB fibre based amplifier over 75.6 km Sterlite SMF [111] 125

Figure 5.29. Schematic diagram of recirculating loop configuration [112] 126

Figure 5.30. Averaged BER versus launch power over the central subchannel of the central superchannel of both upper and lower bands without OPC (black) and with OPC (red) at 1350km. (a). Two superchannels transmitter. (b). Six superchannels transmitter. 128

Figure 5.31(a). Averaged BER versus launch power over the central subchannel of each superchannel from both upper and lower bands without OPC (black) and with OPC (red) in two superchannels configuration.(b). Received spectra at 3600km with dual band OPC. 128

Figure 5.32(a). Averaged BER versus transmission distance over the central subchannel of central superchannel from both upper and lower bands without OPC (black) and with OPC (red) in six superchannels configuration.(b). Received spectra at 2700km with dual band OPC. 129

Figure 5.33. BERs of all the subchannels at their maximum reach with six superchannels configuration. (Black points) without dual band OPC at both low and high frequencies bands at 2025km; (Red points) with dual band OPC at both low and high frequencies bands at 2700km. 129

Figure 5.34. Transmission distances versus number of superchannels at the transmitter without and with dual band OPC [111]. 130

Figure 5.35. Measured BER for the central subchannel of each central superchannel at their maximum reach. (Black points). Without OPC for 2, 4, 6, 8, and 10 superchannels configuration; (Red points). With OPC for 2, 4, 6, 8, and 10 superchannels configuration; 130

Figure 6.1. Experimental setup of transmitter, transmission link, and coherent receiver 137

Figure 6.2(a). Received OSNR versus FW-pump power or BW-pump power. (b). On-off gain versus FW-pump power or BW-pump power. 138

Figure 6.3. Q factors versus launch power over 327.6 km and 352.8km link 140

Figure 6.4. Signal and noise power distributions in (a) 327.6km and (b) 352.8km fibre link [89] 140

Figure 6.5. Transmitted (Dashed) and received (Solid) spectra (0.1 nm resolution bandwidth) in (a) 327.6km and (b) 352.8km fibre link 141

Figure 6.6. Q factors of all the channels measured in (a) 327.6km and (b) 352.8km fibre link 141

Figure 6.7. Experimental configuration of transmission system [127]. 144

Figure 6.8(a). Q factor versus launch power in 327 km link without and with DBP. (b). Q factor versus launch power in 364km link without and with DBP [127]. 145

Figure 6.9(a).Q factors of all the subchannels in 327 km link without and with DBP. (b). Q factors of all the subchannels in 364km link without and with DBP [127]. 145

Figure 6.10. Input (black), received spectra at -7dBm (red) and -4dBm (green) using 0.1nm resolution bandwidth in 364km fibre link 146

1. Introduction

An optic fibre communication system consists of a modulated optical source (transmitter), a transmission fibre link, and an optical receiver at the output end. The attenuation from the transmission fibre ultimately limits the maximum transmission distance [1]. In the early 1980s, the attenuation was mostly combated by the use of an optics-electronics (OE) repeater which was effectively a photo-receiver and a transmitter. The received optical signal was converted into an electrical signal and then regenerated the optical signal using the transmitter [2], but these regenerators were difficult and expensive to implement. From the 1990s, optical amplifiers started to play critical roles in the revolution of telecommunications, because optical amplifiers were able to amplify the optical signal power directly, making the transmission link significantly simplified. Therefore, these in-line optical amplifiers could be used to compensate the loss of multiple fibre spans without any complex signal regenerators. Since then, optical amplifiers became widespread over the long-haul transmission systems.

Nowadays, optical amplifiers are very widely deployed in optical fibre communication systems. Two amplification techniques occupy most of the current market, which are erbium-doped fibre amplifier (EDFA) and Raman amplifier [1,2,3]. EDFA is the most widely used amplification scheme in current market so far, because it is relatively simple to implement and has better pump power efficiency [1,2]. However, Raman amplifier, in particular distributed Raman amplifier, is significantly different from lumped EDFA in the amplification mechanism, which prevents the fibre attenuation along the transmission path. The major advantage of using distributed Raman amplifier is that the signal-to-noise ratio (SNR) can be improved significantly [1]. This is crucial, because widely used advanced modulation formats such as 16QAM require higher signal-to-noise ratios [4,5], compared to direct detection system in the old days. In common with other Raman amplifiers, the gain bandwidth is also adjustable and not limited in C and L bands when using EDFA [6].

Thanks to the availability of powerful Raman pumps, distributed Raman amplifiers have been increasingly deployed in both long-haul and unrepeatered transmission systems [7]. Ideally, the signal power profile should be distributed perfectly uniform [7], which indicates that the transmission link is close to "lossless". This can be nearly achieved by using high order

bidirectional Raman amplification [5,7]. A novel structure of distributed Raman amplifier is Raman fibre laser (RFL) based amplifier. It deploys second order pumping and the passive Fabry Bragg grating (FBG) reflectors to create a first order ultra-long fibre laser to amplify the signal, which significantly reduces the signal power variation and improves the noise performance [7].

1.1 Contents summary and collaboration acknowledgement

The thesis is concentrated on the evaluation and optimisation of different Raman fibre laser based amplification techniques in long-haul and unrepetered coherent transmission systems. Several novel configurations of RFL based amplifiers are characterised, which includes Fabry-Perot fibre laser based amplifier with two FBGs, Fabry-Perot fibre laser based amplifier with single FBG, and random distributed feedback (DFB) fibre laser based amplifier. In long-haul/unrepeatered coherent transmission systems using advanced modulation formats, different RFL based amplifiers are evaluated and optimised to achieve the best transmission performance by balancing the relative intensity noise (RIN) induced penalty, amplified spontaneous emission (ASE) noise, and nonlinear impairment. Furthermore, optimised RFL based amplifiers are proved to be effective to combat the nonlinear impairment and enhance the reach in the mid-link optical phase conjugator (OPC) transmission systems.

Some works in this thesis were collaborated with other researchers, particularly in these very complicated transmission system experiments. As I mainly focused on the experimental work of RFL based amplification and its application in coherent transmission systems, the numerical simulation of signal and noise power distribution of RFL based amplifiers (in Chapter 4 and 5) was performed by Dr Pawel Rosa. I proposed the idea of the comparison of Q factors vs launch power using different RFL based amplifiers (in Chapter 5), but the simulation was performed by Dr Son Thai Le. The optical phase conjugators in section 5.3 were proposed and implemented by Dr Marc Stephens and Prof. Nick Doran for our group experiments, but I was closely involved with the characterisation of the OPC using DP-QPSK WDM signals. The I-Q modulator in DP-QPSK transmitter was initially built by Dr Ian Phillips, but we worked together on the characterisations. Consequently, Dr Ian Phillips, Dr Marc Stephens, and I worked together on the long-haul transmission experiments using single band and dual band OPC (in section 5.3) that initially proposed by Prof. Andrew Ellis. The digital signal processing algorithms used in the

coherent receiver were developed as common resources for our group by Dr Stylianos Sygletos, Dr Paul Harper, and Dr Ian Phillips. The Nyquist DP-16QAM transmitter demonstrated in section 5.3.3 was designed and implemented by Dr Simon Fabbri, Dr Stylianos Sygletos, and Prof. Andrew Ellis. Unrepeatered transmission experiments using DP-QPSK WDM signals were a collaborative work between Dr Pawel Rosa and me. The simulation of signal and noise power profiles presented in section 6.2.2 were provided by Dr Juan Diego Ania-Castanon based on our experimental parameters. In section 6.3, the Nyquist DP-16QAM transmitter was provided by optical network group from University College London (UCL).

Chapter	Activity	Collaborator
2	Simulation of ultra-long Raman fibre laser amplifier	Dr Pawel Rosa
4/5	Simulation of signal and noise power in RFL based amplifier	Dr Pawel Rosa
5	Simulation of Q factor vs signal launch power	Dr Son. T. Le
5	DP-QPSK WDM transmitter design and implementation	Dr Ian. D. Phillips
5	Optical phase conjugator design, implementation, and characterisation	Dr MFC Stephens Dr Ian. D. Phillips Prof. Nick Doran
5	Long-haul transmission experiments using single band and dual band OPC	Dr Ian. D. Phillips Dr Marc Stephens Prof. Andrew Ellis
5	Digital signal processing in coherent receiver	Dr Stylianos Sygletos Dr Paul Harper Dr Ian. D. Phillips
5	Nyquist WDM DP-16QAM transmitter design and implementation	Dr Simon Fabrri Dr Stylianos Sygletos Prof. Andrew Ellis
6	Unrepeatered DP-QPSK WDM transmission experiments using random DFB based amplifiers	Dr Pawel Rosa
6	Simulation of signal and noise power profile in unrepeatered RFL based amplifier	Dr Juan. D. Ania-Castanon

6	Nyquist WDM DP-16QAM transmitter design and implementation	Optical network group from UCL

Table 1.1. Collaboration work

Chapter 2 is devoted to the basic theory behind different optical amplifiers, in particular distributed Raman amplifier which is the main highlight of the thesis. Two most important amplification techniques are explained. The mechanism of EDFA is briefly introduced, because it is the most commonly deployed amplifier. Raman amplifier, particularly distributed Raman amplifier, is explained in detail, including the benefits and potential impairments, bi-directionally pumped distributed Raman amplifications, and high order Raman amplifications.

The overview of long-haul repeatered coherent transmission subsystems is presented in **Chapter 3**. This Chapter 3 explains the methodology to evaluate the transmission performance of an optical amplifier. Different modulations schemes and the functionality of the Mach-Zehnder modulator (MZM) is explained, including the generation of ASK (Amplitude-shift-keying), BPSK (Binary phase-shift-keying), QPSK (Quadrature phase-shift-keying), and the principle of MZM. The configuration and implementation of recirculating loop and coherent receiver is also illustrated. In the end, the transmission impairments including linear impairments, nonlinear impairments, and their compensation techniques, are discussed briefly.

In **Chapter 4**, signal/noise power distributions, RIN performances, and intra-cavity fibre laser mode structures, and Raman gain profiles, are characterised on three different kinds of RFL based amplifiers with different forward and backward pump powers. The first scheme is Fabry-Perot fibre laser based amplification with two fibre Bragg grating (FBG) reflectors. Although forward-pumping can be used to reduce the noise, the RIN being transferred to the signal is also significant. However, there is only random DFB fibre laser using backward pumping only, as opposed to the usual Fabry-Perot fibre laser using bidirectional pumping and two FBGs. For Fabry-Perot fibre laser based amplification with one FBG, the characterisation performances are different from two FBGs based configuration, as the noise performance is worse but the signal RIN increase is also less obvious. The lasing mechanism is similar to two FBGs based scheme, but the Fabry-Perot mode is weaker. For random distributed feedback (DFB) fibre laser based amplification, due to the largest signal power variation, the noise performance is the worst.

However, there is no signal RIN increase no matter how much the FW-pump power is deployed. The lasing mechanism is different from the first two as it is "modeless" random DFB fibre laser all the time.

In **Chapter 5**, the RFL based amplification techniques in long-haul coherent transmission systems are demonstrated in detail. First, in order to evaluate the transmission performance using Raman fibre laser based amplification with two FBGs, a long-haul transmission experiment with 10×100G DP-QPSK (dual-polarisation QPSK) WDM (wavelength division multiplexed) signals is implemented. While using second order forward-pump, the Q factor penalty can be 4.15 dB at 1666 km using symmetric bidirectional pumping. Indeed, RFL based amplification with backward pumping only gives the best transmission performance in two FBGs configuration. We attribute the Q factor penalty to increased RIN of the output signal which is transferred from first order Fabry-Perot fibre laser and increased second order forward-pump power. Second, the similar transmission performances using random DFB fibre laser based amplifier are evaluated and also compared this with other conventional distributed Raman schemes (first order and dual order). The best performance is achieved using backward (BW) biased bidirectional pumped random DFB laser amplifier, as this scheme also significantly suppresses the RIN transfer. Moreover, this scheme is easily modified to meet different link requirement by varying the forward-pump power. Third, the mid-link OPC transmission with different amplification techniques is demonstrated in single band configuration. The transmission performances without and with single band OPC using EDFA, RFL based amplifier with backward-pumping only, and RFL based amplifier with bidirectional pumping are presented. The results shows that RFL based amplification with BW-pumping exceeds dramatically (28% enhancement) in transmission distance due to relatively high symmetry level and no RIN-induced penalty. Furthermore, long-haul transmission performance using BW-pumping only RFL based amplifier and dual band mid-link OPC is also demonstrated. The results show 60% increase in reach (up to 3600 km) for two simultaneously transmitted superchannels and 33% improvement in reach (up to 2700 km) for six superchannels.

In **Chapter 6**, the applications of random DFB fibre laser based amplification technique on the unrepeatered transmission system are demonstrated. First, the unrepeatered transmission experiments in recent years are reviewed. In order to fill the research gap, unreapetered transmission experiment of 1.4 Tb/s DP-QPSK WDM signals over 352.8 km standard single

mode fibre (SSMF) is demonstrated, which turns out to be the highest capacity over this length of fibre without using ROPA or speciality fibre. Then, as more advanced modulation format has drawn a lot of interest, in co-operation with UCL (University College London), unrepeatered transmission experiment is conducted using Nyquist DP-16QAM (Quadrature amplitude modulation) superchannel with random DFB fibre laser based amplification technique and multi-channel digital back propagation (DBP). 7× 10G baud Nyquist DP-16QAM signals with net spectral efficiency (SE) of 6.6 b/s/Hz (the highest net SE at this transmission distance) is successfully transmitted over 364 km ultra-low-loss (ULL) fibre.

Chapter 7 gives the conclusion of the thesis and potential future work.

1.2 Publications

1. **M. Tan**, P. Rosa, S. T. Le, Md. A. Iqbal, I. D. Phillips, and P. Harper, "Transmission performance improvement using random DFB laser based Raman amplification and bidirectional second-order pumping," *Optics Express*, Vol. 24, No.3, 2016.
2. **M. Tan**, P. Rosa, S. T. Le, I. D. Phillips, and P. Harper, "Evaluation of 100G DP-QPSK long-haul transmission performance using second order co-pumped Raman laser based amplification," *Optics Express*, Vol. 23, No. 17, 2015.
3. **M. Tan**, P. Rosa, I. D. Phillips, and P. Harper, "Extended reach of 116 Gb/s DP-QPSK transmission using random DFB fiber laser based Raman amplification and bidirectional second-order pumping," *Optical Fiber Communication Conference (OFC)*, W4E. 1, March 25th, 2015.
4. **M. Tan**, P. Rosa, I. D. Phillips, and P. Harper, "Long-haul transmission performance evaluation of ultra-long Raman fibre laser based amplification influenced by second order co-pumping," *Asia Communications and Photonics Conference (ACP)*, ATh1E. 4, Nov. 13th, 2014. **(Best Student Paper Award)**
5. **M. Tan**, P. Rosa, Md. Iqbal, I. D. Phillips, J. Nuño, J. D. Ania-Castanon, and P. Harper, "RIN Mitigation in Second-Order Pumped Raman Fibre Laser Based Amplification," *Asia Communications and Photonics Conference (ACP)*, AM2E. 6, Nov. 23rd, 2015. **(Best Student Paper Award)**

6. **M. Tan**, P. Rosa, I. D. Phillips, MFC. Stephens, S. Sygletos, A. D. Ellis, and P. Harper, "Transmission comparison of ultra-long Raman fibre laser based amplification with first and dual order Raman amplification using 10× 118 Gbit/s DP-QPSK," *16th International Conference on July* 6th *Transparent Optical Networks (ICTON)*, 2014.
7. A. D. Ellis, **M. Tan**, M. A. Iqbal, M. A. Z. Al Khateeb, V. Gordienko, G. Saavedra. M., S. Fabbri, M. F. C. Stephens, M. E. McCarthy, A. Perentos, I. D. Phillips, D. Lavery, G. Liga, R. Maher, P. Harper, N. J. Doran, S. K. Turitsyn, S. Sygletos, and P. Bayvel, "4 Tbit/s transmission reach enhancement using 10×400 Gbit/s super-channels and polarization insensitive dual band optical phase conjugation," *Journal of Lightwave Technology*, Vol. 34, No. 8, 2016.
8. L. Galdino, **M. Tan,** A. Alvarado, D. Lavery, P. Rosa, R. Maher, J. D. Ania-Castanon, P. Harper, S. Makovejs, B. Thomsen, and P. Bayel, "Amplification schemes and multi-channel DBP for unrepeatered transmission," *Journal of Lightwave Technology*, Vol. 34, No. 9, 2016.
9. L. Galdino, **M. Tan,** D. Lavery, P. Rosa, R. Maher, I. D. Phillips, J. D. Castanon, P. Harper, R. I. Killey, B. C. Thomsen, S. Makovejs, and P. Bayvel, "Unrepeatered Nyquist-PDM-16QAM transmission over 364km using Raman amplification and mulit-channel DBP," *Optics Letters*, Vol. 40, No. 13, 2015.
10. P. Rosa, **M. Tan**, I. D. Phillips, S. L. Thai, J. D. Ania-Castanon, S. Sygletos, and P. Harper, "Unrepeatered DP-QPSK transmission over 352.8 km SMF using random DFB fibre laser amplification," IEEE *Photonics Technology Letters*, Vol .27, No. 11, 2015.
11. MFC. Stephens, **M. Tan**, I. D. Phillips, S. Sygletos, P. Harper, and N. J. Doran, "1.14 Tb/s DP-QPSK WDM polarization-diverse optical phase conjugation," *Optics Express*, Vol. 22, No. 10, 2014.
12. I. D. Phillips, **M. Tan**, MFC. Stephens, M. McCarthy, E. Giacoumidis, S. Sygletos, P. Rosa, S. Fabbri, S. T. Le, T. Kanesan, S. K. Turitsyn, N. J. Doran, P. Harper, and A. D. Ellis, "Exceeding the Nonlinear-Shannon limit using Raman laser based amplification and optical phase conjugation," *Optical Fiber Communication Conference (OFC)*, M3C. 1, March 9th, 2014.
13. MFC. Stephens, **M. Tan**, I. D. Phillips, S. Sygletos, P. Harper, and N. J. Doran, "1THz-bandwidth polarization-diverse optical phase conjugation of 10x114Gb/s DP-QPSK WDM signals," *Optical Fiber Communication Conference (OFC),* W3F. 6, March 9th, 2014.

14. P. Rosa, **M. Tan**, I. D. Phillips, S. T, Le, J. D. Ania-Castanon, S. Sygletos, and P. Harper "Unrepeatered DP-QPSK transmission over 350 km standard fibre using URFL based amplification," *Asia Communications and Photonics Conference (ACP)*, ATh4E. 5, Nov. 13th, 2014.

15. P. Rosa, G. Rizzelli, **M. Tan**, and J. D. Ania-Castanon, "Charaterisation of random DFB Raman laser amplifier for WDM," *Optics Express*, Vol. 23, No. 22, 2015.

16. P. Rosa, G. Rizzelli, **M. Tan**, and J. D. Ania-Castanon, "Optimisation of Random DFB Raman Laser Amplifier," *17th International Conference on Transparent Optical Networks (ICTON)*, July 5th, 2015.

17. A. D. Ellis, I. D. Phillips, **M. Tan**, MFC Stephens, M. E. McCarthy, MAZ Kahteeb, M.A. Iqbal, A. Peretos, S. Fabrri, V. Gordienko, D. Lavery, G. Liga, G. S. Mondaca, R. Maher, S. Sygletos, P. Harper, N. J. Doran, P. Bayvel, and S. K. Turistyn. "Enhanced superchannel transmission using phase conjugation," *European Conference on Optical Communication (ECOC)*, We. 2.6.4, Sept. 30th, 2015.

18. P. Rosa, S. T. Le, G. Rizzelli, **M. Tan**, and J. D. Castanon, "Signal power asymmetry optimisation for optical phase conjugation using Raman amplification," *Optics Express*, Vol. 23, No. 25, 2015.

19. P. Rosa, S. T. Le, G. Rizzelli, **M. Tan**, and J. D. Ania-Castonon, "Signal power asymmetry optimisation for optical phase conjugation using random DFB laser Raman amplification," to *Asia Communications and Photonics Conference (ACP)*, AM3D. 5, Nov. 23rd, 2015.

20. M. McCarthy, S. Sygletos, N. MacSuibhne, **M. Tan**, M. Stephens, I. D. Phillips, P. Harper, N. J. Doran, and A. D. Ellis, "Challenges of developing non-linear devices to achieve the linear Shannon limit," *16th International Conference on Transparent Optical Networks (ICTON)*, July 6th, 2014.

21. S. T. Le, J. E. Prileksy, M. Kamalian, P. Rosa, **M. Tan**, J. D. Ania-Castanon, P. Harper, and S. K. Turistyn, "Optimized nonlinear inverse synthesis for optical links with distributed Raman amplification," *European Conference on Optical Communication (ECOC)*, Tu. 1.1.3, Sept. 29th, 2015.

22. S. T. Le, T. Kanesan, M. McCarthy, E. Giacoumidis, I. D. Phillips, MFC. Stephens, **M. Tan**, N. J. Doran, A. D. Ellis, and S. K. Turitsyn, "Experimental demonstration of data-dependent

pilot-aided phase noise estimation for CO-OFDM," *Optical Fiber Communication Conference (OFC)*, Tu3G. 4, March 9th, 2014.

23. P. Rosa, M. S. Erkilinç, R. Maher, M. Paskov, S. Kilmurray, **M. Tan**, P Harper, I. D. Philips, A. D. Ellis, J. D. Ania-Castañón, B. C. Thomsen, S. Savory, R. Killey, P. Bayvel, "Nyquist-WDM PDM-QPSK transmission over SMF-28 fibre using URFL amplification," *16th International Conference on Transparent Optical Networks (ICTON)*, July 6th, 2014.

2. Optical Amplification

As the light is propagated in the fibre, the power of the light gets attenuated due to the fibre loss. There are two kinds of losses that are extrinsic and intrinsic. The extrinsic loss comes from the process of fibre fabrication, and can be eliminated with the state-of-the-art fibre fabrication facilities [1]. However, the intrinsic loss is fundamental and cannot be removed completely. The intrinsic loss is mainly from the Rayleigh scattering (RS) loss which comes from the microscopic density fluctuation of the core [2,8]. Figure 2.1 shows the experimental attenuation measurement of standard single mode fibre (OFS MC-SM) between 1400 nm and 1600 nm [9]. The fibre complies with ITU G. 652 fibre category [10]. It can be seen that the attenuation is ~0.199 dB/km at 1550 nm. This attenuation ultimately limits the maximum distance that the signal can be transmitted, which shows the necessities of optical amplification [1].

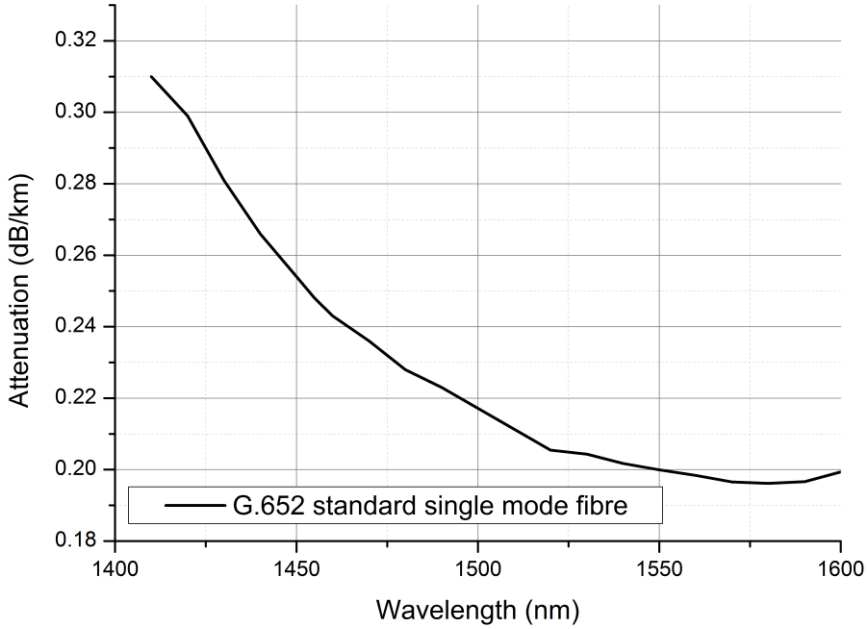

Figure 2.1. Experimental measurement of the attenuation versus wavelength on the standard single mode fibre (OFS MC-SM) [9]

As explained above, the transmission distance is ultimately limited by the fibre attenuation in the transmission systems [1]. This can be overcome in two methods which are signal regenerators and optical amplifiers. Back in the 1980s, the loss limitation was mostly compensated using the OE repeater which was essentially a photo-receiver and a transmitter. The mechanism was that the received optical signal was converted into an electrical signal and then regenerated the optical signal with the transmitter [2]. These regenerators were quite complicated and expensive to

implement, as the WDM transmissions were deployed more widely and individual channels de-multiplexing were required [2]. Alternatively, optical amplifiers could amplify the optical signal power directly without converting them to electrical, making the transmission link significantly simplified. From the middle of 1990s, in-line optical amplifiers were practically used to compensate the loss of multiple fibre spans without any complex signal regenerators for the first time, and started to play critical roles in the revolution of telecommunications.

Nowadays, optical amplifiers are very widely deployed in optical fibre communication systems. In general, depending on how the signal is amplified along the transmission fibre, there are two categories of optical amplifiers known as discrete (lumped) amplifiers and distributed amplifiers. Discrete amplifier means the signal gain is lumped at only a point (or several points) of a transmission line. The signal loss is accumulated over a certain length (typically ~60-80km) of transmission fibre, and then compensated by a discrete amplifier with a short length of gain fibre (i.e. 10 m erbium-doped fibre). In distributed amplifiers, the transmission fibre itself is the gain medium for signal amplification, which indicates that the loss and the amplification occur almost at the same time as the signal is propagated along the transmission fibre.

For discrete amplifiers, there are several categories enabled by different techniques. These are erbium-doped fibre amplifier (EDFA), discrete Raman amplifier, fibre optical parametric amplifier (FOPA), and semiconductor optical amplifier (SOA).

EDFA was studied in 1964 for the first time [3], but became practical in the middle of 1980s [2]. The gain medium was the fibre doped with rare-earth elements [2]. Erbium is the most practical dopant to realise the amplification in C band [2], as the fibre attenuation is the lowest in C band.

Discrete Raman amplifiers mean that a lumped gain fibre is inserted in the transmission link [6]. Due to the small Raman scattering cross-section [5], Raman amplification might be better used for distributed Raman amplification. There are still challenges to design a discrete Raman amplifier such as the gain efficiency. However, discrete Raman amplification can still be an alternative to open up the new gain wavelengths which EDFA cannot cover.

A semiconductor optical amplifier is small-sized, cost-effective, and can be integrated with other semiconductor devices in single small chip, compared with other discrete amplifiers. However, the performance of SOA is usually worse because of its lower gain, higher noise, and higher nonlinearity, which might be not suitable for high speed dense wavelength division multiplexing

(DWDM) transmission [2].

Fibre-optic parametric amplifier is based on the four waves interacting with each other (four-wave mixing) [11,12]. Typically, a short length of highly nonlinear fibre is used as the gain medium and a very powerful pump is required. Unlike EDFA, the gain bandwidth of FOPA is determined by the dispersion and nonlinearity of the fibre medium. Another major advantage of FOPA is that the noise figure of phase-sensitive FOPA can be very low even below the standard quantum limit of 3 dB [13]. FOPA is currently an interesting research topic as a new way of optical amplification, but FOPA is not easily compatible with polarisation division multiplex (PDM) signals [14], which degrades the spectral efficiency of the transmitter.

As opposed to different categories of discrete amplifiers, distributed Raman amplifier is significantly different in the amplification mechanism, which prevents the fibre attenuation and allows the "quasi-lossless" transmission link [7]. Therefore, the advantage of using distributed Raman amplifier is the improvement of signal-to-noise ratio (SNR). In common with other Raman amplifiers, the gain bandwidth is adjustable and not only limited in C and L bands [6].

Currently, most of optical amplifiers deployed in the field are EDFA, due to its high pump-signal efficiency, relatively small size, easy implementation and operation, and cost. However, Raman amplification has attracted many people's attentions since 2000s, thanks to the development of high power pump laser diodes. As the data demand is increasing very rapidly, advanced modulation format has been deployed more and more widely, which requires higher signal-to-noise ratio [4]. This is just where the major advantage of Raman amplification lies. Nowadays, for unrepeatered transmissions, there have been quite a number of applications using first order, second order, or third order distributed Raman amplifiers in the field and under the sea [15]. As long as low cost Raman amplifiers become available, Raman amplifiers would be the first choice when upgrading the existing network [5].

This chapter gives an overview of optical amplification techniques. It starts with a brief description of the most commonly used EDFA. However, Raman amplification is our main concentration which aligns with the highlight of the thesis. In section 2, a detailed description of Raman amplification is presented, including the theory of Raman amplification, the benefits and performance limiting factors of distributed Raman amplifications, and so on. The section 3 demonstrates several advanced structures of distributed Raman amplification schemes, including

bi-directionally pumped Raman amplification and high order Raman amplification.

2.1 Erbium-doped fibre amplification

Erbium-doped fibre amplifiers are very widely deployed in optical communication systems. Compared with Raman amplifiers, the gain efficiency (the ratio between the net gain in dB and the pump power in mW) was much higher (up to 11 dB/mW) using the pump at 980 nm as demonstrated in the 1990s [16]. The gain medium fibre inside EDFA contains erbium ions (Er^{3+}). In order to achieve enough gain in C&L bands, the gain medium fibre needs to be pumped at a proper wavelength. The gain spectrum depends on several factors, including the pumping configurations, the dopant concentration, the length of doped fibre, and so forth [2]. The majority of EDFAs use the pump laser diodes at 980 nm which can provide more than 100 mW pump power [2]. There are a few EDFAs using the pump at 1480 nm, but such EDFAs require higher pump power and longer fibre length due to the low absorption efficiency illustrated in [17].

There are different pumping configurations when designing EDFA, such as forward pumping only, backward pumping only, and bidirectional pumping. Backward pumping only configuration means that the signal and the pump propagate in the opposite directions, and forward pumping means that the signal and the pump propagate in the same direction. In the unsaturated regime when the signal power is very low, forward pumping only and backward pumping only provides nearly the same noise performance. In the saturated regime, backward pumping only provides higher pump-signal conversion efficiency [18]. In the bidirectional pumping configuration, two pumps are located on each side. The advantage of bidirectional pumping is that the population inversion is increased leading to higher gain, and the signal gain is also uniformly distributed along the erbium-doped fibre [2]. Figure 2.2 shows a schematic example of an EDFA with bidirectional pumping.

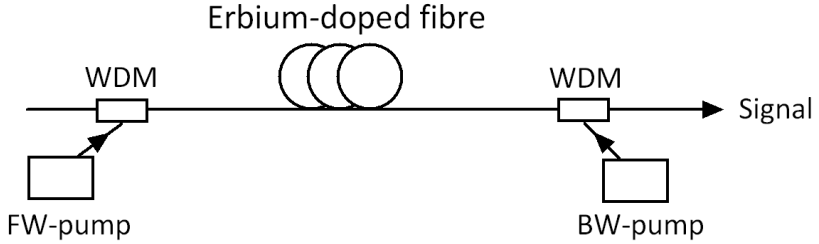

Figure 2.2. Schematic diagram of bi-directionally pumped EDFA

The wide amplification bandwidth and polarisation insensitive gain makes EDFA compatible with multi-channels in C&L band for wavelength division multiplexing (WDM) and polarisation division multiplexing (PDM) application[2]. However, in long-haul transmission systems, the gain flatness is crucial, because even low gain variations between different channels grow exponentially over a chain of fibre spans and amplifiers, resulting in huge power differences between channels. In order to flatten the gain, there are two design considerations which are either passive or active. A passive gain flatten filter can be inserted at the input or output of EDFA [19]. However, due to the loss of the filter, dual-stage EDFA structure is commonly used, and the filter is located in the middle between first stage EDFA and second stage EDFA. The second stage EDFA acts as a power amplifier which determines the final output power, and the first stage EDFA acts as a pre-amplifier with lower gain. Figure 2.3 shows the schematic diagram of a two-stage EDFA. A usual active way to control the gain is to add an input laser signal that is outside the amplification bandwidth, which can flatten the overall gain dynamically [2].

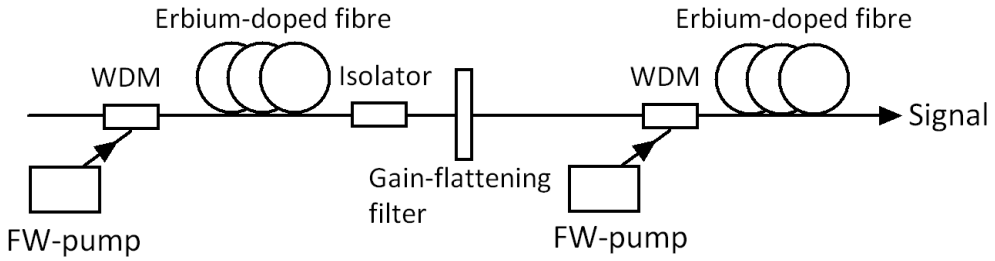

Figure 2.3. Schematic diagram of dual-stage EDFA [4]

2.2 Raman amplification

Raman amplification is based on stimulated Rama scattering (SRS) occur in optical fibres [2,20,21]. The signal and pump are combined into the gain fibre through a WDM coupler. Figure 2.4 shows a general schematic of Raman amplification. Compared with EDFA, the amplification based on SRS can occur at any frequency range as long as the pump at appropriate frequency is available. This indicates that the Raman gain bandwidth can be extended by coupling multiple pumps together [20]. On the other hand, the gain medium can be not only the specialty fibre in particular used for the generation of the Raman gain, but also the transmission fibre itself such as in distributed Raman amplification. Distributed Raman amplification leads to superior noise performance and higher signal-to-noise ratio, resulting in better transmission performance [1,5].

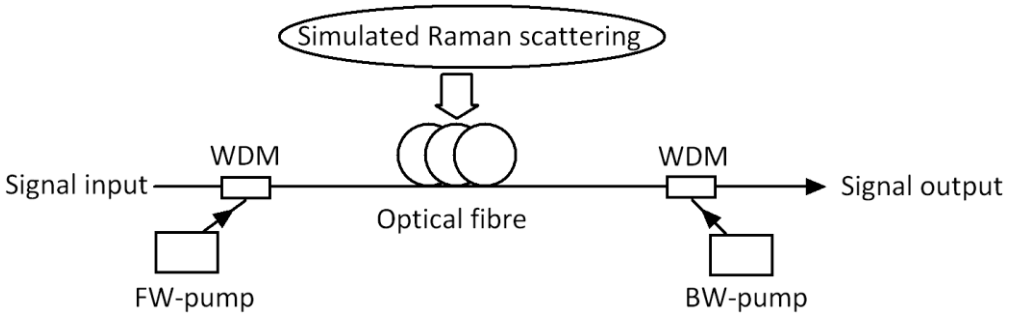

Figure 2.4. Schematic diagram of Raman amplification [20]

2.2.1 Raman amplification in optical fibres

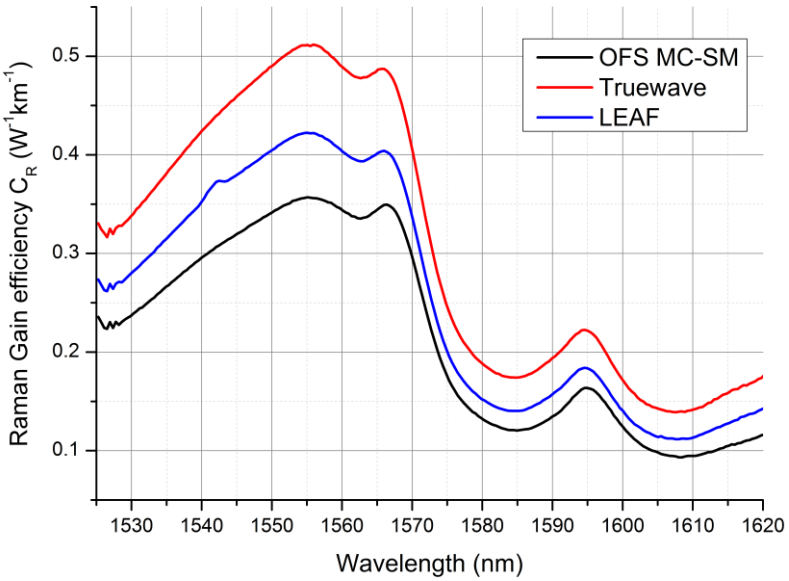

Figure 2.5. Raman gain efficiency versus wavelength using three different fibres. (OFS-MC complies with ITU G. 652 standard, Truewave fibre, and LEAF fibre complies with ITU G.655 standards [9,22,23].

Stimulated Raman scattering (SRS) is the fundamental physics process behind the Raman amplifications. Essentially speaking, SRS enable part of the power transferred from one optical field to another in which frequency is downshifted [21]. During the process of SRS, the pump photon excites a molecule which quickly decays to a lower energy level, and a signal photon is emitted. ω_P and ω_S stands for the optical frequencies of the pump and the signal. $\Omega=\omega_P-\omega_S$ stands for the Raman frequency shift (also called the Stokes shift). The Raman frequency shift associated with the Raman gain coefficient depends on the gain medium. For standard telecom fibre it might be extended up to 40 THz [2], but the gain efficiency peak of this shift is ~13.2 THz [1]. Figure 2.5 shows the experimental measurement of Raman gain coefficient of three different fibres, which the pump at 1455 nm was backward-propagated and the signal was

measured at the output end.

The initial growth of an optical signal is defined in equation (2.1).

$$\frac{dP_S}{dz} = g_R P_P P_S \tag{2.1}$$

Here, g_R is the Raman gain coefficient, P_P and P_S are the powers of the pump and the signal, respectively [1]. But in equation (2.1), it is assumed that the fibre loss is ignored (0 dB/km) and the pump power is constant along with fibre. However, in a practical Raman amplified system, the power distribution of the pump P_P and the signal P_S along the axis of the fibre z should be modified as the following equations:

$$\frac{dP_S}{dz} = g_R P_P P_S - \alpha_S P_S \tag{2.2}$$

$$\xi \frac{dP_P}{dz} = -\frac{\omega_P}{\omega_S} g_R P_P P_S - \alpha_P P_P \tag{2.3}$$

Here, α_S and α_P stands for the fibre attenuation at the signal wavelength and pump wavelength, respectively [1]. g_R stands for the Raman gain coefficient ($W^{-1}m^{-1}$) of the fibre divided by the effective core area of the fibre A_{eff} [1]. ξ means different pumping directions, 1 stands for forward-propagated pumping, and -1 stands for backward-propagated pumping. In equation (2.3), the first term on the right hand side stands for the signal gain (including the pump depletion), and the second term stands for the fibre attenuation. Equations (2.2) and (2.3) are difficult to solve. However, the pump depletion can be ignored because the signal is much smaller compared with the pump power in practical experiments. Therefore, in equation (2.3), the first term on the right equals to 0. As for forward-propagated pumping case (ξ=1), equation (2.3) can be modified to the following one:

$$P_P(z) = P_0 \exp(-\alpha_P z) \tag{2.4}$$

where P_0 is the pump power when z equals to zero [1]. By substituting equation (2.4) into (2.2), we can get:

$$\frac{dP_S}{dz} = g_R P_0 \exp(-\alpha_P z) P_S - \alpha_S P_S \tag{2.5}$$

It is easy to solve the equation (2.5) by integrating, therefore we can obtain,

$$P_S(L) = P_S(0) \exp(g_R P_0 L_{eff} - \alpha_S L) = P_S(0) G(L) \tag{2.6}$$

where L is the fibre length, L_{eff} is an effective length defined in equation (2.7), and $G(L)$ is the net

gain of the signal.

$$L_{eff} = \frac{1-\exp(-\alpha_P L)}{\alpha_P} \tag{2.7}$$

Similarly, the backward pumping configuration is in equation (2.8)

$$P_P(z) = P_0 \exp[-\alpha(L-z)] \tag{2.8}$$

The bidirectional pumping configuration can be expressed similarly in equation (2.9).

$$P_P(z) = P_0\{r_f \exp(-\alpha_P z) + (1-r)\exp[-\alpha_P(L-z)]\} \tag{2.9}$$

where P_0 here stands for total pump power, and r_f stands for the ratio of forward pump power over total pump power.

The equations above shows that the signal is one Stokes shift away from the primary pump laser, and this is called first order Raman pumping. The signal amplified by the pump is called the first Stokes. In second order pumping, when the primary pump power increases gradually to some extent, the first Stokes would be amplified [1,24]. Once the power of the first Stokes is able to generate the Raman gain, it would act as a pump transferring the energy to the amplified signal which is also one Stokes shift away from itself [1]. Therefore, the amplified signal is two Stokes shift away from the primary pump. This is called second order Raman amplification which will be discussed in section 2.3.

In addition, Raman amplification is a very fast process (shorter than a picosecond), which is much faster than EDFA [25]. The Raman gain also has strong polarisation dependence, meaning that the Raman gain on the signal is an order of magnitude higher when the signal and the pump are co-polarised [26]. In order to avoid the polarisation dependent gain, the pump needs to be fully depolarised, such as polarisation multiplexing two pumps at the same wavelength, Lyot depolarisers, and so on [27,28].

2.2.2 Distributed Raman amplification and its benefits

Distributed Raman amplifier is a Raman amplifier that the pump power is extended into the transmission fibre which is also the Raman gain fibre. Distributed Raman amplifications compensate the fibre attenuation along the transmission fibre, compared with discrete amplifications where the gain is provided after the transmission fibre in a discrete location. Figure

2.6 shows a schematic of a bi-directionally pumped first order distributed Raman amplifier.

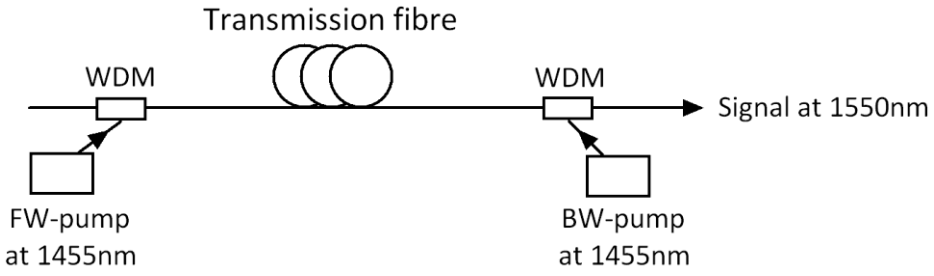

Figure 2.6. Schematic diagram of first order Raman amplification with bidirectional pumping

The research on distributed Raman amplifications developed rapidly since the late 1990s, as the high power pumps became available. A major benefit of using distributed Raman amplification is the improved noise performance due to the fact that the signal gain can be "pushed" toward the middle of the fibre preventing the signal decay, compared with discrete amplification [7]. Figure 2.7 shows an example to compare signal power distributions in a repeatered transmission system.

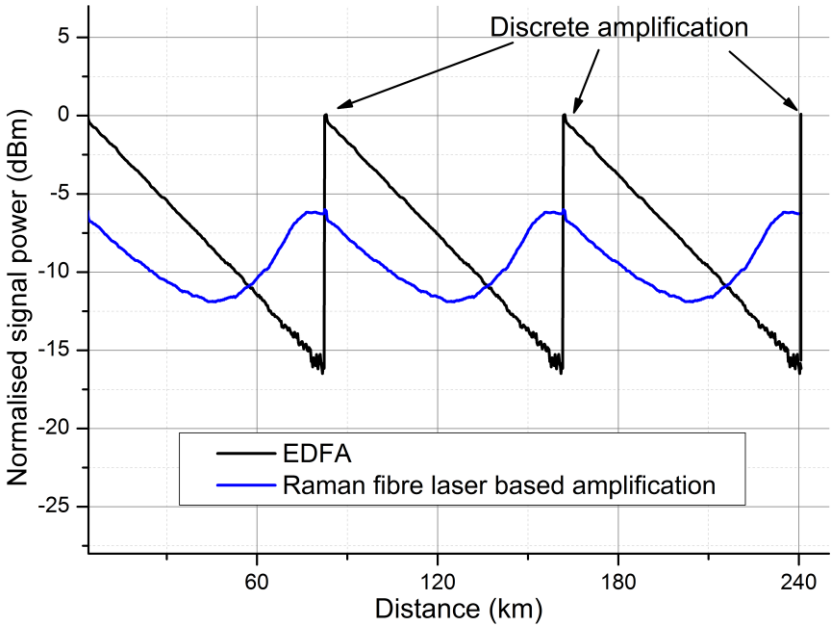

Figure 2.7. Schematic diagram of signal power profiles comparisons using distributed Raman amplification (section 2.3.2 Raman fibre laser based amplification with backward pumping only) and discrete amplification (EDFA) [20,29].

In Figure 2.7, the transmission fibre per span consists of 83 km standard single mode fibre. The signal power distributions are experimental measurements using modified optical time domain reflectometer (OTDR) setup [30]. In order to show the impact of the differences between distributed Raman amplification and discrete amplification, the signal power profiles of the second and third spans are duplicated of the first span. For discrete amplified transmission

system, it can be seen in Figure 2.7 that there is an upper and lower limit for the signal power. If the signal power is too high, the transmission performance will be suffered from the nonlinear impairments which will be discussed in next chapter. Conversely, if the signal power is too low after the fibre attenuation, the noise level will be increased after the amplification [20]. However, compared with discrete amplification, the signal power is distributed more uniformly using distributed Raman amplification, resulting in the noise reduction.

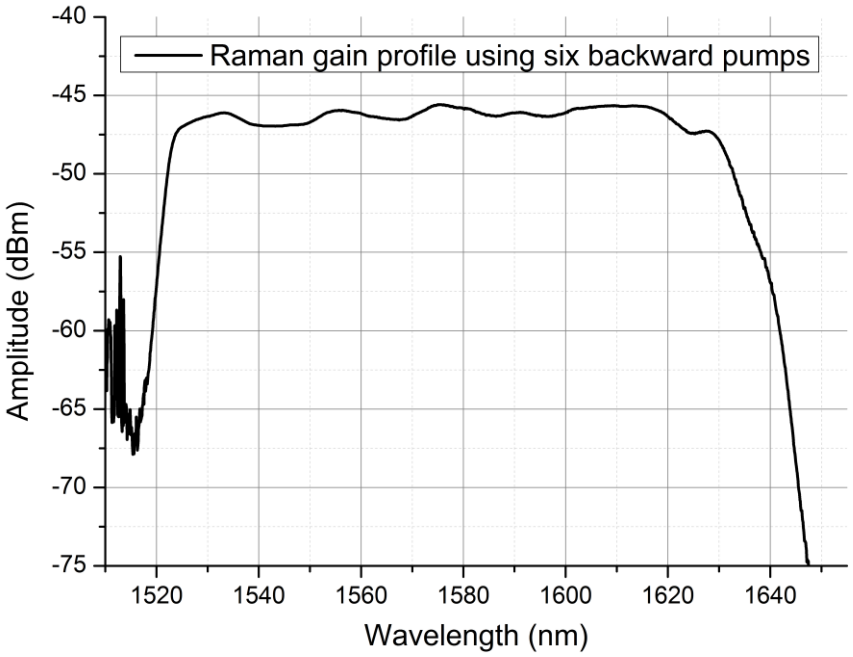

Figure 2.8. Raman gain profile using six backward-propagated pumps [31]

In addition to the noise reduction, the Raman gain bandwidth can be extended by combining multiple Raman pumps at six different wavelengths. Figure 2.8 shows an experimental Raman gain profile using six different wavelengths backward pumps over 83 km SMF (366 mW at 1425 nm, 276 mW at 1444 nm, 171 mW at 1462 nm, 133 mW at 1476 nm, 49 mW at 1491 nm, and 162 mW at 1508 nm). It can be seen that the Raman gain bandwidth could be extended up to 100 nm with +/- 1.2 dB gain variation [31]. Further optimisation on the gain profile variation can be used more pumps (i.e. 12 wavelengths pumps), which results in the gain variation of only +/- 0.5 dB and the gain bandwidth of over 100 nm [32].

2.2.2.1 Improved noise performance of distributed Raman amplifications

The noise in the EDFA comes from the undesirable photon of spontaneous emission which is

amplified together with the signal [2], which is called amplified spontaneous emission (ASE) noise. The changes in signal-to-noise ratio after the amplifier is defined as the noise figure (NF) as shown in equation (2.10)

$$NF = \frac{SNR_{in}}{SNR_{out}} \tag{2.10}$$

As presented in [1,27], the NF can be simplified as shown in equation (2.11).

$$NF = 2n_{sp}\frac{G-1}{G} + \frac{1}{G} \tag{2.11}$$

G stands for the net gain and n_{sp} stands for the population inversion factor which is defined in equation (2.12). Here, N_1 and N_2 stands for the ground and excited state, and σ_e and σ_a represents the fibre emission and absorption cross sections [2,5].

$$n_{sp} = \frac{\sigma_e N_2}{\sigma_e N_2 - \sigma_a N_1} \tag{2.12}$$

From equation (2.11), when the gain is large enough, the first term on the right equals to $2n_{sp}$, and the second term equals to 0. The smallest n_{sp} can be equal to 1 from the equation (2.12). This means the minimum noise figure is 2 in linear units which equals to 3 dB due to the quantum limit [2].

For distributed Raman amplifier, the ASE refers to spontaneous Raman scattering which comes from shot noise, signal-spontaneous beat (signal-ASE) noise, and spontaneous- spontaneous beat (ASE-ASE) noise [27]. Shot noise is a fundamental source associated with the nature of the photon. Signal-ASE noise is the intensity fluctuations due to the interaction between the signal and ASE in the same polarisation when they propagate in the same direction [27]. Signal-ASE is dominated over ASE-ASE noise as the ASE-ASE power level is relatively low. Therefore, in the case of shot noise and signal-ASE noise, the noise figure can be expressed in linear units as equations (2.13) and (2.14) [27].

$$NF \approx \frac{2P_A^+(L)}{h\omega B_{ref} G} + \frac{1}{G} \tag{2.13}$$

$$NF = \frac{P_S(0)}{h\omega B_{ref} OSNR_{out}} + \frac{1}{G} \tag{2.14}$$

where $P_A{}^+$ stands for the power of ASE in one polarisation, B_{ref} stands for the reference

bandwidth, and $h\omega$ represents the energy of the photon. The first term here represents the noise from signal-ASE, and the second term represents the shot noise. In this way, the NF can be calculated or measured experimentally.

Alternatively, the NF can be also estimated by the integration of signal power profile. The spectral density evolution N_s of the optical wavelength can be expressed as the equation (2.15) in [33].

$$\frac{dN_s}{dz} = -\alpha_s\left[N_s - \frac{h\omega_s}{2}\right] + g_R P_P\left[N_s + \frac{h\omega_s}{2}\right] \tag{2.15}$$

The spectral density of the output optical noise is

$$N_s = G\frac{h\omega_s}{2} + (G-1)\frac{h\omega_s}{2} + 2\alpha_s G D_{inv}\frac{h\omega_s}{2} \tag{2.16}$$

$$D_{inv} = \int_0^L \left[\frac{1}{G(z)}\right]dz \tag{2.17}$$

The input noise can be defined as the vacuum definition [33] and considered as the white Gaussian in a certain optical bandwidth, the noise figure of distributed Raman amplifier is defined as the equation (2.18) [33].

$$NF = \frac{N_s}{\frac{Gh\omega_s}{2}} = 1 + \frac{G-1}{G} + 2\alpha_S\int_0^L [\frac{1}{G(z)}]dz \tag{2.18}$$

$$G(z) = \frac{P_S(z)}{P_S(0)} \tag{2.19}$$

Equation (2.19) shows the definition of the signal gain $G(z)$. $P_S(0)$ can be treated as a constant, and $P_S(z)$ represents the signal power distribution along the fibre. The integration of $1/P_S(z)$ between 0 and L equals to the area formed by the reciprocal of signal power profiles in linear units. Therefore, if the net gain G remains the same, the noise figure is proportional to this area. This means that the use of forward pumping will reduce this area due to higher signal power value and consequently improve the noise figure. Additionally, it can be also seen that using discrete amplification would give the largest area, which leads to the worst noise figure.

In the case that cascaded amplifiers are used in repeatered transmission systems, the total noise figure of these amplifiers can be expressed in equation (2.20).

$$NF_{total} = NF_1 + \frac{NF_2 - 1}{G_1} + \frac{NF_3 - 1}{G_1 G_2} + \ldots\ldots\ldots \quad (2.20)$$

Here, NF_i and G_i stands for the noise and the on-off gain of the i^{th} amplifier in linear units, indicating that the noise figure is mostly determined by the first amplifier if the on-off gain is relatively high.

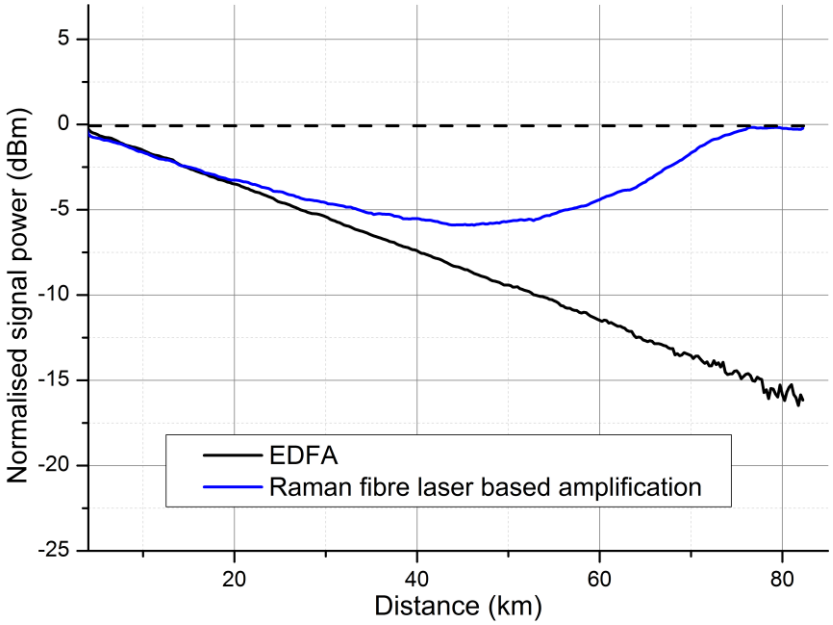

Figure 2.9. Signal power profiles using distributed Raman amplifier and discrete amplifier

As illustrated in Figure 2.9, the noise performance of 83 km standard single mode fibre using EDFA and second order distributed Raman amplifier with BW-pumping (explained in section 2.3.2) are compared. In the first case using EDFA, after the signal is propagated over 83 km SMF, the signal-to-noise ratio does not degrade. In terms of equation (2.14), the noise figure of the passive 83 km span equals to *1/G* which is 16.6 dB in dB assuming the attenuation is 0.2 dB/km. In terms of equation (2.20), the total noise figure is equivalent to the case that the first amplifier is the passive span and the second one is an EDFA. Therefore, the total noise figure in dB can be calculated by the passive span loss plus the noise of EDFA which is 19.6 dB assuming the EDFA is ideal (3 dB noise figure).

Under the circumstance of distributed Raman amplifier with second order backward pumping, it shows that distributed Raman amplifier coverts the last ~30 km fibre into a preamplifier stage of the next span, decreasing the passive span to ~50 km [27]. Therefore the noise figure is reduced significantly to only ~13 dB [34].

The effective noise figure is commonly used in distributed Raman amplifier. This effective noise figure can be derived when the noise figure of an imaginary discrete amplifier is placed after the fibre span, but the total noise figure remains the same as the original distributed Raman amplifier, which means the noise figure of this imaginary discrete amplifier can be negative [1,27]. For example, in this second order distributed Raman amplifier with backward pumping, the effective noise figure equals to -3.6 dB [34] Therefore, the noise figure of a distributed Raman amplifier is significantly better than a discrete amplifier like EDFA. As presented in [15,24,35,36], the optical signal-to-noise ratio (OSNR) performances using distributed Raman amplification are usually higher by 5~7 dB (depending on the configuration of distributed Raman amplifier) compared with EDFA. This might potentially lead to the improvement of transmission performance, in particular using advanced modulation format which requires higher OSNR [4].

2.2.3 Performance limitation factors of distributed Raman amplifications

Several advantages of using distributed Raman amplifications have been reviewed, but there are still several challenges which limit the transmission performance when using distributed Raman amplifiers. Some challenges can be overcome, for example, the polarisation dependent gain can be mitigated by several depolarisation techniques [26,28]. However, for other impairments like relative intensity noise (RIN) from the forward-propagated pump, it might be difficult to fully compensate such impairment.

2.2.3.1 Multiple path interference

In optical fibres, Rayleigh backscattering (RS) is a well-known effect which occurs in all the types of fibres, and also the major reason of the fibre attenuation [1,15]. However, some photons would be reflected twice. Due to Rayleigh scattering, the signal photons are reflected to the backward-propagated direction. This effect can be ignored due to its very low power level which is usually more than 40 dB smaller than the signal power [1]. However, some of the backscattered photons are reflected again into the forward-propagated direction [15]. This is called double Rayleigh scattering (DRS). Figure 2.10 shows a schematic diagram of Rayleigh scattering and double Rayleigh scattering mechanism in the fibre.

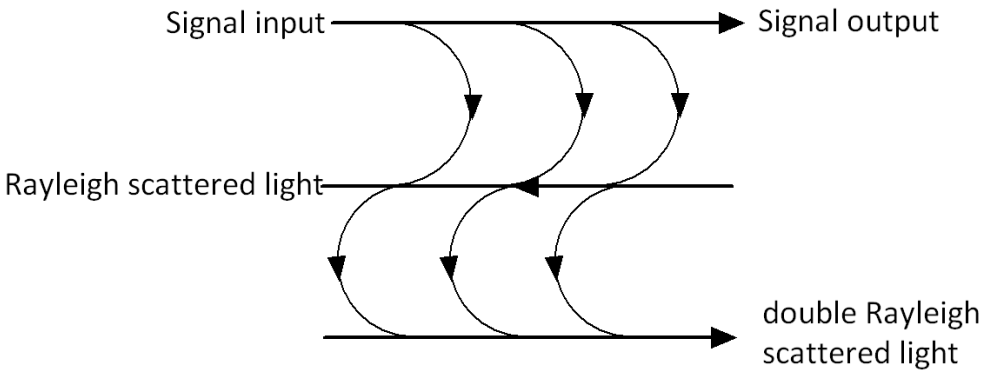

Figure 2.10. Schematic of double Rayleigh scattering mechanism in the fibre [1]

The light due to double Rayleigh backscattering would be also amplified, but it is incoherent with the signal light because the DRS interaction exists in the whole long-distance transmission fibre [15], indicating that the DRS light is a noise source for the receiver. This causes multiple path interference (MPI) which sets the ultimate limit for the maximum Raman gain that can be applied before MPI dominates [27].

The process of Rayleigh scattering, double Rayleigh scattering and the signal propagation can be expressed by the following equations.

$$\frac{dP_S}{dz} = g_R P_P P_S - \alpha_S P_S \tag{2.21}$$

$$-\frac{dP_{RS}}{dz} = g_R P_P P_{RS} - \alpha_S P_{RS} + kP_S \tag{2.22}$$

$$\frac{dP_{DRS}}{dz} = g_R P_P P_{DRS} - \alpha_S P_{DRS} + kP_{RS} \tag{2.23}$$

Equation (2.21) is the same as equation (2.2), which describes the signal propagation along the fibre. g_R is normalised Raman gain coefficient. P_{RS} and P_{DRS} stands for the power of Rayleigh backscattered light and double Rayleigh backscattered light, respectively. k equals to $\alpha_R S$, where α_R is the loss due to Rayleigh backscattering and S represents the Rayleigh capture coefficient indicating how much the backscattered light is captured [1,27].

In addition, beside DRS-induced MPI, two reflectors in a distributed Raman amplified system at the signal wavelength can also lead to MPI [27]. A fraction of the signal light would be delayed due to the reflection between two reflectors [37]. In this case, MPI would be exacerbated due to the Raman gain, because the delayed signal would be amplified again.

MPI relates to the ratio of the signal power, similar to 1/OSNR (optical signal-to-noise ratio) [15]. Due to the incoherent property of MPI, the MPI-induced penalty would add up linearly as

the number of the amplified span increases, indicating that the Raman gain is further restricted. However, if the Raman gain is less than 15 dB, the MPI-induced penalty is insignificant [15]. It is also advised that less DRS-induced MPI would be generated if more Raman gain can be provided by the forward-propagated pump, because when the gain is generated near the input section of the fibre, the amplified DRS light must pass the attenuation of the majority of the fibre in the middle twice, which significantly decreases the power of the DRS light [27].

2.2.3.2 Relative Intensity Noise

Another performance limitation factor in distributed Raman amplification is relative intensity noise (RIN) of the signal transferred from the pumps. Due to the extremely fast process of stimulate Raman scattering (a few femtoseconds), if there are any intensity fluctuations in pump lasers, the signal power is likely to get influenced and amplified by the Raman gain. This leads to large fluctuations of signal at the end of output [1]. Here, RIN is defined as the ratio of intensity fluctuation of the pump power over averaged pump power [1]. In other words, RIN is the ratio between the noise power spectral density and the total power [38]. Because of the intensity noise, the fluctuation causes the change of photocurrent in the photo-receiver. In the electrical domain, it can be expressed in equation (2.24) [38].

$$RIN(\omega) = F\left\{\frac{\left\langle \left(P_r - P_{ave}\right)^2 \right\rangle}{P_{ave}^2}\right\} \tag{2.24}$$

where P_{ave} is the averaged optical power and P_r stands for the received optical power. F stands for the Fourier transform [38]. The equation can be simplified as equation (2.25) below [38].

$$RIN = \frac{S_P(\omega)}{\Re^2 P_{ave}^2} \tag{2.25}$$

Here, $S_P(\omega)$ represents the spectral density of the electrical noise power, and $R^2P_{ave}{}^2$ is the averaged signal power [38]. The RIN can be measured using a low-noise photo-receiver and an electrical spectrum analyser (ESA) [39], and the detailed experimental setup will be discussed in Chapter 4.

The RIN transfer between the signal and the pump is defined as a function in equation (2.26).

$$H(\omega) = \frac{RIN_s(\omega)}{RIN_P(\omega)} \tag{2.26}$$

The extent of RIN transfer depends on the specific pumping configuration, the noise frequency, and the pump power (the Raman gain) [1]. In forward pumping configuration which the signal and the pump are propagated in the same direction, the noise from the forward pump would be superimposed onto the signal noise gradually through the interactions over many kilometres [40]. However, in backward pumping configuration, the time of crossover between the signal and the pump is very short. The noise from the backward pump is averaged over the fibre before reaching the signal [1]. Therefore, the RIN transfer from the backward (BW) pump is insignificant, compared to forward (FW) pumping configuration. In addition, the Raman gain provided by the FW-pump (related to the FW-pump power) would also have an impact on the RIN, indicating that a higher Raman gain would result in the increase of RIN transfer to the signal [1]. RIN transfer can be measured using external modulated Raman pumps with a network analyser as illustrated in [41]. Figure 2.11 shows an example of the measured RIN of the signal increasing with higher forward pump power second order Raman fibre laser based amplifier (details can be found in section 2.3.2) over 83 km standard single mode fibre with two FBGs on both sides [7,42].

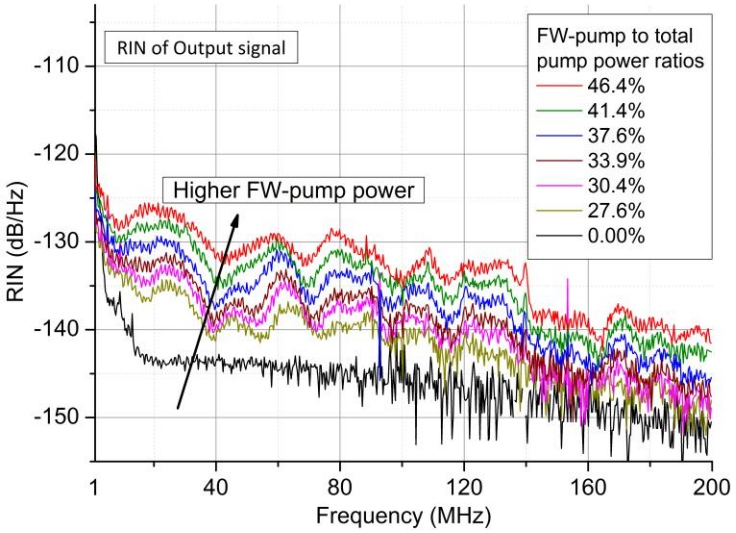

Figure 2.11. Measured RIN of the signal at the output end using URFL based amplifier [42]

The RIN from the forward pump would not only increase the RIN of the signal, but also cause relative phase and polarisation noise of the signal [43,44]. The relative phase noise is originated from the cross-phase modulation (XPM), and the relative polarisation noise of the signal would

be harmful when using polarisation division multiplexed (PDM) modulation format [43].

Fabry-Perot semiconductor lasers with multiple modes are commonly used as Raman pumps. Consequently, the RIN of such laser is ~-110 dB/Hz which is typically higher than single mode distributed feedback (DFB) laser (~-140 dB//Hz). But if the DFB laser is used as a Raman pump, the linewidth of DFB laser is too narrow which would cause undesired stimulated Brillion scattering (SBS) [40]. SBS refers to the third order nonlinear effect which the light is scattered in the opposite direction and not beneficial to the actual Raman amplification [40]. Alternatively, Raman fibre lasers are also typically used as Raman pumps due to their very high output power. However, the RIN of Raman fibre lasers are usually higher (> -105 dB/Hz) than the Fabry-Perot semiconductor lasers. The lowest RIN of Raman fibre laser pump on the market is between -120 and -130 dB/Hz [45] as shown in Figure 4.7 in Chapter 4.

The RIN of the pump is difficult to eliminate, because the RIN, the output power, and the linewidth, are required to be taken into consideration simultaneously. However, it might be able to suppress or avoid the RIN-induced penalty on the signal by adjusting distributed Raman amplifier structure accordingly. In [136], by intensity-modulating the low power semiconductor laser pump in dual order pumping configuration, the RIN transfer could be suppressed. In [47,48] proposed by the author of this thesis, based on a random distributed feedback fibre laser based amplifier, it enabled the use of bidirectional second order pumping without increasing the RIN of the signal [48]. This will be further discussed and investigated in detail in Chapters 4 and 5. In addition, the RIN-induced penalty might be able to be compensated in coherent transmission systems using optimised phase estimation (PE) algorithm and nonlinear polarisation crosstalk canceller (NLCC) algorithm in digital signal processing (DSP) of coherent receiver[43,49].

2.3 Advanced Raman amplification techniques

2.3.1 Bi-directionally pumped distributed Raman amplifications

As explained in section 2.2.2.1, the noise figure of distributed Raman amplifier can be improved if using more FW-pump power [33], as the gain of the signal occurs near the input section of the fibre. Due to higher OSNR requirement when using advanced modulation format, this shows the need for distributed Raman amplifier with bidirectional pumping to achieve low noise figure

(FW-pumping) and enough gain (BW-pumping) [1]. Figure 2.12 shows the schematic of dual order pumping scheme in which the seed (pump) at 1455 nm is amplified by second order pump at 1366 nm [50]. Figure 2.13 shows the comparison of experimentally measured signal power profiles along the fibre between bidirectional pumping and backward pumping only. In Figure 2.13, the signal power variation was ~6 dB using backward pumping only. Once using symmetrical bidirectional pumping (the FW-pump power equals to the BW-pump power), the variation was reduced significantly to ~1.6 dB. This led to the effective noise figure improvement from ~-3.6 dB using backward pumping only to ~-7.6 dB using bidirectional pumping [46].

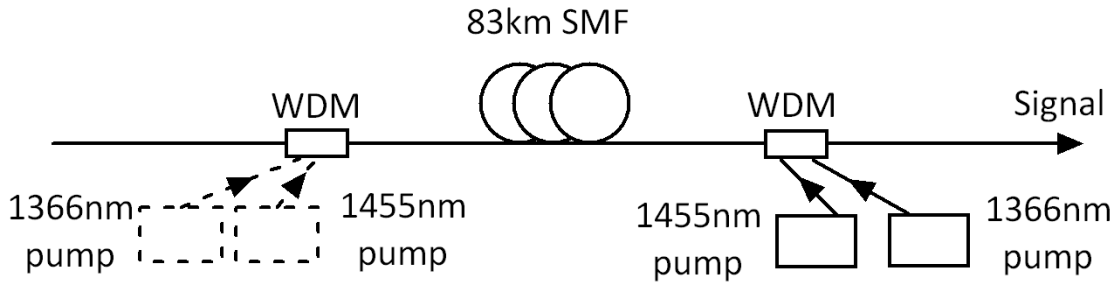

Figure 2.12. Schematic of dual order pumping configuration [50]

Another benefit of using bidirectional pumping is the reduced gain/OSNR tilt at the output end of the fibre when amplifying WDM channels with very broadband bandwidth [1]. This is because the shortest wavelength suffers from the additional loss due to the stimulated Raman scattering between signals from the shortest to the longest wavelength [27]. On the other hand, there are also stimulated Raman scattering between pumps, resulting in the amplification of the longest wavelength pump. These effects lead to the tilt of gain profiles at the output, indicating that the OSNR of the signal at the shortest wavelength is the worst. The gain/OSNR tilt can be eliminated by specifically applying forward pumps at short wavelengths [15,51].

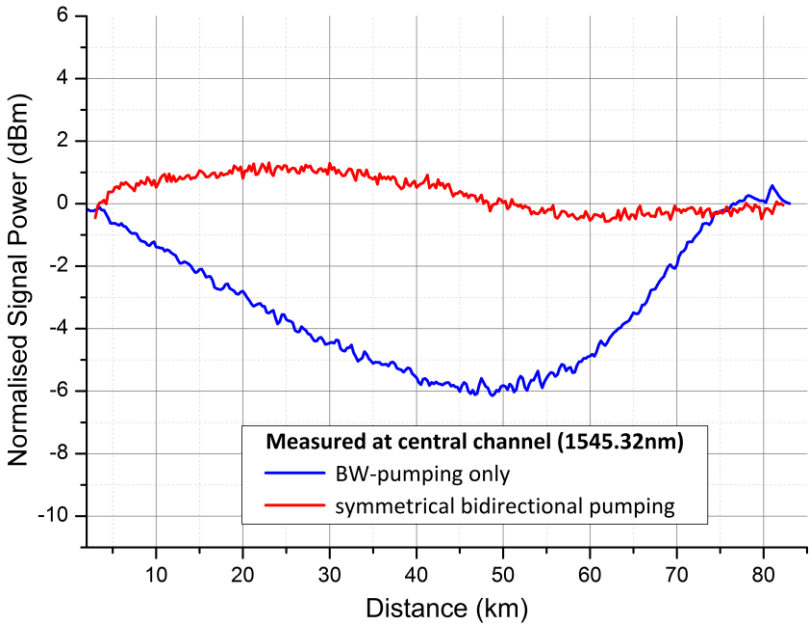

Figure 2.13. Signal power profiles using bidirectional pumping and backward pumping only

2.3.2 High order distributed Raman amplifications

It has been shown that bidirectional Raman pumping can improve the noise figure by the use of FW-pumping. In addition, high order Raman pumping can also have similar improvement on the noise figure. High order distributed Raman amplification means that the primary pump is two or more Stokes frequency shifts away from the signal. For example, in dual order Raman pumping scheme, the pumps at 1366 nm (second order pump) and 1455 nm (first order pump) are combined to amply the signal within C band. Third order Raman pumping configuration is also available and has been deployed for unrepeatered transmission in the field [52,53]. Up to six order Raman pumping configuration has been investigated in [54]. Figure 2.14 shows the schematic diagram and the pump powers of dual order/first order backward pumping scheme.

In dual order pumping scheme, the role of second order pump is to amplify the first order pump so that the gain for the signals is "pushed" further away from the pump [50]. For example, in the case of backward pumping only, the gain of the signal can occur further away from the output end of the transmission fibre using second order Raman pumping, compared to first order backward pumping only. Figure 2.15 shows the measured signal power profiles using dual order backward pumped amplifier and first order backward pumped amplifier over 83 km standard single mode fibre. Signal power variations using first order backward pumping only was ~8.5 dB,

compared with only ~6 dB variation using dual order backward pumping with relatively low first order seed power and ~7.2 dB with higher first order seed power. Note that the first order pump power needs to be much lower than second order pump power in order to maximise the noise reduction benefit [34,47]. Such dual order pumping configuration can be also applied on the forward pumps making it bidirectional pumping, which leads to further minimisation of signal power profile similar to the red signal profile shown in Figure 2.13.

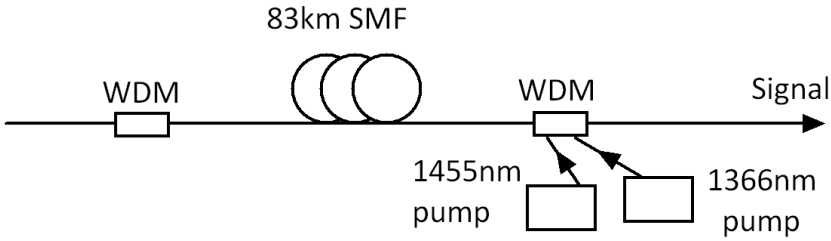

1455nm BW-pump (mW)	1365nm BW-pump (mW)
9.3	1190
50	946
590	0

Figure 2.14. Schematic diagram and the pump powers of dual order pumping scheme

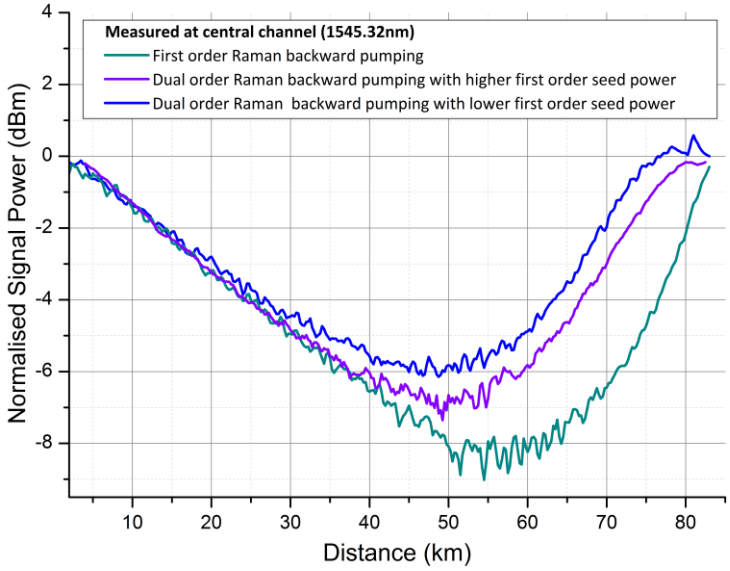

Figure 2.15. Signal power profiles using dual order and first order Raman amplifier with BW-pumping only

A novel second order distributed Raman amplifier scheme is Raman fibre laser (RFL) based amplifier, in which a first order ultra-long Raman fibre laser can be seen as a virtual first order pump generated by second order Raman pump and two fibre Bragg gratings (FBGs) reflectors [7]. Two FBGs centred at 1455 nm with 3 dB bandwidth of 0.5 nm and high reflectivity (>95%)

are located at each end of the transmission fibre. The centre wavelength of passive FBG can be changed in terms of the gain requirement. The resultant first order laser together with second order pump amplifies the signal at C band. This scheme is distinguished from dual order pumping scheme, because it simply uses one pump instead of two pumps at two wavelengths [47]. RFL based amplifier with bidirectional Raman pumping can achieve very low signal power variation (+/- 0.8 dB) over 83 km fibre, which turns the transmission fibre into quasi-lossless (near ideally flat power profile) and significantly improves the noise figure [7,34,42]. Figure 2.16 shows a schematic diagram of second order RFL based amplification scheme.

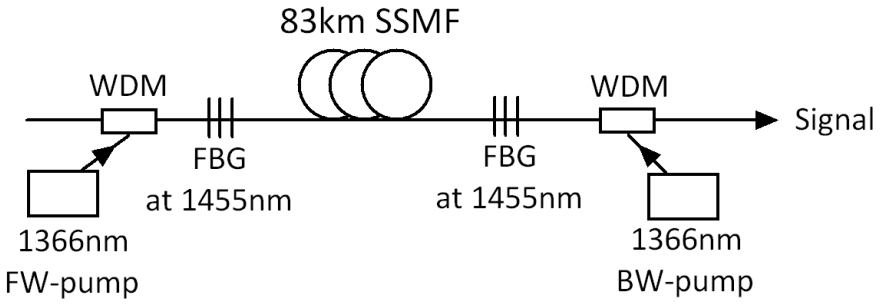

Figure 2.16. Schematic diagram of Raman fibre laser based amplification

The signal and noise power distributions can be expressed by solving a set of ordinary differential equations (ODE) which considers all the related crucial effects, such as double Rayleigh scattering, the pump depletion, and so on [5,7].

$$\frac{dP_{P1}^{\pm}}{dz} = \mp\alpha_1 P_{P1}^{\pm} \mp g_1 \frac{\omega_1}{\omega_2} P_{P1}^{\pm}\left[P_{P2}^{+} + P_{P2}^{-} + 4h\omega_2\Delta\omega_2\left(1+\frac{1}{e^{h(\omega_1-\omega_2)/k_BT}-1}\right)\right] \pm \varepsilon_1 P_{P1}^{\mp} \tag{2.24}$$

$$\frac{dP_{P2}^{\pm}}{dz} = \mp\alpha_2 P_{P2}^{\pm} \pm g_1\left[P_{P2}^{\pm} + 2h\omega_2\Delta\omega_2\left(1+\frac{1}{e^{h(\omega_1-\omega_2)/k_BT}-1}\right)\right](P_{P1}^{+} + P_{P1}^{-})$$

$$\mp g_2 \frac{\omega_2}{\omega_s} P_{P2}^{\pm}\left[P_S + N_S^{+} + N_S^{-} + 4h\omega_S\Delta\omega_S\left(1+\frac{1}{e^{h(\omega_2-\omega_s)/k_BT}-1}\right)\right] \pm \varepsilon_2 P_{P2}^{\mp} \tag{2.25}$$

$$\frac{dP_s}{dz} = -\alpha_s P_s + g_2 P_s (P_{P2}^{+} + P_{P2}^{-}) \tag{2.26}$$

$$\frac{dN_S^{+}}{dz} = -\alpha_s N_s^{+} + g_2\left[N_S^{+} + 2h\omega_S\Delta\omega_S\left(1+\frac{1}{e^{h(\omega_2-\omega_s)/k_BT}-1}\right)\right](P_{P2}^{+} + P_{P2}^{-}) + \varepsilon_S N_s^{-} \tag{2.27}$$

$$\frac{dN_S^{-}}{dz} = \alpha_s N_s^{-} - g_2\left[N_S^{-} + 2h\omega_S\Delta\omega_S\left(1+\frac{1}{e^{h(\omega_2-\omega_s)/k_BT}-1}\right)\right](P_{P2}^{+} + P_{P2}^{-}) - \varepsilon_S (P_s + N_s^{+}) \tag{2.28}$$

where the + and – stands for the forward and backward direction, respectively. *1* and *2* stands for

the pump at 1366 nm and the lasing at 1455 nm, respectively. ω_P and ω_S represents the frequency of the pump and the signal, respectively. $\Delta\omega_P$ represents the effective bandwidth of the pump and $\Delta\omega_S$ means the bandwidth of the signal. g is the Raman coefficient for each Raman scattering process. ε stands for double Rayleigh scattering coefficient.

The boundary conditions of the ODE above are as below [7].

$$P_{P1}^{+}(0) = P_{P1}^{-}(L) = P_0 \tag{2.29}$$

$$P_{P2}^{+}(0) = R_1 P_{P2}^{-}(0) \tag{2.30}$$

$$P_{P2}^{-}(L) = R_2 P_{P2}^{+}(L) \tag{2.31}$$

$$N_s^{+}(0) = N_0 \tag{2.32}$$

$$N_s^{-}(L) = 0 \tag{2.33}$$

$$P_s(0) = P_{IN} \tag{2.34}$$

where R_1 and R_2 stands for the reflectivity of the FBG near the forward pump and the backward pump [5].

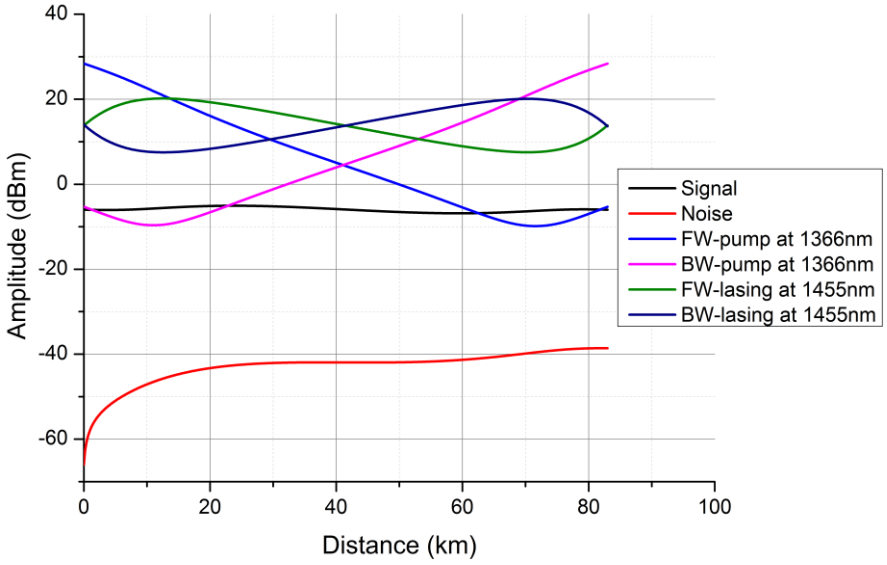

Figure 2.17. Simulation of Rama fibre laser based amplifier with bidirectional pumping and two FBGs [5]

After these ODEs are solved [7], the power distributions of signal, noise, FW-pump, BW-pump, FW-lasing, and BW-lasing, can be obtained and shown in Figure 2.17 for RFL based amplifier with two FBGs over 83 km SMF span [5,7]. The simulation parameters are listed in table 2.1 [9]. It can be seen that the signal power variation is +/- 0.8 dB which agrees with experimental data.

Bi-directionally-propagated first order lasing is generated by second order pumps and the reflection of FBGs, forming an ultra-long 83 km Fabry-Perot cavity. In this simulation, the reflectivity of both two FBGs is 95%. In Chapters 4 and 5, a novel scheme based on random distributed feedback laser with second order bidirectional pumping and single FBG is proposed to avoid the RIN transfer and improve the transmission performance. This model can be also used to simulate this random DFB laser based scheme by minimising the FBG near the input close to zero [55].

Parameters	**Symbol**	**Value**	**Unit**
FW-pump power	P_2^+	0.7	W
BW-pump power	P_2^-	0.7	W
Signal frequency	ω_S	194	THz
Raman gain coefficient at 1366nm	g_1	0.51	$W^{-1}km^{-1}$
Raman gain coefficient at 1455nm	g_2	0.36	$W^{-1}km^{-1}$
Rayleigh scattering coefficient at 1366nm	ε_1	1×10^{-4}	km^{-1}
Rayleigh scattering coefficient at 1455nm	ε_2	6×10^{-5}	km^{-1}
Rayleigh scattering coefficient at 1545nm	ε_s	4.3×10^{-5}	km^{-1}
Attenuation at 1366nm	α_1	0.33	dB/km
Attenuation at 1455nm	α_2	0.26	dB/km
Attenuation at 1545nm	α_s	0.2	dB/km
Plank's constant	h	6.62×10^{-34}	Js
Boltzmann's constant	k_B	1.381×10^{-23}	J/K
Temperature	T	298	K

Table 2.1. Simulation parameters [5]

Although the signal power profile and noise figures can be minimised using high order Raman pumping, a disadvantage is that the pump-signal efficiency is further decreased compared to

EDFA and first order distributed Raman amplifier. Therefore, it might be not very cost-effective to deploy such scheme in long-haul repeatered transmission system with many in-line amplifiers, but it doesn't affect the fact that the noise figure and potential transmission performance would be improved using high order scheme [56].

2.4 Summary

This chapter 2 is devoted to the basic theory of optical amplifiers, in particular distributed Raman amplifier which is the main highlight of the thesis. In section 2.1, the mechanism of EDFA is briefly introduced in order to compare with distributed Raman amplifier in the following sections. Section 2.2 is concentrated on Raman amplifier. In section 2.2.1, a set of two equations which describes the signal and pump power distributions is explained. In the following section 2.2.2, distributed Raman amplification and its benefit are illustrated. The main benefit of distributed Raman amplification lies in the significant noise figure/SNR improvement compared to discrete amplification, which consequently improves the OSNR of the signal and potentially the transmission performance. In section 2.2.3, multiple path interference and relative intensity noise are discussed. It shows that MPI can cause insignificant penalty if the Raman gain is relatively small and bidirectional pumping would help decrease the MPI penalty. For the RIN from the forward pump being transferred to the signal, it might introduce significant penalty in particular for long-haul repeatered transmission. There are mainly two ways to overcome or compensate the RIN-induced optically or electrically. Optically overcoming the RIN-induced penalty can use very low RIN pump if possible, or the RIN can be avoided by designing a distributed Raman amplifier as in references [47,48,136]. Electrically compensation of RIN-induced penalty means that digital signal processing (DSP) algorithms can be optimised for reducing such RIN-induced penalty, including relative phase noise and relative polarisation noise [43,49]. In section 2.3, two advanced Raman amplification techniques are reviewed, which are bidirectional pumping and high order pumping. Bidirectional pumping would reduce the noise figure and improve the noise performance, but the use of forward pumping can be problematic if the RIN problem is not properly solved. High order pumping would similarly decrease the noise figure but at the expense of using more pump power. In particular, a novel second order Raman fibre laser based amplifier with two FBGs is explained in detail in this section. This

scheme creates a first order ultra-long Raman fibre laser to assist the amplification of the signal, as opposed to conventional dual order/first order Raman amplifier.

3. Transmission Subsystems

In Chapter 2, different optical amplification techniques including EDFA, conventional distributed Raman amplification, and second order Raman fibre laser based amplification, are reviewed from the theory perspective,. However, when different optical amplification techniques are compared with each other, the most convincing way is to deploy the optical amplifier in coherent transmission system and see what the transmission performance would be. Here, in this chapter, the overview on the coherent transmission subsystems is discussed, which includes different modulation techniques, the Mach-Zehnder modulator (MZM), the recirculating loop, the coherent receiver, and potential transmission impairments.

3.1 Modulation schemes and optical modulators

3.1.1 Modulation schemes

In order to enable a continuous wave (CW) signal to carry information, the signal needs to be modulated by applying some changes accordingly on one or more properties. These changes can be applied on the amplitude, frequency, phase, polarisation state, and so on. Back in the 1980s, only the amplitudes of the optical carrier signal in most of the transmitters were varied [2]. The reason why the phase modulated transmitter was not widely used was the complexity to demodulate the signal at the receiver at that time [58]. With the rapid progress of semiconductor devices and digital signal processing (DSP), this made various modulation formats possible. For example, the modulation of multiple properties (amplitude and phase simultaneously) on the optical carrier signal would increase the spectral efficiency (bit/s/Hz) which is defined as the ratio between the data bit rate (bit/s) and the bandwidth of the signal (Hz). As we know, the electric filed $E(t)$ of an optical carrier signal can be expressed as equation (3.1).

$$E(t) = pA\cos(\omega_0 t + \theta) = p\,\mathrm{Re}[A\exp(i\omega_0 t + i\theta)] \tag{3.1}$$

Here, p stands for the polarisation unit vector, a stands for the amplitude, θ is the phase, and ω_0 stands for the frequency. This indicates that there are four properties that can be modulated on the optical carrier signal, that are the amplitude, phase, frequency, and polarisation [2,58]. In

digital transmission systems without considering the polarisation, these are called amplitude-shift keying (ASK), phase-shift keying (PSK), and frequency-shift keying (FSK). The complex phasor C is defined as $C=A\exp(i\theta)$, which can generate the constellation diagram in order to observe the modulation format more intuitively. The real and imaginary parts of C is plotted along both X and Y axes, respectively [4].

Most of optical modulation techniques in telecom were OOK (On-off keying) or ASK at 2.5 and 10 Gbit/s in the 1980/1990s which only allowed the variation of the amplitude of the carrier signal. In terms of equation (3.1), there are two points along the real axis for the constellation diagram of OOK/ASK signal, indicating that the amplitude of the signal changes from 0 to a without any change in the phase or frequency.

Similarly, PSK is the modulation format which allows the phase change on the carrier signal. Unlike the ASK signal which is switched on and off accordingly, the PSK signal is always switched on (the amplitude might remain the same), and the information is carried on the phase shift. However, the PSK signal cannot be demodulated by direct detection, because no information can be detected or kept if the optical signal is directly detected without coherently combining with a local oscillator (LO) [2,5]. The simplest PSK modulation format is binary PSK (BPSK) which the phases of the carrier signal are distinctively chosen (typically 0 and π). Alternatively, the carrier signal can be differentiated in the way that the phase difference between two neighbouring symbols is changed by 0 or π. This modulation format is called differential PSK (DPSK). For example, if the difference in phase between the n_{th} and $n+1_{th}$ is 0, it can be defined that the $n+1_{th}$ bit remains at the same level. If the phase difference is π, the $n+1_{th}$ bit level gets changed/inversed. The use of DPSK modulation enables the phase of the carrier signal to remain relatively stable over much shorter time (only 2 bits), unlike many bits using BPSK especially at the time that there is no phase variation [2]. Therefore, DPSK modulation format is more tolerant to the phase noise, and there would be lower requirement for the linewidth of the transmitter laser and local oscillator, because the wider laser linewidth results in more phase noise at the receiver [59].

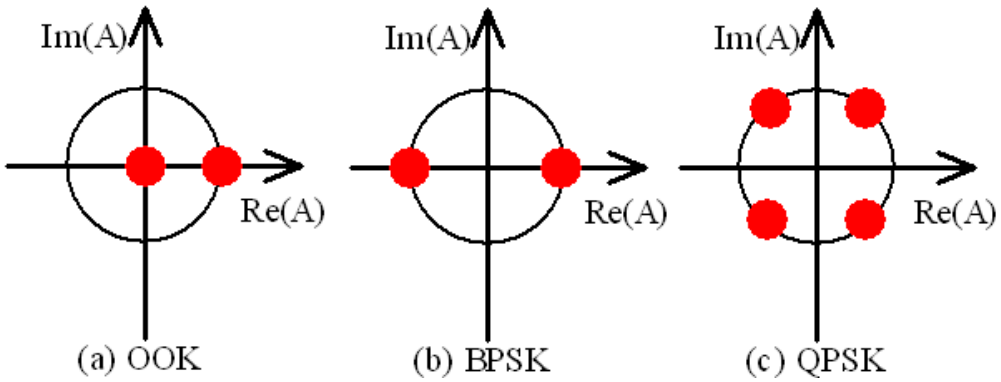

Figure 3.1. Constellation diagrams of OOK, BPSK, and QPSK

However, neither the BPSK nor DPSK modulation is helpful to improve the spectral efficiency and the total capacity, because the BPSK is similar to ASK or OOK in the sense that only two different values are varied from one property of the carrier signal. On one hand, because of the limitations and cost of semiconductor based device, the modulated baud rate (B_s) is not able to increase infinitely, as -3 dB bandwidths of frequency response for most of semiconductor lasers are still less than 25 GHz [2]. Therefore, to increase the data rate without increasing the modulation baud rate B_s was a promising solution. On the other hand, the rapid progress of coherent detection and digital signal processing makes more advanced modulation format possible. A common example is quadrature-phase-shift-keying (QPSK) modulation which the carrier phase is allowed to take four different values, such as $\pi/4$, $3\pi/4$, $5\pi/4$, and $7\pi/4$. More importantly, unlike ASK or BPSK, the QPSK signal can transmit 2 bits per symbol. Figure 3.1 shows the constellation diagrams of OOK (ASK), BPSK, and QPSK.

As shown in Figure 3.1(c), the information can be allocated as four possible combinations of two bits (00, 01, 10, and 11), which corresponds to four values of carrier phase [57]. Consequently, the symbol rate (also called the baud rate B_s) is decreased by half using QPSK modulation, compared with ASK or BPSK modulation. The relationship between the bit rate and baud rate is defined in the following equation (3.2).

$$B = B_s \log_2(M) \tag{3.2}$$

In QPSK, M equals to 4 and $B=2B_s$, which means the bit rate is twice the baud rate. Compared with OOK and BPSK modulation, if the baud rate remains the same, the bit rate of QPSK signal is twice leading to a double total capacity. Obviously, more advanced modulation format

can be achieved by increasing the variant M. For example, if eight distinct values are allocated to the phase of the carrier signal and three bits are allowed to transmit simultaneously, the bit rate is three times higher than the baud rate. This modulation technique is called 8-PSK as illustrated in Figure 3.2(a).

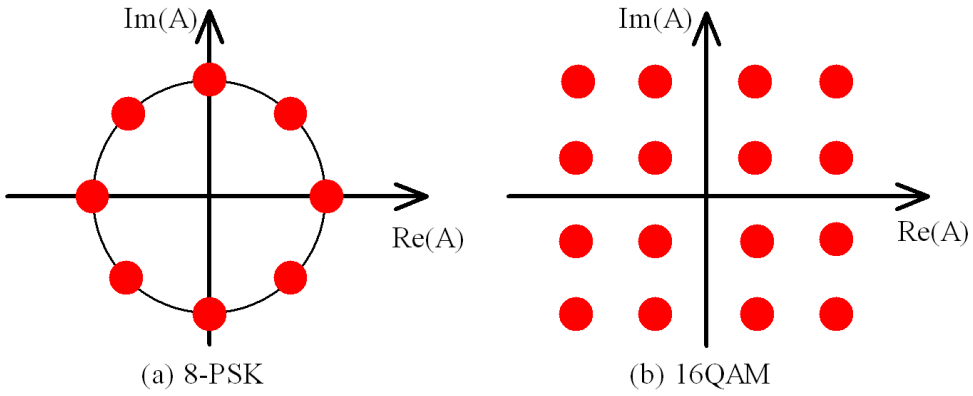

Figure 3.2. Constellation diagrams of (a) 8-PSK; (b)16QAM

In Figure 3.2(a), only the different values of carrier signal phase are varied from symbol to symbol. However, if the amplitude and phase of the carrier signal can be changed at the same time, more bits can be transmitted at the same time, resulting in higher spectral efficiency and total capacity. In Figure 3.2(b), two amplitude values and four phase values are allocated for each symbol, which is called 16-quadrature amplitude modulation (16QAM). 16 symbols located as a square grid are deployed to increase the variant M to 16 [58]. In this case, four bits per symbol can be transmitted, indicating that the baud rate is further decreased by half than QPSK if the bit rate remains the same.

Now it is known that QPSK allows two bits per symbol and 16QAM allows four bits per symbol. To sum up, the essence to increase the spectral efficiency is to increase the number M in equation (3.2). Alternatively, the spectral efficiency can be also increased two times by combing two orthogonally polarised signals together. Although the polarisation state of the signal is random when transmitted over the fibre, the relative polarisation states remain orthogonal [2]. This polarisation division multiplex (PDM) technique would further decrease the baud rate by half. For example, 100G dual polarisation-QPSK (DP-QPSK) has been widely deployed in telecoms, and the baud rate of the modulator is ~25 G baud.

3.1.2 Mach-Zehnder modulator (MZM) and its functionality

The optical signal modulation techniques are divided into two categories in general, which are direct modulations and external modulations [60,61]. In direct modulation, the laser diode can be modulated directly through the electrical signal that drives the laser diode and carries the message [62]. The major drawback of direct modulation is that it can only be used for relatively low data rates (<5 Gb/s) due to the pulse distortion and frequency chirp [2,62]. For external modulation, electro-absorption modulator (EAM) and Mach-Zehnder modulator (MZM) are widely used for optical modulators [60,63]. However, MZM is the most commonly used modulator and the main device of 100G DP-QPSK modulator in the following experiments. For the MZM used in telecommunications, the electro-optic effect of $LiNbO_3$ waveguide is usually used because the effective refractive index can be changed when the external voltage is applied [2]. In this way, the changing refractive index results in the phase change when the light passes through the device. The phase modulation can be also converted into amplitude modulation using a Mach-Zehnder configuration [57]. Figure 3.3 shows the schematic diagram of a typical MZ modulator.

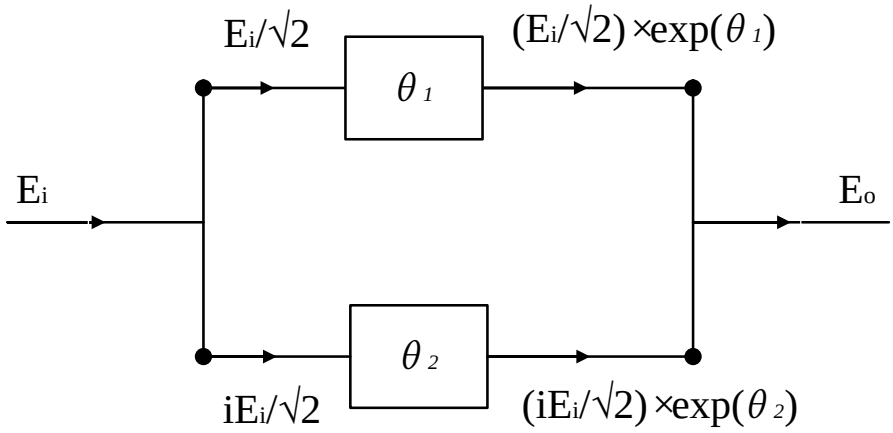

Figure 3.3. The schematic diagram of MZM [2]

The input field E_i is split by a 3 dB coupler into two equal arms. Different phase shifts are added by applying required voltages on two arms, and combined together through another 3 dB coupler [2,57]. The phase shifts applied on two arms can be expressed in the following equation (3.3)

$$\theta_j = \frac{\pi V_j(t)}{V_\pi} \tag{3.3}$$

where j is the arm path 1 or 2, V_j is applied voltage on the arm, and V_π is voltage that produces a

π phase shift [2]. The output field is as follows in equation (3.4).

$$E_o = \frac{1}{2} E_i (e^{i\theta_1} + e^{i\theta_2}) \tag{3.4}$$

So the transfer function of the modulator is shown in equation (3.5),

$$t_m = \frac{E_o}{E_i} = \cos\left[\frac{1}{2}(\theta_1 - \theta_2)\right] \exp\left[\frac{i(\theta_1 + \theta_2)}{2}\right] \tag{3.5}$$

Therefore, MZM can be functioned as an amplitude modulator or a phase modulator. For the former as an amplitude modulator, voltages in two arms should be $V_2(t)=-V_1(t)+V_b$, where V_b is a constant bias voltage. In equation (3.5), $\theta_1+\theta_2$ equals to the constant. In this case, the power transfer function of an amplitude modulator should be expressed in equation (3.6).

$$T_m(t) = |t_m|^2 = \cos^2\left[\frac{\pi}{2V_\pi}(2V_1(t) - V_b)\right] \tag{3.6}$$

For the latter used as a phase modulator, the same bias voltages are applied to two arms, meaning that $\theta_1=\theta_2$ and $V_1 = V_2$. The transfer function of a phase modulator can be expressed in equation (3.7).

$$t_m = \exp(i\theta_1) \tag{3.7}$$

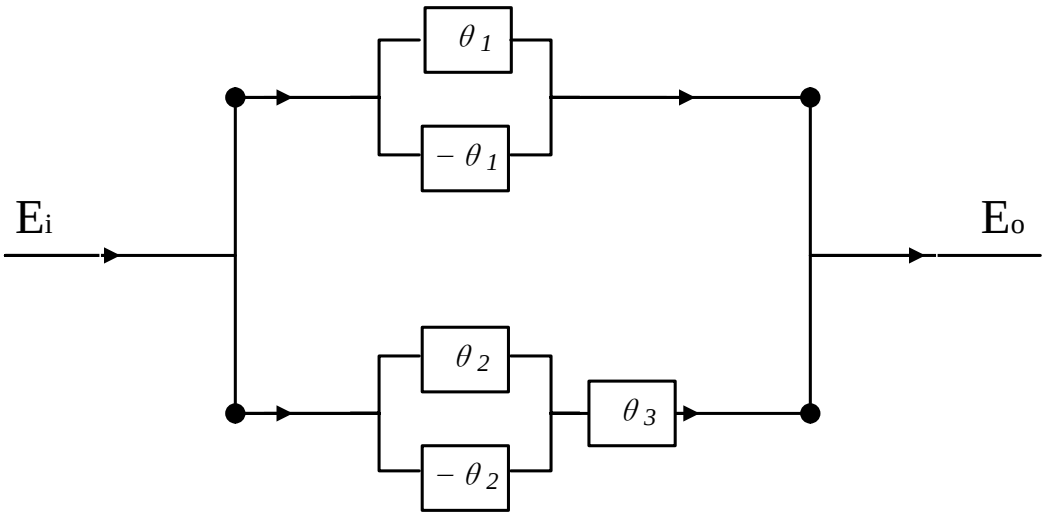

Figure 3.4. Schematic diagram of QPSK modulator nesting three MZMs [2,58]

It has been known that a single MZM might be able to change both amplitude and phase at the same time by changing the voltages V_1 and V_2 properly, but cannot change two quadratures (In-phase and Quadrature) independently [2]. As illustrated in the last section, QPSK is able to transmit two bits per symbol, meaning that the spectral efficiency is doubled. To enable

modulating two quadratures and generate QPSK signal, the structure combining three MZMs is a commonly used technique. Two internal MZMs on both arms should be operated in terms of "push-pull" regime which means $\theta_1=-\theta_2$ (V_1 and V_2 are operated with the opposite phase) [57,58], and introduce two phase shifts of 0 and π on both two arms. The output signal from each internal MZM is actually BPSK signals. As for the outer MZM, by applying the voltages V_3, it is biased to produce a constant $\pi/2$ shift between the phases of two outputs of internal MZMs (I and Q). In this way, a quadrature signal that there is $\pi/2$ phase difference in between is generated. By combining all three MZMs together, there are four possible phase shifts ($\pi/4$, $3\pi/4$, $5\pi/4$, and $7\pi/4$) given by $(\pm1\pm i)/\sqrt{2}$. A schematic diagram of QPSK generator nested by three MZMs is shown in Figure 3.4.

3.2 Recirculating loop

In a real repeatered in-line long-haul transmission system, the optical signal is transmitted over many amplified fibre spans. The schematic diagram of a repeatered system is shown in Figure 3.5. However, a recirculating loop is essentially a timed controlled transmission line which allows optical signal propagated from I/P (input) to O/P (output) multiple times to simulate multi-span in-line transmission system [38,64], which significantly reduces the cost of an expensive in-line transmission system by using only one span repeatedly.

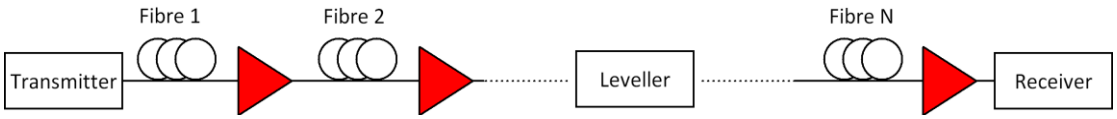

Figure 3.5. Schematic diagram of straight in-line system

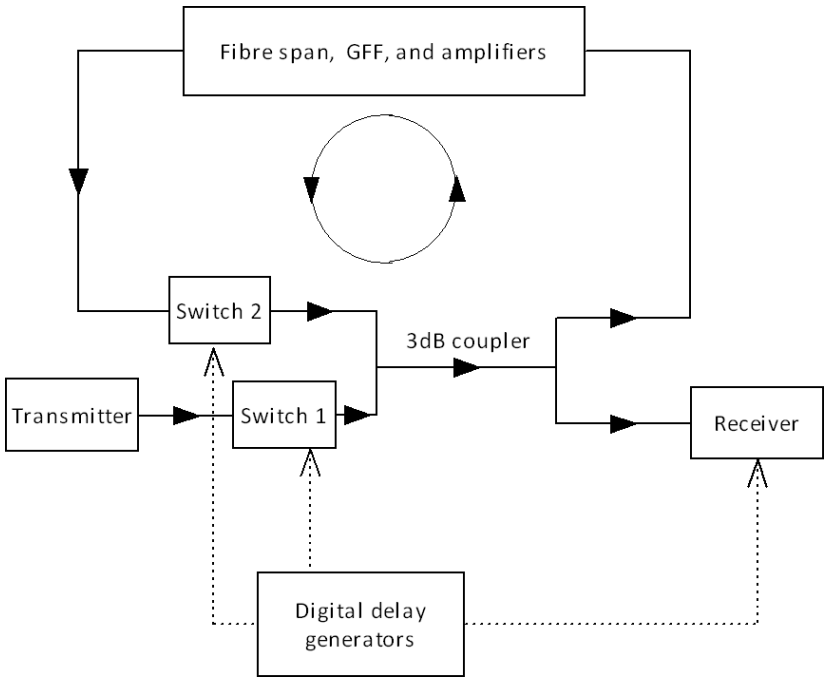

Figure 3.6. A recirculating loop schematic diagram (Solid line: optical signal transmission; dotted line: electrical signal)

The schematic diagram of a typical recirculating loop is illustrated in Figure 3.6. Acousto-optic modulators (AOMs) are usually used as fast response optical switches due to their excellent extinction ratio (~50 dB) and polarisation diversity [64]. As shown in Figure 3.6, the signal is transmitted through switch 1 and split into two paths through a bidirectional 3 dB coupler. One output is toward the direction into the recirculating loop, and the other is toward the receiver path. Along the recirculating loop path, a transmission span with associated amplified chain, a gain flatness filter (GFF), an EDFA, and switch 2 (loop switch) are placed. The loss of the transmission span is compensated by the associated amplification technique. The GFF is used to flatten the output spectrum from the amplified span. An additional EDFA might be used to compensate the loop specific loss from the switches, 3 dB couplers, GFF and so on. Alternatively, if the loss from the amplified span is not fully compensated, the remaining loss from the amplified span can be also compensated by this EDFA in the loop. If the amplified span is enabled by backward Raman amplification, the scheme should be called hybrid EDFA/Raman amplification [137]. The external triggers of switch 1 (switch at the input) and switch 2 (loop switch) are provided by digital delay generators (DDGs), which are responsible for controlling the timings of the loop so that a certain number of recirculations can be applied.

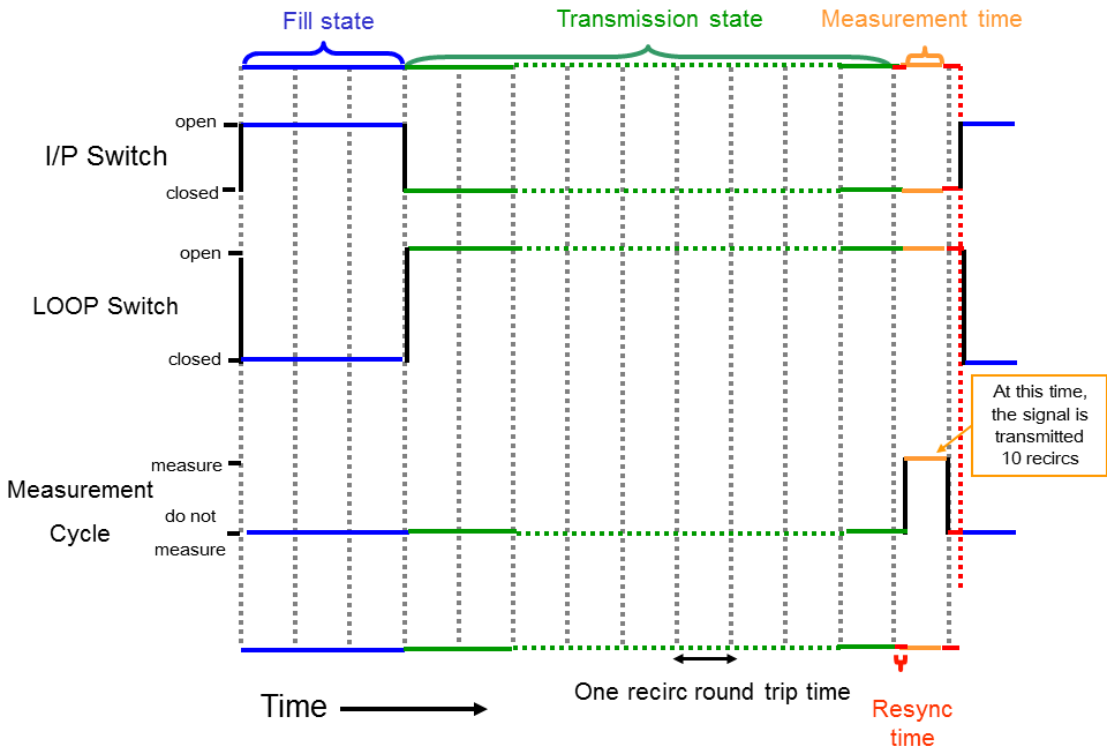

Figure 3.7. Timing controls of recirculating loop [64,65]

Figure 3.7 shows the timing controls and switching states of a typical recirculating loop design. For the operations of a recirculating loop, there are usually two switching states: filling state and transmission state (looping state). For the filling state, the switch 1 is set to transmit the signal, meaning that the signal can go through the switch 1 but get blocked before the switch 2, because the switch 2 is set to block the signal at the moment. This means the loop is filled with optical signals in order to avoid multi-path interference [38]. For the transmission state, the switch 1 is set to block "new" input signal and the switch 2 is set to transmit so that the optical signal which are already in the loop can transfer required roundtrip recirculations within the loop, and then tested with the receiver at the loop O/P path. To measure the signal transmitted after desired numbers of recirculations, a trigger is injected into the receiver and enables the receiver to capture the signal only within specific period of time [65]. Because the signal is transmitted in the exactly same path many times, everything would be accumulated, including signal power, ASE noise, the amplifier noise, and so on [38]. Also, in a recirculating loop, when the signal propagates through the loop, it suffers from the loss of the loop components such as 3 dB coupler, splitting tap and so forth. So an optical amplifier (mainly EDFA in the loop) is required to compensate

the power loss accurately, which makes sure that the input and output optical powers of each recirculation are always the same. A convenient way to monitor this is to use 1% tap at the loop output. The monitored signal is detected by a low speed photo-detector, and the electrical output is connected to a low speed oscilloscope [38,65]. The scope needs to be also triggered by a digital delay generator correctly. Amplitudes of waveforms displayed in the scope are corresponded to the average signal optical power in each recirculation [38]. If the power is not adjusted accurately leading to positive or negative net gain, the signal power level displayed on the oscilloscope will increase or decrease step by step after each recirculation. For example, if the output power from the first recirculation is higher than the input, the output power after the second recirculation would be higher by the same amount than the output after the first recirculation. This would cause much higher power after many recircualtions [64]. Additionally, for WDM transmission systems, the amplitude of each channel after each recirculation are required to be levelled by GFF, otherwise the differences in amplitude between each channel would be expanded significantly after a number of recirculations.

Speaking of the advantages of recirculating loop, it is very easy to build, cost-effective and small sized, because only one set of the equipment is required instead of multiple sets. However, compared with real in-line transmission systems, there are a few drawbacks or differences which need to be resolved or realised. First, the signal is gated by complex timing control both in the recirculating loop and the receiver part, which might be difficult to implement if the loop is non-standard configuration. Second, it is a concatenation of the same components in the recirculating loop. This artificial periodicity is very rare to happen in real in-line systems [38,64]. Though polarisation periodicity can be eliminated using polarisation scrambler, an additional loss of ~5 dB would be introduced. Third, the recirculating loop suffers from the excess loss from switches, 3dB couplers, and additional components, which requires additional gain from the amplifier after each recirculation, effectively increasing the total noise.

3.3 Coherent receiver

Coherent detection becomes a significant research interest so rapidly, because it can decode the information with phase modulation and convert it to the amplitude variations [58]. This is extremely helpful for advanced modulation formats which contains both amplitude and phase

information in order to improve the spectral efficiency and total capacity [2,4,58]. In addition, the use of coherent detection significantly increases the sensitivity of the receiver, which is very important for the unrepeatered transmission link [5].

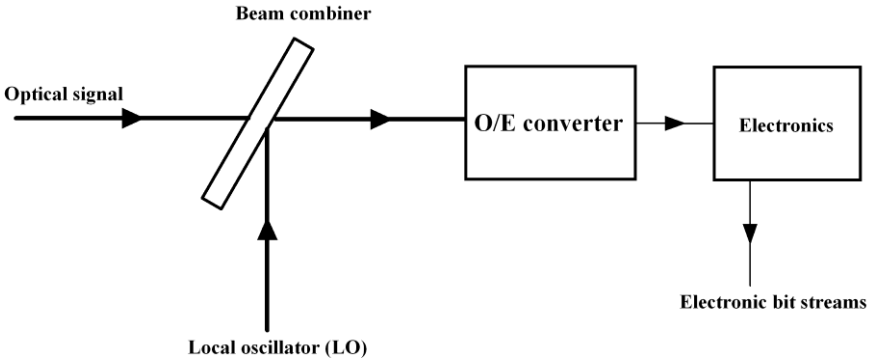

Figure 3.8. Schematic diagram of coherent detection mechanism [2]

The basic idea of coherent detection is shown in Figure 3.8. At the receiver, a narrow linewidth laser is used as local oscillator (LO). Optical signal is combined with the LO using WDM coupler in practice. The complex field of optical signal is shown in equation (3.7) and LO signal is shown in equation (3.8) [2,58].

$$E_s = A_s \exp[-i(\omega_s t + \theta_s)] \tag{3.7}$$

$$E_{LO} = A_{LO} \exp[-i(\omega_{LO} t + \theta_{LO})] \tag{3.8}$$

A, θ, and ω stands for amplitude, phase and frequency, respectively. Optical power P into O/E converter is given by

$$P = |E_S + E_{LO}|^2 \tag{3.9}$$

$$P(t) = P_S + P_{LO} + 2\sqrt{P_S P_{LO}} \cos(\omega_{IF} t + \theta_S - \theta_{LO}) \tag{3.10}$$

In equation (3.10), $P_s=A_s^2$, and $P_{LO}=A_{LO}^2$ [2]. ω_{IF} represents the difference in frequency between the signal and the LO, which is ω_s-ω_{LO}, and $\nu_{IF}=\omega_{IF}/2\pi$ is the intermediate frequency *IF*.

There are two different coherent detections techniques which are homodyne detection and heterodyne detection [2]. In homodyne detection, there is no difference in frequency between the LO and signal. From the equation (3.10), it can be seen that the received optical power contains the phase of the LO (θ_{LO}). This means that the fluctuation of θ_{LO} can cause the fluctuation of the total optical signal power, but the phase difference between the signal and the LO is required to be constant. The implementation of such a phase lock device can lock the phase difference, but it

is quite complicated [2], leading to the coherent receiver design difficult.

In heterodyne detection, it requires two stages to demodulate the optical signal. The carrier frequency needs to be first downconverted to the intermediate frequency, and the resultant electrical signal is to recover the bit stream electronically [2,5]. Although the 3 dB penalty in SNR exists in heterodyne detection [4], the advantage of such an expense is that the phase lock loop is no longer required, indicating that the coherent receiver design is simplified significantly. In practice, the phase fluctuations of signal and LO can be suppressed by using narrow linewidth (~100 kHz) laser diode which gives less phase noise [2,66,67].

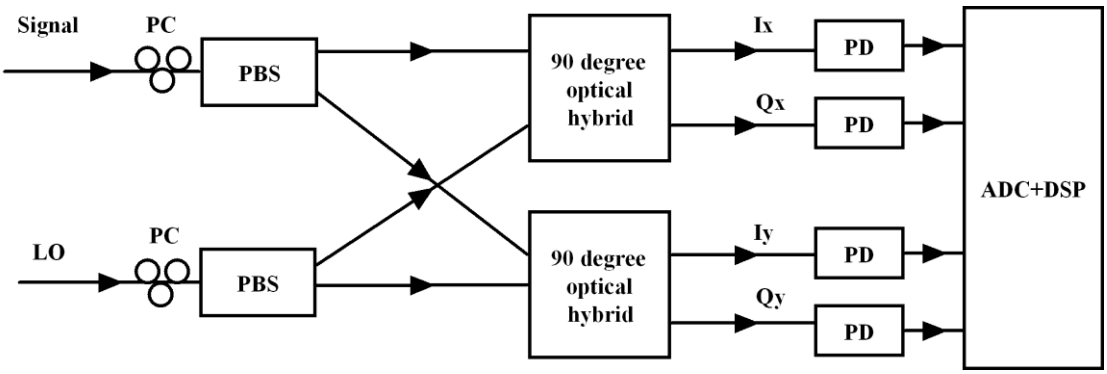

Figure 3.9. A schematic diagram of coherent detector on the PDM signal

As explained in section 3.1, QPSK enables the transmission of two bits per symbol. With polarisation division multiplexing, four bits per symbol can be achieved by PDM-QPSK (DP-QPSK). The coherent receiver that can demodulate such signal is designed as below in Figure 3.9. The received PDM signal and LO are separated into two orthogonal polarisations by polarisation beam splitter (PBS). The polarisation controller before PBS is to make sure of the signal and LO polarised at 45ºand -45º. After PBS, the co-polarised signal and the LO are fed into two 90º optical hybrids. In this way, the phase and polarisation multiplexed signal can be divided into in-phase (I) and quadrature (Q) part for both X and Y polarisations using two 90º optical hybrids [2,57]. The four signals were detected by four photo-detectors (PDs) and followed by a real time oscilloscope for analogue to digital conversion (ADC) and digital signal processing (DSP).

The 90º optical hybrid shown in Figure 3.9 is essentially two 2×2 fibre couplers combined together with a 90º phase shift on one arm of a 2×2 fibre coupler [68]. The schematic of an optical hybrid is shown in Figure 3.10. In this way, the real and imaginary parts of the signal

detection can be realised [57].

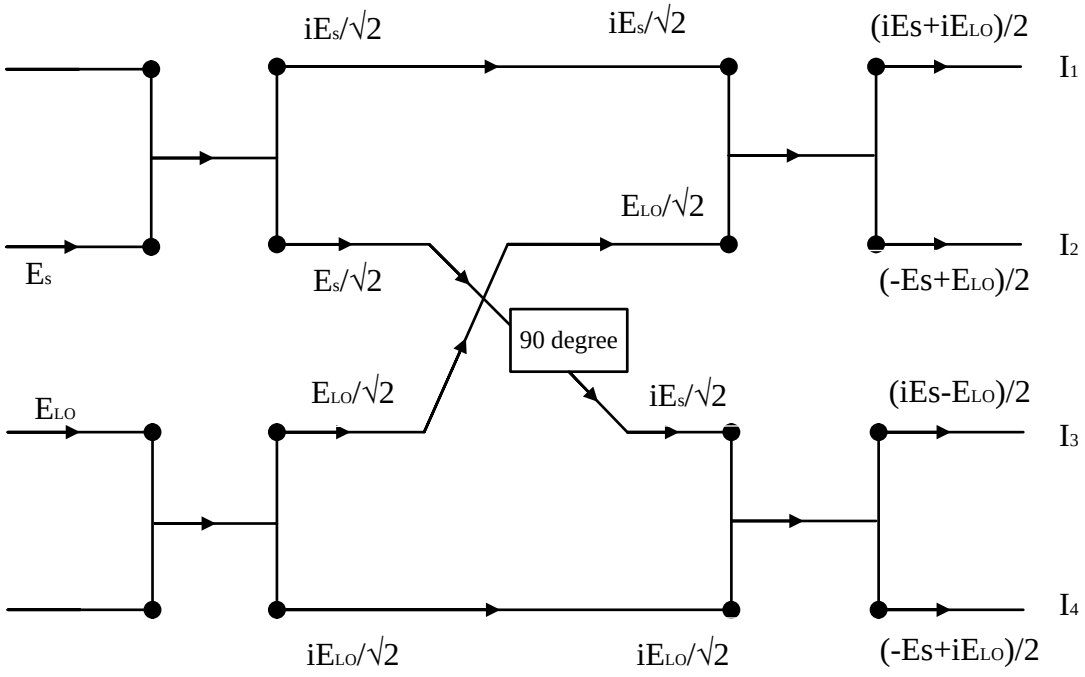

Figure 3.10. A schematic diagram of a 90 degree optical hybrid [57]

In terms of Figure 3.10, the following expressions of photocurrents for each photo-receiver can be obtained. From these equations, E_s^2 and E_{LO}^2 are the amplitudes which do not include any phase information, meaning that they can be easily filtered out by a DC block [57]. By subtracting I_1 and I_2 as well as I_3 and I_4, the In-phase (real parts) and Quadrature (imaginary parts) is left.

$$I_1 \propto \left| i\frac{E_s + E_{LO}}{2} \right|^2 = \frac{1}{4}(E_S^2 + E_{LO}^2 + 2\,\mathrm{Re}\{E_s E_{LO}^*\}) \tag{3.11}$$

$$I_2 \propto \left| -\frac{E_s - E_{LO}}{2} \right|^2 = \frac{1}{4}(E_S^2 + E_{LO}^2 - 2\,\mathrm{Re}\{E_s E_{LO}^*\}) \tag{3.12}$$

$$I_3 \propto \left| \frac{iE_s - E_{LO}}{2} \right|^2 = \frac{1}{4}(E_S^2 + E_{LO}^2 + 2\,\mathrm{Im}\{E_s E_{LO}^*\}) \tag{3.13}$$

$$I_4 \propto \left| \frac{-E_s + iE_{LO}}{2} \right|^2 = \frac{1}{4}(E_S^2 + E_{LO}^2 - 2\,\mathrm{Im}\{E_s E_{LO}^*\}) \tag{3.14}$$

3.4 Transmission impairments

For a long-haul transmission system, the system performance can be achieved at the optimum

launch power which should be the trade-off between linear impairments and nonlinear impairments [2,57]. This assumption is based on a general EDFA-amplified systems, and the additional potential impairments (i.e. RIN, MPI) brought by Raman amplifier has been discussed in section 2.2.3. When the signal power is very low, the linear impairment dominates the performance, because the fibre can be treated as linear medium, and the nonlinear impairments can be ignored. When the signal power is high, the Kerr effect is triggered and the system performance is degraded [69]. Kerr effect is a nonlinear effect that the refractive index of fibre changes with the optical signal intensity when propagated over optical fibres [70].

The optical signal propagated in the fibre can be expressed by the modified nonlinear Schrodinger equation (NLSE), as shown in equation (3.15).

$$\frac{\partial A}{\partial z} = -\frac{\alpha}{2}A - \frac{i}{2}\beta_2 \frac{\partial^2 A}{\partial T^2} + \frac{1}{6}\beta_3 \frac{\partial^3 A}{\partial T^3} + i\gamma |A|^2 A \tag{3.15}$$

Here, A stands for the complex amplitude of the signal, z stands for the propagated distance in km, and α stands for the coefficient of fibre attenuation [2]. β_2 and β_3 means the group velocity dispersion (GVD) and dispersion slope, respectively. T is the time and γ is the Kerr nonlinearity coefficient [2,69]. It can be seen that the nonlinearity term (the last one in equation (3.15)) is corresponded to the amplitude (intensity) of the signal [1].

For linear impairments, the ASE noise is fundamental and unavoidable impairment and never eliminated completely [57,71,72]. ASE noise increases with the numbers of amplifiers in the transmission system. In order to generate less noise, distributed Raman amplification with high order bidirectional pumping can be used, which offers much lower noise figure than EDFA. Also, it is helpful to deploy the low loss fibre when the desired transmission distance is fixed, which means the attenuation of the fibre is reduced. In addition to ASE noise, chromatic dispersion (CD) and polarisation mode dispersion (PMD) can be harmful to the system performance, but these two impairments can be fully compensated using digital signal processing [73], and won't affect the upper limit of a transmission system [57].

In terms of the transmission performance, nonlinear impairments are of high interest, because such nonlinearities can cause strong effects on the signal which might lead to significant performance degradation. In other words, if the nonlinear impairments can be effectively compensated, the transmission performance improvement would be also significant.

For transmission system, there are two types of nonlinearities: intra-channel and inter-channel. Due to the Kerr effect, the phase of the signal can be modulated by the signal itself [1]. This is called self-phase modulation (SPM) which mainly occurs in single channel transmission system. The SPM could lead to unwanted frequency chirp of optical pulses due to the nonlinear phase shift varied with time [2,57]. Consequently, the frequency chirp results in the increase of the signal bandwidth and pulse broadening. In a dense WDM transmission system, the nonlinear phase shift phenomenon could be not only caused by the power of the signal, but also by the power of adjacent channels [2], which is cross-phase modulation (XPM). XPM might cause the signal distortion, depending on the walk-off between the signal and adjacent channels. For WDM systems which the channels are widely separated, the XPM-induced effect can be neglected due to two pulses in different channels overlap for very short time. However for the systems with very close channel spacing, the XPM-induced effect would generate if the pulses in adjacent channels overlap long enough [2]. In addition, four-wave-mixing (FWM) could also occur if at least two or three signals at different frequencies are propagated together. Three optical signals with frequencies ω_1, ω_2, and ω_3, the photon energy can be transferred to the fourth one which its frequency equals to $\omega_4=\omega_1\pm\omega_2\pm\omega_3$. In FWM process, the actual frequency of the fourth signal depends on the phase matching condition [2]. The crosstalk between signals and FWM products, and the depletion on the signal would lead to the degradation of the system performance [2,57].

There are several methods to combat such nonlinear impairments. Two typical examples are digital back propagation (DBP) which compensates the nonlinearity digitally and optical phase conjugation (OPC) which compensate it optically [74,75]. For DBP, using the back-propagation algorithm in the digital domain, it solves the inverse NLSE in order to calculate what has been transmitted and recover from the received signal [75]. However, this requires very significant computational load [76], which is highly impractical in real transmission system. For OPC system, there are two types of OPC system. One is transmitter based OPC system, which the phase conjugation occurs at the transmitter. The other is mid-link OPC system, which the OPC is located in the middle of the link. If the equation (3.15) is complex conjugated, the chromatic dispersion term β_2 and nonlinear coefficient γ would be both inverted, meaning that both chromatic dispersion and nonlinearity before the OPC can be cancelled by these after the OPC [69]. There has been a lot of research interest looking at this mid-link OPC, because the OPC

can combat both intra-channel and inter-channel nonlinear impairments [76]. Details of OPC and its application in long-haul transmission will be demonstrated in Section 5.3, together with the use of Raman fibre laser based amplification.

3.5 Bit error rate and Q factor

Generally, bit error rate (BER) is defined as the number of bit errors divided by the total number of transmitted bits over a certain time interval. In digital transmission systems, the received current value I fluctuates with bit stream. The decision circuit compares the current value I with a threshold value I_D [2]. If the bit is 1 and $I>I_D$, or the bit is 0 and $I<I_D$, there is no error. However, if bit 1 comes with $I<I_D$, or bit 0 comes with $I>I_D$, an error occurs. BER is defined in equation (3.16).

$$BER = p(1)P(0/1) + p(0)P(1/0) \tag{3.16}$$

Here, $p(1)$ and $p(0)$ stands for the probabilities that the receiver receives bits 1 and 0, respectively. $P(0/1)$ is the probabilities that decides 0 when 1 is actually received, and $P(1/0)$ is the probability that decides 1 when 0 is received. As $p(1)$ and $p(0)$ has the same probability to occur, it means both $p(1)$ and $p(0)$ equals to 0.5. Therefore, the BER can be written as equation (3.17).

$$BER = 0.5[P(0/1) + P(1/0)] \tag{3.17}$$

$P(0/1)$ and $P(1/0)$ are given by equation (3.18) and (3.19), and the complimentary error is defined as equation (3.20).

$$P(0/1) = \frac{1}{2} erfc(\frac{I_1 - I_D}{\sigma_1 \sqrt{2}}) \tag{3.18}$$

$$P(1/0) = \frac{1}{2} erfc(\frac{I_D - I_0}{\sigma_0 \sqrt{2}}) \tag{3.19}$$

$$erfc(x) = \frac{2}{\sqrt{\pi}} \int_x^{\infty} \exp(-y^2) dy \tag{3.20}$$

In these equations, I_D stands for the threshold value. σ_1 and σ_0 stands for the variance for bit 1 and 0, respectively. BER is minimised when the I_D is optimised, and the optimised I_D is given in the equation (3.21) [2].

$$I_D = \frac{\sigma_0 I_1 + \sigma_1 I_0}{\sigma_0 + \sigma_1} \tag{3.21}$$

Q parameter is introduced and the definition is shown in equation (3.22).

$$Q = \frac{I_1 - I_D}{\sigma_1} = \frac{I_D - I_0}{\sigma_0} \tag{3.22}$$

Therefore, BER can be expressed as equation (3.23) to demonstrate the relationship between Q parameter and BER.

$$BER = \frac{1}{2} erfc\left(\frac{Q}{\sqrt{2}}\right) \tag{3.23}$$

Here, it can be known that larger Q parameter means lower BER value, so Q parameter can be used as a metric to evaluate the transmission performance. In the following chapters, Q factor is defined as equation (3.24) [57], which is essentially 20 times multiplied by $\log_{10}$(Q parameter).

$$Q = 20\log_{10}[\sqrt{2} \times erfcinv(2 \times BER)] \tag{3.24}$$

3.5 Summary

In this chapter, the overview of long-haul coherent transmission subsystems is presented. In section 3.1, different modulations schemes and the Mach-Zehnder modulator's functionality is explained, including the mechanisms of ASK, BPSK, and QPSK, the principle of MZM, and so forth. In section 3.2, the recirculating loop configuration and implementation is illustrated. The recirculating loop provides a cost-effective way to simulate what occurs in a real in-line transmission system. In section 3.3, the basic principle of coherent detection is explained. In section 3.4, the transmission impairments including linear impairments, nonlinear impairments, and their compensation techniques, are briefly discussed. Coherent transmission system is the methodology to verify the transmission performance of Raman fibre laser (RFL) based amplification techniques which will be experimentally presented in Chapter 5.

4. Raman Fibre Laser Based Amplification

In Chapter 1, several optical amplification techniques are reviewed from the theory perspective, including EDFA, conventional distributed Raman amplification, Raman fibre laser (RFL) based amplification, and so forth. In this chapter, the focus is on the experimental investigations of second order RFL based amplification schemes which are the highlight of the thesis. Generally speaking, second order RFL based amplification is a distributed Raman amplification technique which requires a depolarised second order pump (typically around 1366 nm if the amplified signal is at C band) and passive FBGs to generate first order Raman fibre laser. The second order pump together with induced Raman fibre laser is used to amplify the signal [78]. However, due to different generation mechanisms of Raman fibre laser, in general, there are two Raman fibre laser regimes [42]. One is the Fabry-Perot (F-P) fibre laser which the whole fibre between two reflectors forms the Fabry-Perot laser cavity. The Fabry-Perot fibre laser can be either achieved by two high reflectivity FBGs or single high reflectivity FBG plus a very weak Fresnel reflection. The other one is random distributed feedback (DFB) fibre laser. This random DFB fibre laser can be generated due to the resonant mode reaching the lasing threshold in a distributed cavity formed by a distributed feedback (Rayleigh scattering) and a high reflectivity FBG [56,79]. In this case, the cavity length is not fixed, because Rayleigh scattering is distributed over the fibre [80]. Note that there are several generation mechanisms of random DFB fibre lasers, but here only the half-opened mechanism is discussed due to the highest pump power efficiency [79]. In this chapter, both RFL based amplification techniques are characterised from different perspectives, including signal/noise power distributions, relative intensity noise (RIN), electrical/optical spectra, and so forth. These characterisations results help give us a better understanding of RFL based amplification and support the long-haul/unrepeatered coherent transmission performances which will be demonstrated in Chapter 5 and 6.

4.1 Fabry-Perot fibre laser based amplification with two FBGs

4.1.1 Experimental setup

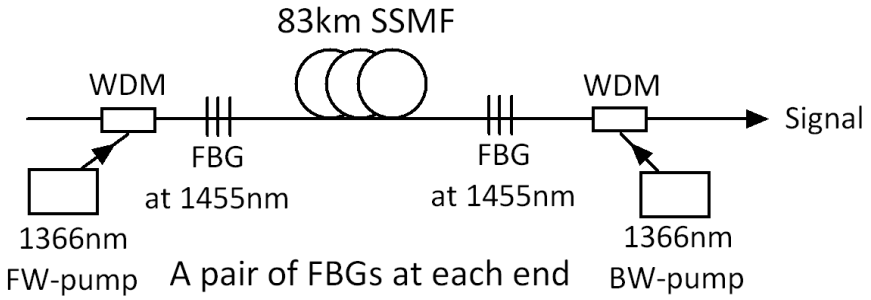

Figure 4.1. Schematic diagram of F-P fibre laser based amplification with two FBGs

In the Fabry-Perot laser based amplification scheme, a matched pair of high reflectivity (>~95%) FBGs centred at 1455 nm with a 3 dB bandwidth of ~0.5 nm were used with one located at each end of an 83 km standard SMF span [7]. Highly depolarised second order continuous wave (CW) pumps at 1366 nm from both directions created an ultra-long Fabry-Perot cavity (83 km cavity length) fibre laser at the wavelength specified by the FBGs [42], when the pump powers were large enough to overcome the lasing threshold [47]. The resultant fibre lasing at 1455 nm and the pump at 1366 nm provided the amplification for the signals in the C band [78]. Figure 4.1 shows the schematic of Fabry-Perot fibre laser based amplification with two FBGs.

FW-pump power (dBm)	BW-pump power (dBm)	FW-pump power ratio
0.0	31.2	0.0%
25.5	29.7	27.6%
26.0	29.6	30.4%
26.5	29.4	33.9%
27.0	29.2	37.6%
27.5	29.0	41.4%
28.0	28.6	46.4%

Table 4.1. Second order FW-pump power, BW-pump power, and FW-pump power ratio

As seen from table 4.1, the FW-pump and BW-pump powers were adjustable subject to the requirement of the transmission link. FW-pump power ratio represents the ratio between the FW-pump power and total pump power. Note that the pump powers listed in Table 4.1 were

used to compensate the ~16.5 dB loss from the SMF span. In consequence, the adjustment of FW-pump and BW-pump powers would lead to the change of signal/noise power distribution along the transmission fibre.

4.1.2 Signal/noise power distribution along the fibre

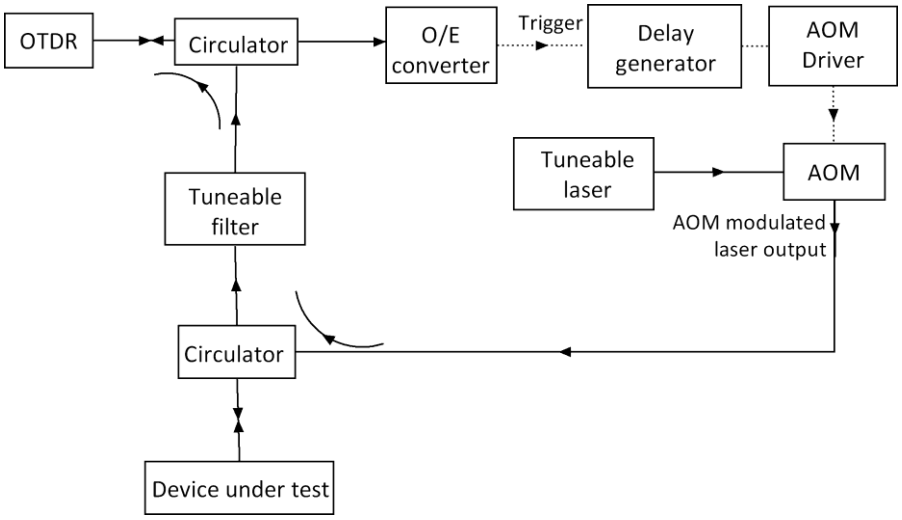

Figure 4.2. Schematic diagram of modified OTDR setup [30]

Signal power distributions along the fibre with different FW- and BW-propagated pump powers were measured at 1545.32 nm with a modified optical time-domain reflectometer (OTDR) setup as illustrated in Figure 4.2 [30]. The OTDR was used to monitor the signal power distributions traces. Meanwhile, there was a built-in pulsed Fabry-Perot semiconductor laser at 1550 nm in the OTDR. The pulsed laser was converted by an O/E convertor and the electrical pulse was used to modulate an external tuneable laser via an AOM. In this way, a pulsed laser with tuneable wavelength was created. Then, the pulsed laser was fed into the Raman amplified span under test and reflected into the OTDR via two circulators, and the signal power distributions could be obtained from the OTDR.

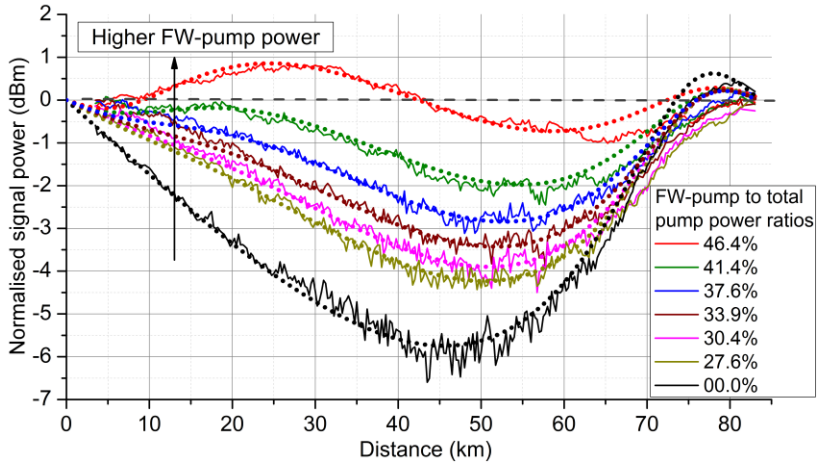

Figure 4.3. Experimental data (solid line) and simulations (dotted line) of signal power distributions with different pump powers [42].

Figure 4.3 shows both the experimental (solid) and simulated (dotted) signal power distributions [7,42]. The signal power distributions were the mutual effect of second order pump power profiles at 1366 nm and first order Raman fibre laser power profiles at 1455 nm [7,55] . . For each pump power combination, signal power variation (SPV) was calculated as the difference between the maximum and minimum power value along the span. This SPV was used as a metric to compare different pumping schemes. The lowest SPV of only ~1.6 dB over 83 km SMF was achieved with symmetric bidirectional pumping (FW-pump power ratio 46.4%). With BW-pumping only (no FW-pumping), the SPV increased up to ~5.6 dB. This shows that the use of second order FW-pumping gave a significant reduction in SPV and increases the signal power, which in principle reduces the amplifier noise figure [33].

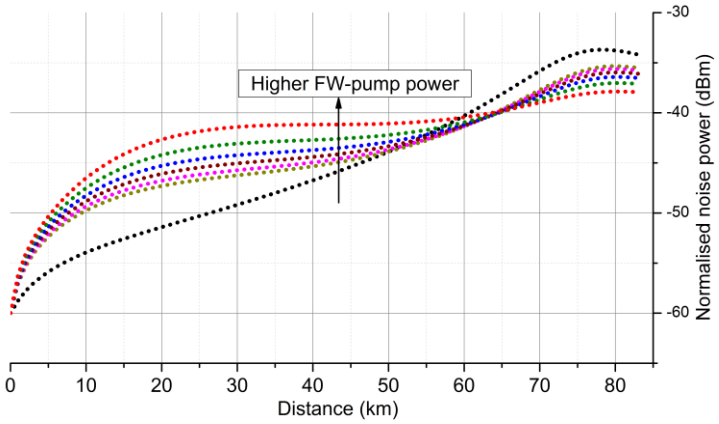

Figure 4.4. Simulated noise power distributions with different pump powers [42].

Figure 4.4 demonstrates the simulated noise power distributions of Fabry-Perot fibre laser based

amplification with different pump powers [7,42]. The noise at the output end was reduced by ~4 dB using symmetric bidirectional pumping, compared with BW-pumping only. In terms of the best noise performance only, the FW-pump power ratios need to be as high as possible. However, considering this Raman amplified span in long-haul transmission system, the optimum launch power value is due to the trade-off between the noise and nonlinear impairment (without considering the RIN-induced penalty) [81], indicating that the minimised SPV and uniformly distributed signal power profiles would help achieve the optimum transmission performance using high order symmetric bidirectional pumping instead of FW-pumping only.

4.1.3 Relative intensity noise

Relative intensity noise is a very important parameter in Raman amplification, because it is the change in pump source normalised by the total light intensity [15,40]. The lifetime of gain generation from the pump is very short (a few femtoseconds) in Raman amplification [40], indicating that the noise from the pump source would be transferred to the signal through the amplification process. In particular, in FW-pumped scenario, the signal and the pump source are propagated over fibre at the same directions, and the noise from the pump will be superimposed on the signal noise [15,40,82]. However, in BW-pumped scenario, the signal and the pump source are propagated at opposite directions. The time of mutual influence between the signal and the pump is very short and the noise from the BW-pump is averaged before reaching the signal [27,83], meaning that the pump noise is difficult to get transferred to the signal. In particular, it is clear that the FW-pumping can reduce the noise, but also increase of RIN on the signal [42]. It means that, in this Fabry-Perot fibre laser amplification, the use of FW-pump would introduce a benefit due to the noise reduction and a penalty due to the RIN increase simultaneously. The consequence brought by these two contrary effects will be demonstrated in detail in Chapter 5. Overall, the RIN from the pump being transferred to the signal is very important and might be harmful in long-haul coherent transmission.

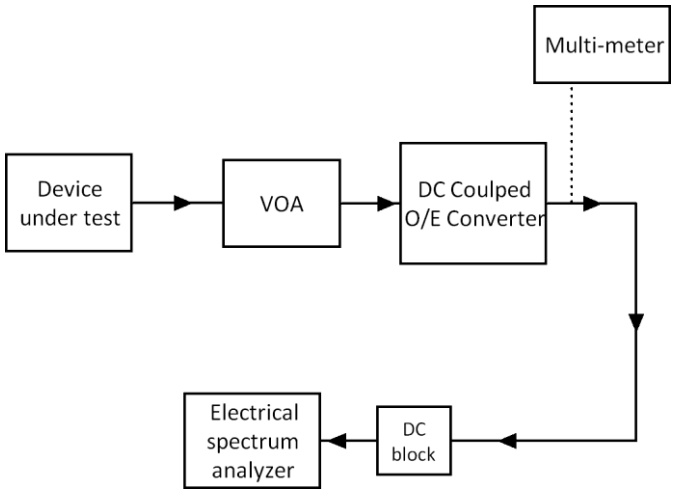

Figure 4.5. Schematic diagrams of RIN measurement setup

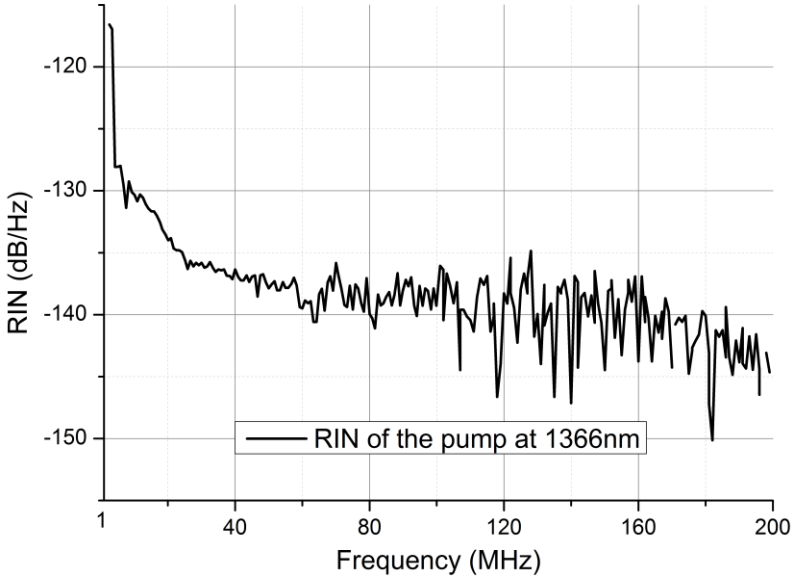

Figure 4.6. Measured RIN of second order pump at 1366 nm

The schematic design of the RIN measurement is shown in Figure 4.5, as illustrated in [84,85]. The setup for the RIN measurement was based on an ultra-low-noise receiver and an electrical spectrum analyser (ESA) ranging from 1 MHz up to 200 MHz. Figure 4.6 shows the measured RIN of the second order pump at 1366 nm. Note that the RIN levels (~-120 dB/Hz) of our pumps are likely to be the lowest on the market for fibre laser based pumps [45].

As shown in Figure 4.7, the RIN of the output signal at 1545.32 nm was measured after one span from a CW low RIN (~-145 dB/Hz) tuneable laser source, and the FW-propagated Fabry-Perot fibre laser through a 5% splitter was measured.

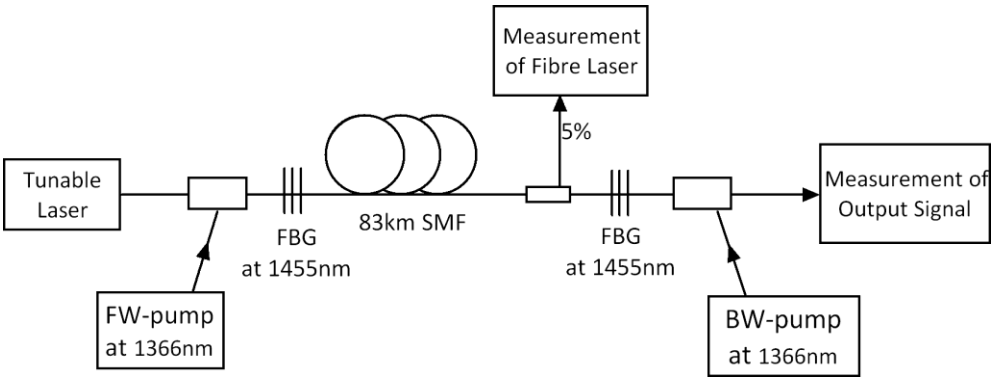

Figure 4.7. Schematic diagrams of RIN measurement on the signal and induced fibre laser

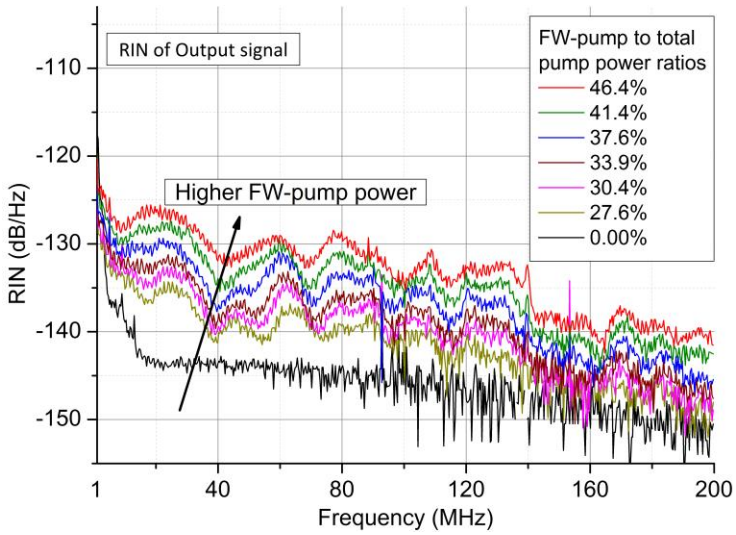

Figure 4.8. Measured RIN of the signal at the output end

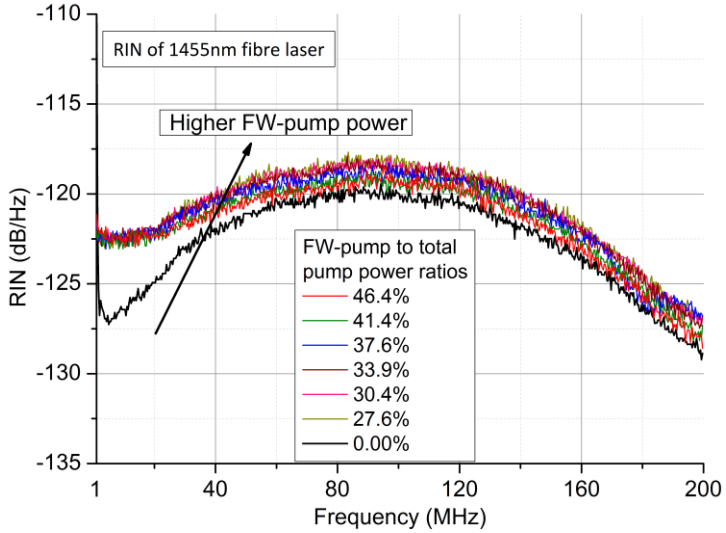

Figure 4.9. Measured RIN of the FW-propagated induced fibre laser

Figure 4.8 shows that there was an increase of up to ~18 dB in output signal RIN as the FW-pump power ratio was increased from 0% to 46.4% FW-pumping ratio. The RIN increase was already very significant (up to 9 dB) from 0% to only 27.6% FW-pumping ratio. Once the ratio was above 27.6% FW-pumping, the RIN was increased gradually (1 dB per step) as

FW-pumping ratio was increased step by step. Figure 4.9 shows the RIN for the induced fibre laser at 1455 nm. The RIN was very similar for all the configurations and reached the maximum value of -118 dB/Hz at ~100 MHz. However in the BW-pumping only scenario, the fibre laser RIN was slightly lower at -120 dB/Hz at around 100 MHz, but there was up to 9 dB reduction in the low frequency range below 40 MHz. Overall, it can be obviously seen that there were some significant differences in RIN between the BW-pumping scheme and all the other schemes using FW-pumping.

4.1.4 Electrical/optical spectra of induced Raman fibre laser

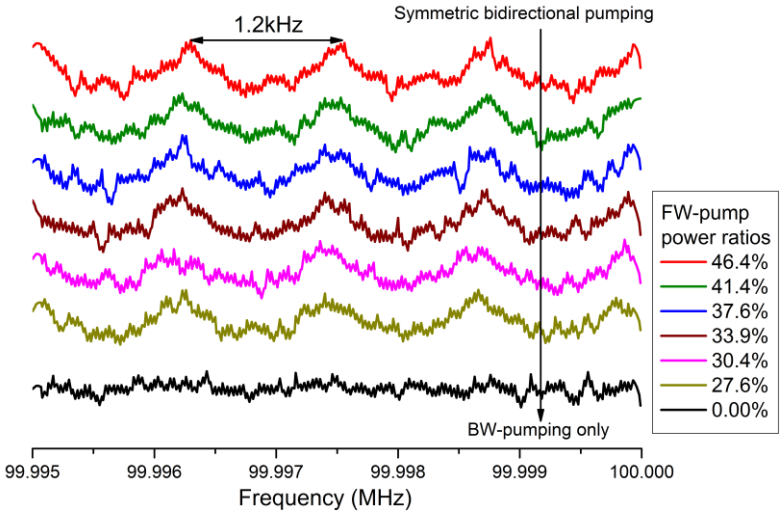

Figure 4.10. Measured electrical spectra of the FW-propagated induced fibre laser

Figure 4.10 shows the measured intra-cavity electrical spectra of the FW-propagated fibre laser at 1455 nm for different FW-pump powers. Note that the traces in Figure 4.10 are deliberately offset to aid the comparison, meaning that the relative amplitude is not important. Similar to Figure 4.8, there was also a clear difference in the intra-cavity electrical spectra between BW-pumping only and bidirectional pumping schemes. The electrical spectra in Figure 4.10 indicate that there were two regimes of fibre lasing. For all the bidirectional pumping schemes there was a laser mode spacing of ~1.2 kHz corresponding to an 83 km Fabry-Perot cavity, meaning that the transmission span was effectively an ultra-long Raman Fabry-Perot cavity fibre laser. In this configuration with two FBGs, this mode spacing was independent of FW-pump power, because it only corresponded to the length of the cavity (i.e. the transmission fibre span)

and the refractive index which determined the mode spacing [86], as demonstrated in equation (4.1). $\triangle\nu$ stands for the mode spacing, c is the light of speed, n means the refractive index of the fibre, and L is the length of the cavity.

$$\Delta\nu = \frac{c}{2nL} \tag{4.1}$$

However, no mode spacing was observed in BW-pumping only scheme, therefore we concluded that a 'modeless' random distributed feedback (DFB) fibre laser with a half-opened cavity was created [87], indicating that the laser was generated within a cavity formed by the FBG on one side and distributed Rayleigh backscattering from the fibre itself on the other side (acting like a distributed 'mirror') [79]. In this case, there was no fixed cavity length (30-40 km depending on the pump power) for random DFB fibre laser because of the distributed random Rayleigh backscattering from the fibre [80]. Overall, these results show that even with closed cavity with two FBGs, a random DFB fibre laser can be still achieved, as opposed to the usual Fabry-Perot fibre laser with bidirectional pumping.

This could also contribute to the RIN performances of the output signal discussed in previous section. Among the schemes using the FW-pump, the pump RIN was transferred from both the first order Fabry-Perot cavity fibre laser and the second order FW-pump to the signal, which causes various penalties [43,51]. The signal RIN increased with increasing the FW-pump power. For BW-pumping only scheme, it was mainly because the absence of the second order FW-pump decreased the RIN transfer. In addition to this, the RIN of the induced Raman fibre laser was also lower in the low frequency range because it was a short cavity length (<40 km) random DFB laser rather than Fabry-Perot laser (83 km) [7,79]. The RIN of the fibre laser would get transferred to the output signal more severely for Fabry-Perot laser based amplification with longer cavity [88].

Note that there could be exceptions that the span between two FBGs is too long (i.e. ＞270 km) [86], the induced fibre laser with symmetrical bidirectional pumping is still random DFB fibre laser instead of Fabry-Perot fibre laser. The reason is that the pump power is not able to reach the FBG on the other side due to the high attenuation of such long fibre, but the Rayleigh backscattering from the fibre would reflect the pump back resulting in the generation of a random DFB fibre laser. With two FBGs, two independent random DFB fibre lasers are located

near the input and output sections of the fibre, forming a bi-directionally pumped random DFB laser based amplification [24,89]. This amplification technique can be deployed for unrepeatered coherent transmission which will be demonstrated in Chapter 6.

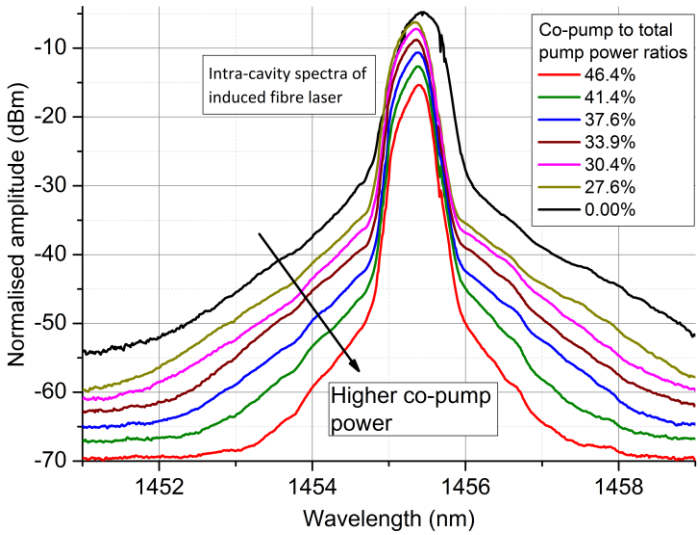

Figure 4.11. Measured optical spectra of the FW-propagated induced fibre laser

Figure 4.11 shows the measured optical spectra of the ultra-long Fabry-Perot fibre laser at 1455 nm with different pumping schemes. The 3 dB bandwidth of the fibre laser was reduced with higher FW-pump power, from 0.5 nm with BW-pump only to 0.3 nm with the highest FW-pump power ratio. Consequently, the linewidth of the fibre laser was decreased leading to higher stimulated Brillouin scattering (SBS) which might contribute to the transmission performance degradation [40].

4.1.5 Raman gain profile

The Raman on-off gain profile was measured as a difference between the output signal and the input signal using an OSA (optical spectrum analyser) with an ASE noise as an input optical signal. Figure 4.12 shows that the Raman gain profiles with two FBGs centred at 1455 nm were the same for all the pump power combinations, which just compensated the loss from the fibre at 1545 nm (0 dB net gain). It can be noticed that the peak-to-peak gain variation was up to +/-0.65 dB over 30 nm bandwidth. However, as illustrated in [9], the gain profiles and variation would change if the overall on-off gain was changed. For example, if the Raman on-off gain is set to be 25 dB (9 dB net gain) which requires more FW- and BW-pump power, the gain variation

would be larger as shown in [5]. The more pump power, the more gain variation, and vice versa.

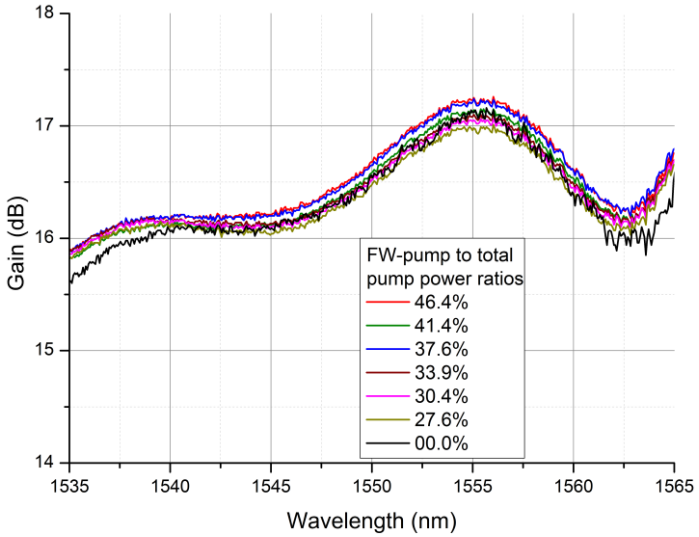

Figure 4.12. Measured Raman profiles for different pump power combinations

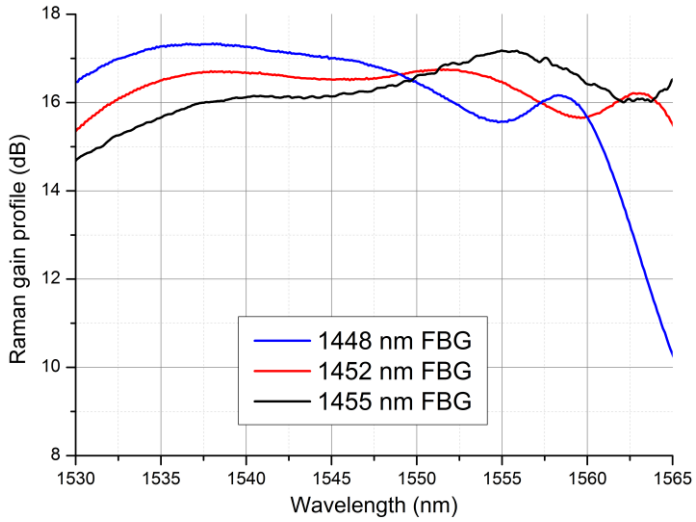

Figure 4.13. Measured Raman profiles for Fabry-Perot fibre laser based amplification technique with FBGs at different wavelengths

The Raman gain profiles and variations can be easily modified by adjusting the centre wavelength of the FBG, as shown in Figure 4.13. As the FBG was centred at 1452 nm, the peak-to-peak gain variation between 1535 nm and 1555 nm was very small (within +/-0.25 dB variation). So this amplification scheme was easily adjustable in terms of on-off gain requirement. Alternatively, if very strict gain flatness or wide gain bandwidth was required, it was still very simple to achieve the target, such as adding another pair of FBG at short or long wavelengths, injecting a small amount of first order pump power, and so forth [90,91].

4.2 Fabry-Perot fibre laser based amplification with one FBG

In the last section, it has been demonstrated the characterisation of Fabry-Perot fibre laser based amplification with two FBGs. It has been found that once bidirectional pumping was used, a first order Fabry-Perot fibre laser was generated. Here, the Fabry-Perot fibre laser based amplification with one FBG will be discussed in detail.

4.2.1 Experimental setup

The experimental setup of F-P fibre laser based amplification with one FBG was illustrated in Figure 4.14. The only difference from two FBGs configuration was that the FBG near the input end was removed, and a flat cleaved connector was used instead, because the input WDM was 1×3 WDM that allowed a ~3.4% (measured) Fresnel reflection in the 1420-1480 nm range. Alternatively, the configuration might be achieved using an FBG reflector with ~3.4% reflectivity.

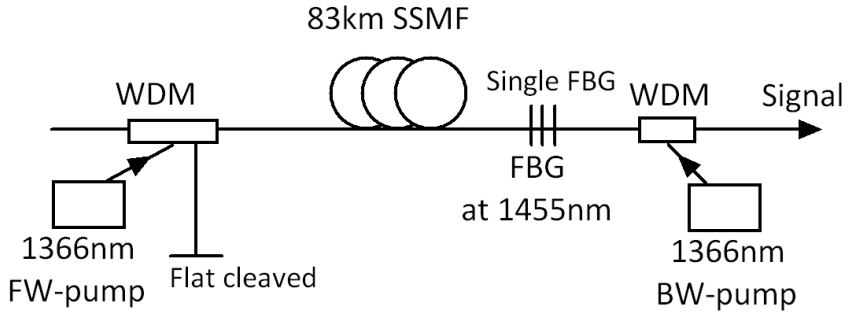

Figure 4.14. Schematic diagram of F-P fibre laser based amplification with one FBG

FW-pump (dBm)	BW-pump (dBm)	FW-pump power ratio
0	31	0%
27.5	30.3	35.0%
28.7	29.9	43.6%
29.7	29.4	51.7%
30.3	28.9	58.1%

Table 4.2. Second order FW-pump power, BW-pump power, and FW-pump power ratio

The pump powers combinations were listed in Table 4.2. Similar to Table 4.1, the pump powers used here also compensated the loss from the 83 km SSMF.

4.2.2 Signal/noise power distribution along the fibre

As demonstrated in Figure 4.15(a), signal power distributions along the fibre with different pump powers were measured at 1545.32 nm with a modified OTDR setup [30]. Experimental (solid) and simulated (dotted) data are both presented [5,7,42].. As expected, to some extent, the more FW-pump power, the smaller the signal power variation [92]. With 58.1% or 51.7% FW-pump power ratios, the SPV was minimised to only ~3 dB. The simulated noise power distributions in Figure 4.15(b) show that, using more FW-pump power decreased the noise at the output end, resulting in higher optical signal to noise ratio [92]. Still, it was not the case that the FW-pump power could be as high as possible, because the optimum signal launch power should be limited by the trade-off between ASE noise and nonlinear impairment, and high signal power would cause high nonlinearity [81].

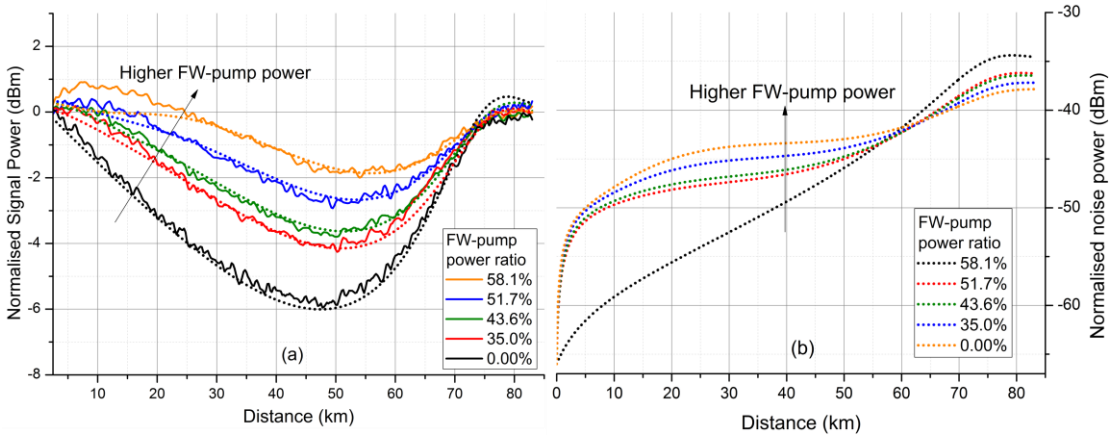

Figure 4.15(a). Experimental data (solid line) and simulations (dotted line) of signal power distributions with different FW-pump power. (b). Simulated noise distributions (dotted line) with different FW-pump powers [48].

4.2.3 Relative intensity noise

The output signal from Fabry-Perot fibre laser based amplification with one FBG was measured with RIN measurement setup demonstrated in Figure 4.7. From Figure 4.16, the signal RIN was increased very little from 0% to 43.6% FW-pump power ratio, but the signal power variation was decreased from ~5.8 dB to only ~3.8 dB. This means that the signal RIN didn't increase while the SPV was improved by increasing the FW-pump power. More importantly, using this signal RIN mitigation method might have the potential of avoiding the RIN-induced penalty on the

long-haul coherent transmissions [42,43], as well as improving the transmission performance due to the better signal to noise ratio. However, if the FW-pump power was further increased, the signal RIN started to increase, up to ~10 dB higher when the highest FW-pump power (58.1% FW-pump power ratio) was applied.

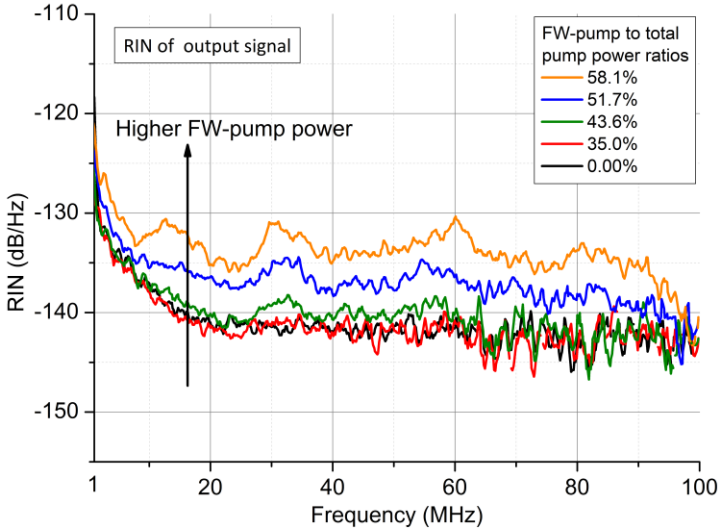

Figure 4.16. Measured RIN of the signal at the output end

4.2.4 Electrical spectra of induced Raman fibre laser

Figure 4.17 shows the measured mode structure of the FW-propagated fibre laser. For the scheme with BW-pumping only, it was also a "modeless" random DFB fibre laser. However, for all the other pumping schemes with FW-pumping, we can see clearly that there was ~1.2 kHz mode spacing, indicating that an 83 km Fabry-Perot cavity was formed to generate an ultra-long Raman fibre laser even when the reflectivity near the input end was low (~3.4%). The ~1.2 kHz mode spacing was independent of the FW-pump power after the threshold was reached, which was only related to the length and the refractive index of the fibre [86]. Overall, with a FBG near the output and very low reflectivity mirror near the input, a Fabry-Perot Raman fibre laser was generated when using bidirectional pumping.

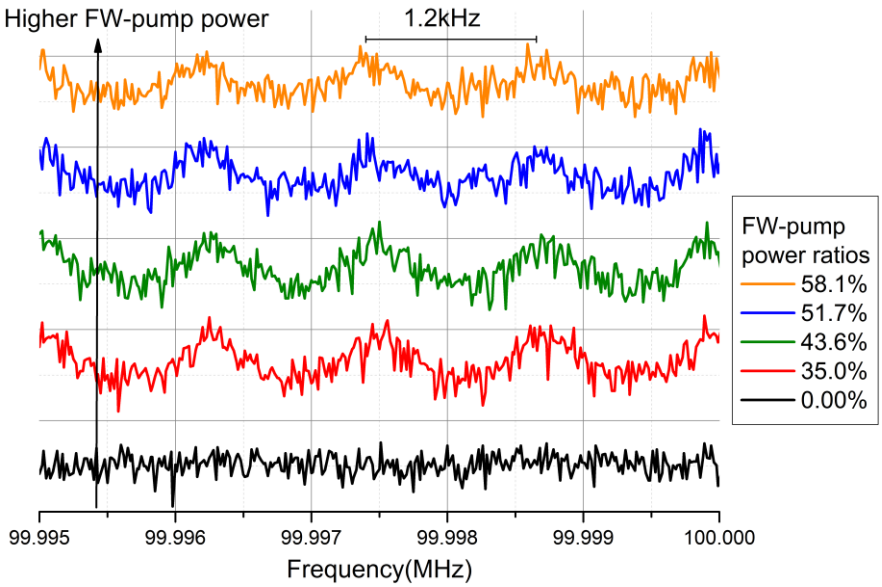

Figure 4.17. Measured electrical spectra of the FW-propagated fibre laser

4.3 Random DFB fibre laser based amplification with one FBG

4.3.1 Experimental setup

The mechanism using single FBG to form an Fabry-Perot fibre laser based amplification was discussed in the previous section. However, the reflectivity near the input section was further reduced to close to zero (measured result of 0.04%), achieved by replacing with an angled connector instead. The schematic diagram of such an amplifier is illustrated in Figure 4.18.

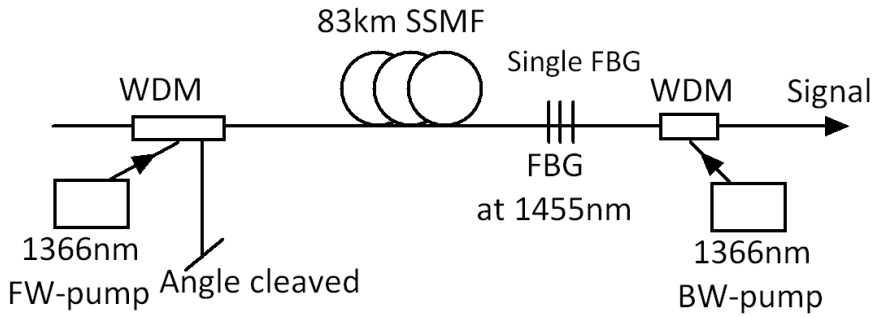

Figure 4.18. Schematic diagram of random DFB fibre laser based amplification with one FBG

FW-pump (dBm)	BW-pump (dBm)	FW-pump power ratio
0	31	0%
27.5	30.6	33.1%
28.7	30.5	39.7%
29.7	30.4	45.6%
30.3	30.4	49.7%

Table 4.3. Second order FW-pump power, BW-pump power, and FW-pump power ratio

The FW-pump and BW-pump powers are demonstrated in Table 4.3. Note that the pump powers were only to compensate the loss of 83 km SSMF.

4.3.2 Signal/noise power distribution along the fibre

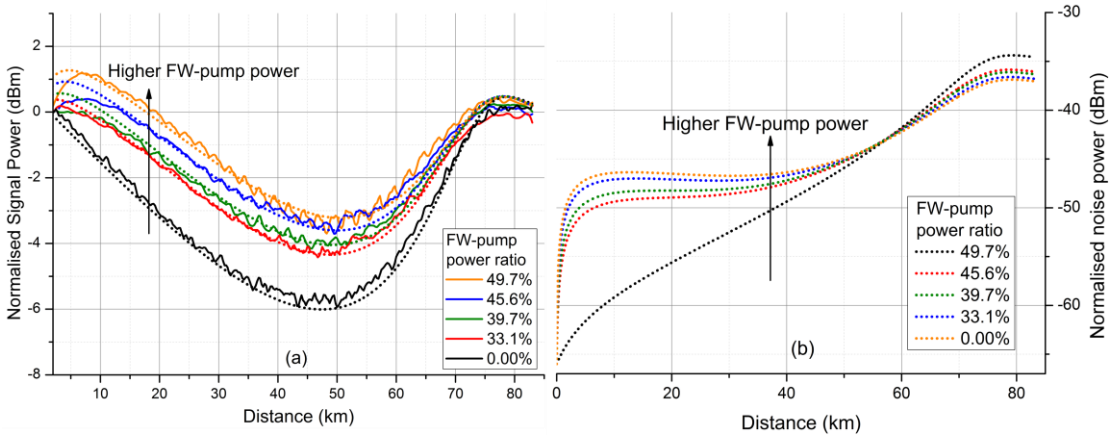

Figure 4.19(a). Experimental data (solid line) and simulations (dotted line) of signal power distributions with different FW-pump power. (b). Simulated noise distributions (dotted line) with different FW-pump powers [48].

The signal and noise distributions along the fibre were shown both experimentally (solid line) and theoretically (dotted line) in Figure 4.19 [7,42].. The highest SPV was around ~6 dB with no FW-pumping, and the lowest SPV was below 4 dB with 45.6% or 39.7% FW-pumping ratios. Using more FW-pump power, the gain near the input end was pushed into the beginning of the fibre only within 10 km. However, for the scheme with the FW-pump power ratio of 45.6%, there was a sharp signal power increase near the input section of the fibre. That could potentially affect the transmission performance, because the optimum signal power in order to achieve the

best balance between noise and nonlinearity would be lower resulting in OSNR degradation, and the nonlinear impairment corresponded to the signal power [2,48,81]. In addition, this random DFB fibre laser based amplification would be also very beneficial for long-haul transmission system with mid-link OPC, as the symmetry of the span is crucial for the transmission performance improvement [92,93]. As illustrated in [92], more than 97% symmetry level can be achieved using this amplification technique over 62 km SMF.

4.3.3 Relative intensity noise

The RIN of the signal at the output end was demonstrated in Figure 4.20. It is obviously seen that the signal RIN remained the same over the whole range, no matter how much the FW-pump power was fed into the amplifier, indicating that the RIN increase was completely mitigated. This RIN mitigation was very important for long-haul coherent transmission, as the transmission performance would be only limited by the trade-off between the noise and nonlinearity without suffering from RIN-induced penalty [48,81].

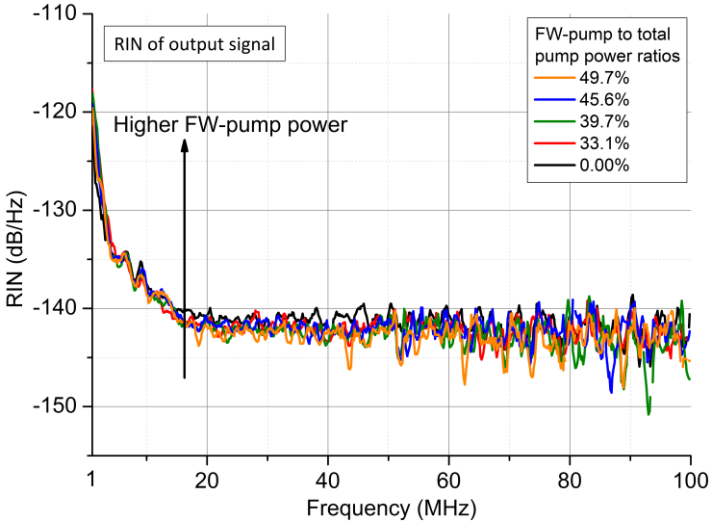

Figure 4.20. Measured RIN of the signal at the output end

4.3.4 Electrical spectra of induced Raman fibre laser

Figure 4.21 shows the measured mode structure of induced fibre laser with different pump powers. It can be seen that there was no mode using BW-pumping only or bidirectional pumping, which confirms that it was random DFB fibre laser [56,79,87]. It means that the laser was generated due to the resonant mode reaching the lasing threshold in a distributed cavity formed

by Rayleigh scattering from the fibre and an FBG, as explained in section 4.1.4.

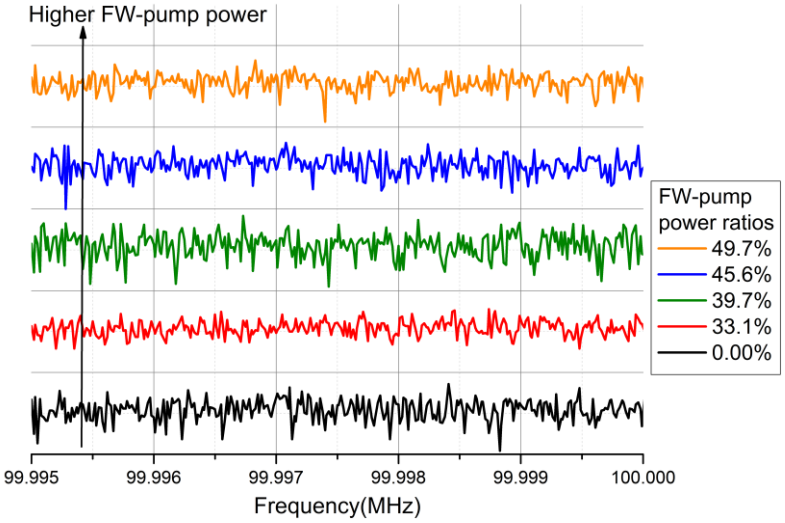

Figure 4.21. Measured electrical spectra of the FW-propagated fibre laser

4.4 Comparisons of Fabry-Perot fibre laser based amplification and random DFB fibre laser based amplification

It has been shown that Raman fibre laser (RFL) based amplification with second order pump and fibre Bragg grating (FBG) is a simple and flexible Raman amplification technique. In section 4.1, with two FBGs on both sides two different Raman fibre lasing regimes contributed to the amplification, when forward and backward pump powers were changed slightly. These were random DFB lasing and Fabry-Perot lasing. An interesting feature of using backward pumping only is that a random Rayleigh backscattering distributed feedback (DFB) fibre laser can be generated even in a closed cavity, as opposed to the usual Fabry-Perot lasing obtained when using bidirectional pumping [42]. In section 4.2, a novel Fabry-Perot fibre laser based amplification configuration was studied, in which single FBG was located near the output end of the amplifier but a low level of back reflection near the input end was allowed. Furthermore, in section 4.3, when the reflector near the input end was completely removed, random DFB fibre laser was formed for both BW-pumping only and bidirectional pumping scenarios. Here, three Raman fibre laser based amplification schemes are compared from several aspects including signal power distributions, the RIN of the output signal, and the mode structures of induced fibre laser.

4.4.1 Experimental setup

Schematic diagrams for three Raman schemes have been demonstrated in each section. Here, the Fabry-Perot fibre laser with two FBGs is named as R1, Fabry-Perot fibre laser with one FBG as R2, and random DFB fibre laser as R3. For schemes R1 and R2, the fibre laser was random DFB laser using BW-pumping only and Fabry-Perot fibre laser when using bidirectional pumping. For scheme R3, the fibre laser would be random DFB fibre laser for both BW-pumping only and bidirectional pumping. A potential benefit of random DFB lasing is that the cavity length of a random laser is much shorter (30-40 km) compared to a Fabry-Perot cavity laser. This means the RIN transfer could be reduced due to this shorter cavity [88,94].

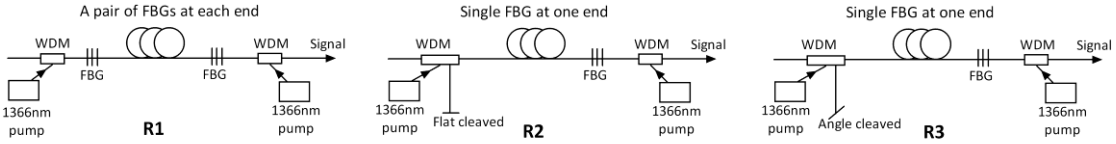

FW-pump (dBm)	BW-pump (dBm)	FW-pump power ratio
0	31.2	0%
26.5	29.4	33.9%
27.0	29.2	37.6%
27.5	29.0	41.4%
28.0	28.6	46.4%

(a)

FW-pump (dBm)	BW-pump (dBm)	FW-pump power ratio
0	31	0%
27.5	30.3	35.0%
28.7	29.9	43.6%
29.7	29.4	51.7%
30.3	28.9	58.1%

(b)

FW-pump (dBm)	BW-pump (dBm)	FW-pump power ratio
0	31	0%
27.5	30.6	33.1%
28.7	30.5	39.7%
29.7	30.4	45.6%
30.3	30.4	49.7%

(c)

Figure 4.22. Schematic diagrams and pump powers of amplification schemes R1, R2, and R3.

The tables in Figure 4.22 show the pump powers used in the experiment. For all the configurations the Raman gain was set to counterbalance the ~16.5 dB attenuation of the fibre. The FW-pump was varied from zero (BW-pumping only) to the point where the minimum power variation along the span was achieved (excluding the last point in R3). Three additional points were measured between the end points. Note that although the same absolute FW-pump powers are compared for the configurations shown in Figures 4.22(b) and (c) they correspond to different FW-pump over total pump power ratios as the BW-pump had to be adjusted differently to keep the gain fixed. For scheme R1, lower FW pump powers was used as a consequence of much higher 1455 nm reflectivity at the input end.

4.4.2 Results and discussions

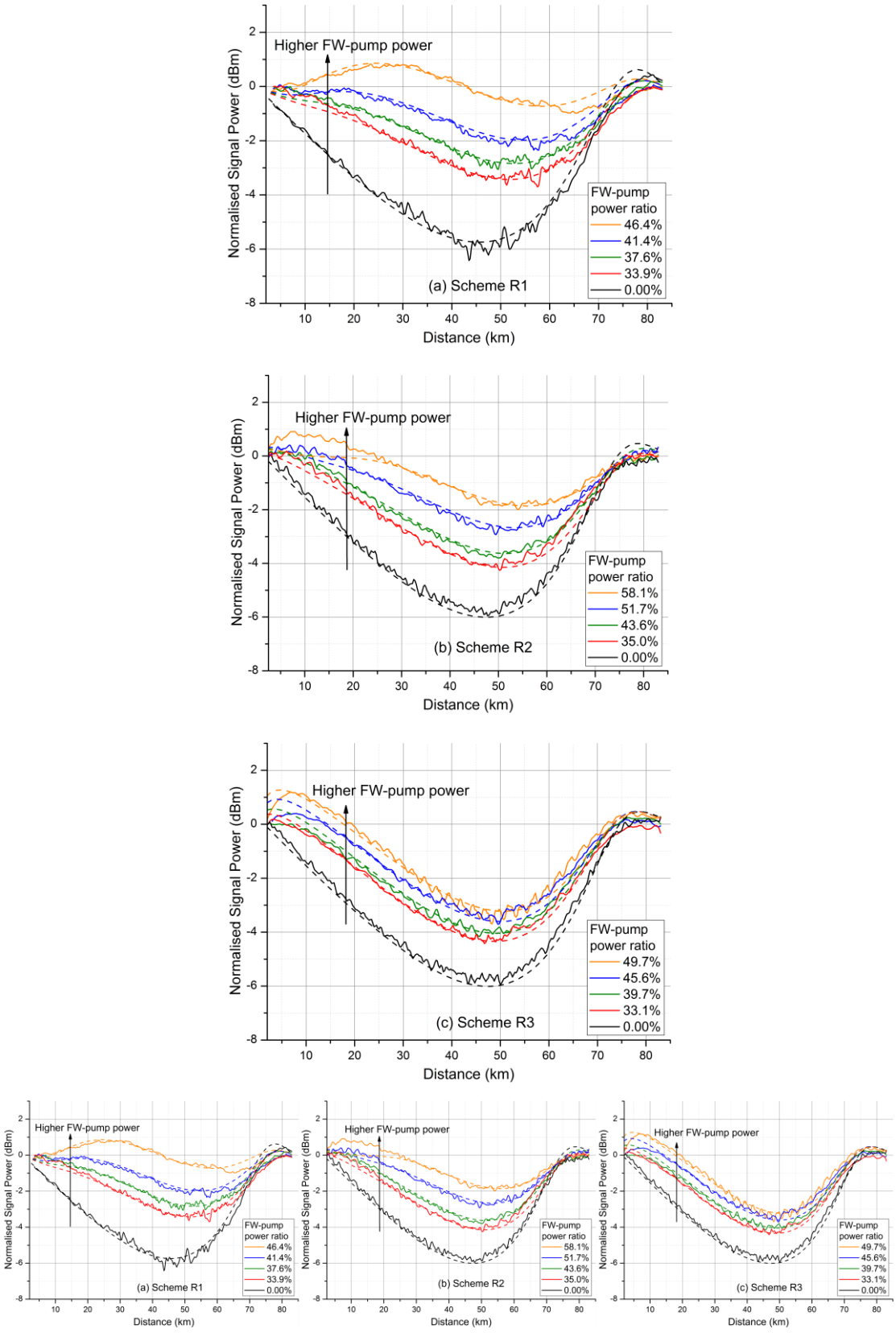

Figure 4.23. Experimental (solid) and simulated (dashed) signal power profiles using the schemes (a). R1, (b) R2, and (c) R3. [48]

Figure 4.23 shows the signal power evolutions along the fibre for different pumping schemes measured at 1545.32 nm using a modified OTDR setup [30]. As we know, the SPV value is important because the minimised SPV would help achieve the best trade-off in transmission performance [2,22,81]. For all the schemes with BW-pumping only, the signal power distributions were almost the same, indicating that there was no difference between each other. For scheme R1 the lowest SPV of ~1.6 dB was achieved with symmetric bidirectional pumping (FW-pump power ratio of 46.4%). For scheme R2 with low back reflection at the input end, the lowest SPV was increased to ~3 dB achieved by either symmetrical pumping or predominantly FW-pumping, Scheme R3 reduced the back reflection level to only 0.04%. The lowest SPV was then increased to ~4 dB with either 45.6% or 39.7% FW-pumping ratios. Scheme R1 with highest input end reflectivity gave the lowest signal variation along the fibre, which indicates the lowest noise figure amplification among three schemes. For schemes R2 and R3, the gain near the input end was pushed into the fibre only within 10-20 km instead of more than 30 km using scheme R1. For scheme R3, there was a sharp increase at the beginning of the fibre. That could harm the transmission performance, and the optimum signal launch power would be lower to avoid the nonlinearity which would result in OSNR degradation, because if the system performance is limited by the fibre nonlinearity and noise, the ideal signal power profile should be totally flat [81,95]. Overall, it can be seen that with lower reflection at the input end, the minimum SPV was increased from only ~1.6 dB to ~4 dB, and the noise performance was worse. In addition, the FW-pump power and consequently total pump power was increased, as lower reflection level near the input was used, which means that the pump power efficiency decreased.

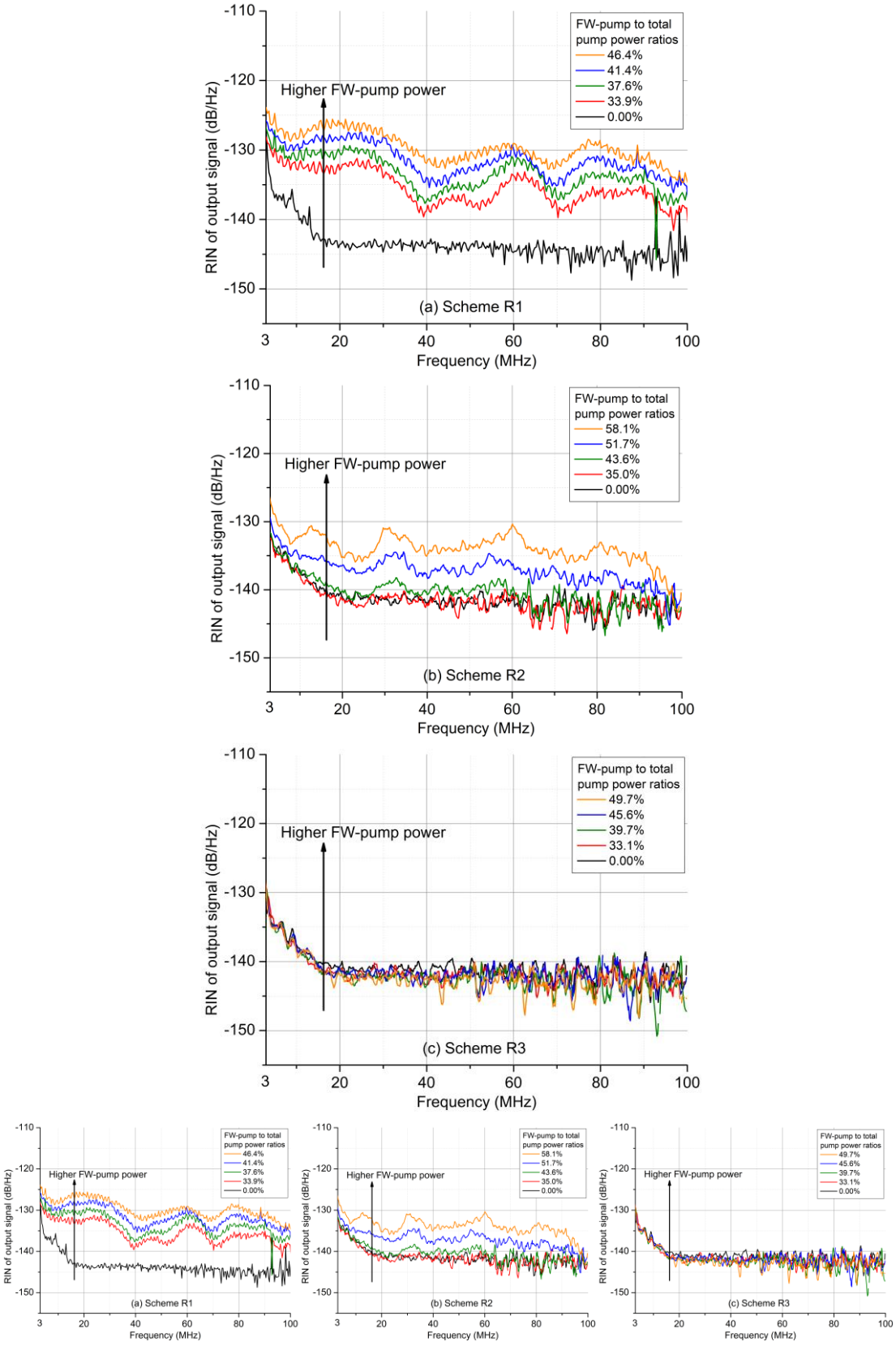

Figure 4.24. RIN of the output signal using pumping schemes (a). R1, (b). R2, and (c). R3.

RIN characteristics of the signal at the span output were experimentally investigated for all the pumping schemes and are shown in Figure 4.24. The results for pumping scheme R1 is shown in

Figure 4.24(a) that the RIN of the signal was increased up to ~18 dB from 0% to 46.4% FW-pumping ratios, compared with BW-pumping only scenario. For scheme R2, the increase in signal RIN was less significant than scheme R1, and the maximum increase was reduced to ~10 dB. If only considering the blue curve in Figure 4.24(b) which also gave the smallest SPV, the RIN increase was only up to ~5 dB. In this sense, the growth of in the signal RIN has obviously been suppressed. In this configuration, using FW-pumping power ratio of below 43.6% might be potentially RIN-induced penalty free, leading to less Q factor penalty in long-haul coherent transmission [42]. Using scheme R3, there was no RIN increase for any FW-pump power ratio. This is particularly important, because now the system is only limited by nonlinearity and ASE noise without suffering any RIN transfer [48].

The reason why the RIN of the signal didn't increase for R2 and R3 was that the minimised reflectivity near the input end led to the reduced efficiency of the Stokes shift (from second order pump to first order laser) in forward-propagated direction [55,96,97]. This resulted in the majority of signal amplification that came from the generation of the backward-propagated weak mode F-P laser (R2)/short-cavity random DFB laser (R3). When second order FW-pump power was relatively low, second order FW-pump amplified the backward-propagated weak F-P mode laser/short-cavity random DFB laser, which was still able to reduce the SPV and improve the noise performance. As second order FW-pump power further increased, for scheme R2, the FW-propagated F-P laser was amplified to provide a small amount of gain for the signal near the input which resulted in the increase of signal RIN as shown in Figure 4.2.4(b), but the RIN increase was lower due to the lower FW-propagated laser power thanks to the reduced efficiency of Stokes shift, compared to the F-P laser with two high reflectivity reflectors [42,55,97]. For scheme R3, with higher second order FW-pump power, the FW-propagated random DFB laser was also amplified. Due to even lower FW-propagated laser power, this would further decrease the RIN transferred to the signal, which mitigated the RIN even using higher second order FW-pump power [97].

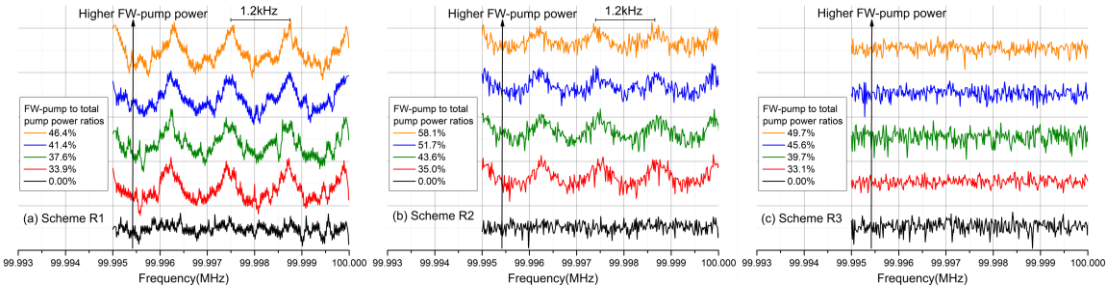

Figure 4.25. Intra-cavity forward-propagated laser mode structures (a) R1, (b). R2, and (c).R3.

The intra-cavity forward-propagated laser mode structures for three Raman amplification schemes are shown in Figure 4.25. Clearly Fabry-Perot fibre laser modes (83 km cavity length) were observed for schemes R1 and R2 with R1 showing stronger mode structure in Figure 4.25(a). It can be also seen in Figure 4.25(c) that a "modeless" random DFB fibre laser was generated for scheme R3.

4.4.3 Summary

Detailed comparisons of different RFL based amplification schemes are presented, including signal/noise power profiles, RIN of the signal at the output end, and intra-cavity laser mode structures. Our results show that reducing the 1455nm reflectivity near the input end can significantly mitigate RIN transfer to the signal in second-order 1366nm pumped amplifiers. This allows the increase of FW-pump power, leading to improved transmission performance.

4.5 Summary and conclusion

In this chapter, signal/noise power profiles, RIN performances, and intra-cavity fibre laser mode structures, and Raman gain profiles, are characterised on three different kinds of RFL based amplifiers when different forward and backward pump powers were applied. The first one was the Fabry-Perot fibre laser based amplification with two FBGs. It was found that although FW-pumping with the FBG near the input end could be used to improve the best noise performance, the signal RIN also increased significantly. This might cause severe RIN-induced penalty on the long-haul transmission performance [42,43], which will be demonstrated in Chapter 5. In addition, it was also found for the first time that there was random DFB fibre laser with BW-pumping only, as opposed to Fabry-Perot fibre laser using bidirectional pumping. As for

Fabry-Perot fibre laser based amplification with one FBG, the characterisation results were slightly different from two FBGs configuration, as the noise performance was worse but the signal RIN increase was much lower, in particular below 43% FW-pump power ratio. The lasing mechanisms were similar to two FBGs based scheme, but the Fabry-Perot mode of induced fibre laser was much weaker. For random DFB fibre laser based amplification, due to the largest signal power variation, the noise performance was the worst. However, there was no signal RIN increase no matter how much the FW-pump power was fed. The RIN mitigation was because of the reduced Stokes shift efficiency of the FW-pump, thanks to the reduced reflectivity near the input end. The lasing mechanism remained as random DFB fibre laser all the time. These findings provide possible solution to the well-known RIN issue of a bi-directionally pumped RFL based amplification technique in a repeatered long-haul coherent transmission system. By further optimising the reflection level at the input section, there might be a "sweet spot" which can achieve the trade-off among RIN-induced penalty, ASE noise, and nonlinearity [48].

5. Long-haul Coherent Transmission Using Raman Fibre Laser Based Amplification

In the previous chapter, different Raman fibre laser (RFL) based amplification techniques are investigated from several aspects, including signal/noise power distributions, relative intensity noise, RFL mode structure, and so forth. It is shown that using FW-pump power makes the signal and noise power distribution more uniform, but can increase the RIN of the signal depending on the configuration of the RFL based amplifier. There are two categories of fibre lasing when different pump powers/configurations are deployed, which were Fabry-Perot fibre lasing and random DFB fibre lasing. In this chapter, the performances of Fabry-Perot fibre laser and random DFB fibre laser based amplifiers are both evaluated in the long-haul coherent transmission systems. Moreover, in order to effectively combat the nonlinear impairment, Raman fibre laser based amplifiers are deployed in the long-haul mid-link optical phase conjugation (both single band and dual band) coherent transmissions system.

5.1 Evaluation of 100G WDM-QPSK long-haul transmission system using Fabry-Perot fibre laser based amplification with two FBGs

In Fabry-Perot fibre laser based amplification with two FBGs, it has been shown in the previous chapter that using second order bidirectional pumping can reduce the intra-span signal power variation (SPV) to an almost negligible ~+/- 0.8 dB for an 80 km transmission span [7]. This is in principle close to the ideal distributed amplification to minimise the noise. However, while using more FW-pump power, the RIN of the signal was also increased. In conventional first order or dual order distributed Raman amplification schemes, the penalty using bidirectional pumping due to relative intensity noise (RIN) transferred from the FW-propagated pump, has been studied in direct detection systems both numerically and experimentally [41,82,83], but only investigated numerically in coherent transmission systems [43].

Here, a detailed evaluation of transmission performance in a long-haul 100G DP-QPSK WDM coherent transmission system is presented, by varying FW-propagated second order pump power within the RFL based amplification scheme (two FBGs). Based on these pumping schemes, we

experimentally measured and quantified the Q factor penalty with FW-pump power ratios and transmission performances of up to 7082 km in a long-haul transmission system. Using symmetric bidirectional pumping, the maximum transmission distance was reduced to 1666 km with a Q factor penalty of 4.15 dB compared to BW-pumping only. These results were also compared with numerical simulation results which excluded RIN, to further quantify the RIN induced penalty. It was found that, although using FW-pumping could distribute the gain more uniformly and minimise the amplification noise, the introduced Q factor penalty was too high regardless of any noise figure reduction. We attributed this Q factor penalty to increased RIN of the output signal which was transferred from increased FW-pump power and induced fibre laser.

5.1.1 Experimental setup

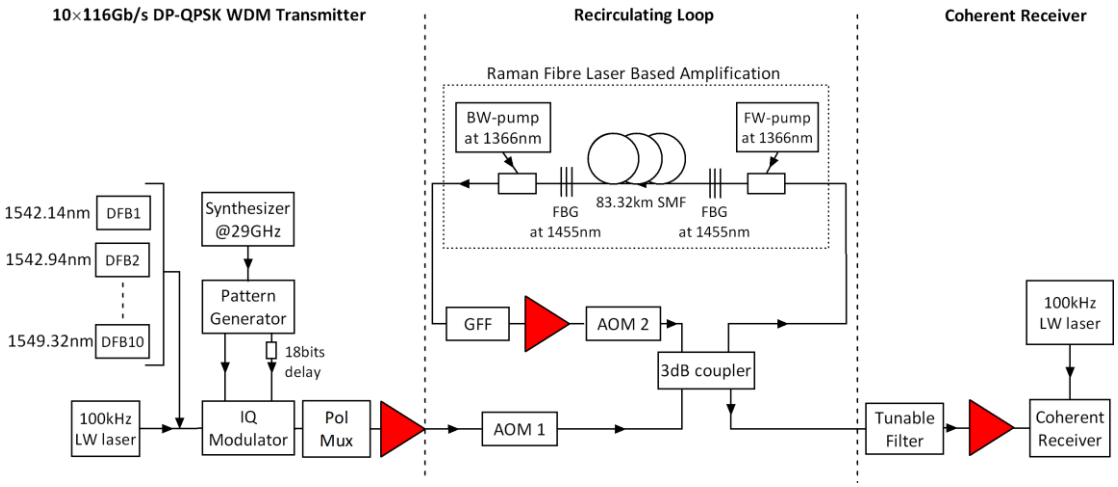

Figure 5.1. Experimental setup of DP-QPSK WDM transmitter, recirculating loop using Raman fibre laser based amplification technique, and coherent receiver.

In the RFL based amplification scheme with two FBGs, as illustrated in section 4.1.1, a matched pair of ~95% reflectivity FBGs with a centre peak at 1455 nm and a 3 dB bandwidth of ~0.5 nm were used with one located at each end of an 83.32 km standard SMF span. Highly depolarised second order pumps at 1366 nm with RIN of approximately -120 dB/Hz were used to create an ultra-long Raman fibre laser at 1455 nm. The resultant fibre lasing at 1455 nm and pump at 1366 nm provided the amplifications for the WDM signals in the C band [78].

To evaluate the influence of increased FW-pump power, a recirculating loop experiment was conducted using the setup shown in Figure 5.1. The transmitter consisted of ten DFB lasers with

100 GHz spacing ranging from 1542.14 nm to 1549.32 nm. A 100 kHz linewidth tuneable laser was used as the "channel under test" while the corresponding DFB laser was switched off during the measurement cycle. The multiplexed signals were QPSK modulated with normal and inverse 2^{31}-1 PRBS patterns at 29 Gb/s with a relative delay of 18 bits between I (in-phase) and Q (quadrature). A polarisation multiplexer with a delay of 290 bits between the two polarisation states gave the resultant 10×116 Gb/s DP-QPSK signals. An EDFA was used before launching into the recirculating loop. The transmission span in the recirculating loop was 83.32 km SMF-28 with a total loss of ~17.6 dB including 16.5 dB from SMF-28 fibre and 1.1 dB from two WDMs. The AOM, 3 dB coupler, gain flattening filter within the loop, and WDMs gave a total loss of ~12 dB, which was compensated by a single stage EDFA at the end of the loop. The ~12 dB loop specific loss could degrade the OSNR of the signal, but this impact could be relatively mitigated by using multiple fibre spans in the loop. The limit of the availability of pumps prevented us from using multiple spans. The receiver was a standard polarisation-diverse coherent detection setup using a 25 GHz bandwidth real time oscilloscope. DSP was used offline with standard algorithms including signal normalisation, low pass filtering, down sampling, dispersion compensation, clock recovery, polarisation recovery (constant modulus algorithm) and phase recovery [29,98]. Q factors were defined as the equation (3.24), and calculated from bit wise error counting over two million bits.

FW-pump power (dBm)	BW-pump power (dBm)	FW-pump power ratio
0.0	31.2	0.0%
25.5	29.7	27.6%
26.0	29.6	30.4%
26.5	29.4	33.9%
27.0	29.2	37.6%
27.5	29.0	41.4%
28.0	28.6	46.4%

(a)

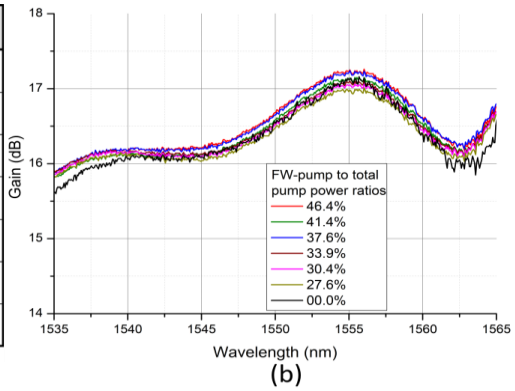

(b)

Figure 5.2(a).Second order FW-pump, BW-pump power, and FW-pump power ratio used in the experiments; (b). Raman gain spectra using different pump power ratios.

The pump powers listed in Figure 5.2(a) were used to compensate for the ~16.5 dB loss from the transmission fibre span. The Raman gain spectra with the input of ASE noise in Figure 5.2(b) show +/- 0.6 dB Raman gain variations across the whole C band with similar spectra for all the

pumping configurations.

5.1.2 Transmission Results and discussions

Experimental (solid lines) and simulated (dotted lines) signal/noise power evolutions along the fibre with different FW-pump and BW-pump powers are demonstrated in Figure 5.3.. Signal power variation (SPV) was defined as the difference between the maximum and minimum power value along the span. The lowest SPV of ~1.6 dB was achieved with symmetric bidirectional pumping. With BW-pumping only, the SPV reached ~5.6 dB. This shows that the use of second order FW-pumping gave a significant reduction in SPV and the increase in signal power, which also reduced the amplifier noise.

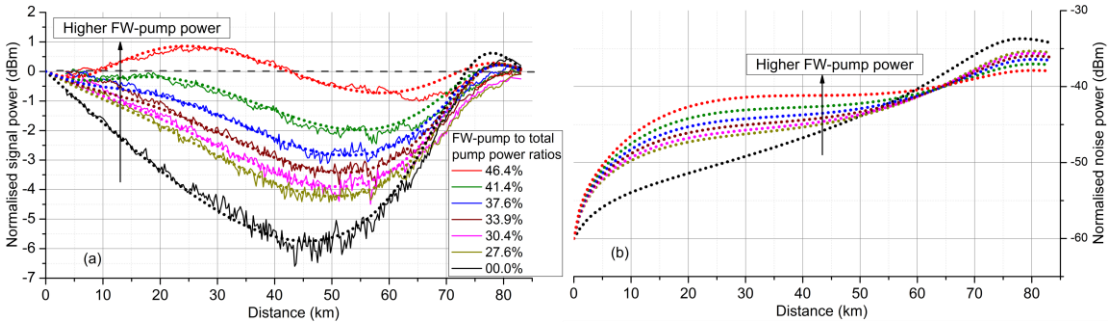

Figure 5.3(a). Experimental data (solid line) and simulations (dotted line) of signal power distributions with different FW-pump power. (b). Simulated noise distributions (dotted line) with different FW-pump powers [42].

If the system performance is limited by the fibre nonlinearity and the ASE noise generated from optical amplifiers, a transmission performance improvement can be expected by using symmetric bidirectional FW-pumping to distribute the gain more uniformly because of the associated reduction in the noise figure. In order to support this argument, a numerical simulation on the performance of WDM DP-QPSK system was conducted while taking into account the power and noise distribution profiles for each pumping scheme. The simulation setup was similar to the experimental one, where 10×29 Gbaud DP-QPSK channels with 100 GHz spacing were transmitted over 20 recirculations. As a large number of channels were simulated, a random sequence of length 2^{16}-1 was used instead of a PRBS of length 2^{31}-1 adopted in the experiment. The generated signal was oversampled four times providing a total simulation bandwidth of ~4 THz. The propagation of the signal in the fibre link was simulated using the well-known

split-step Fourier method, with a step size of ~1 km using the signal power profiles shown in Figure 5.3(a). The Raman noise was modelled as Gaussian noise, which was added to the signal after each step (~1 km), following the simulated noise profiles shown in Figure 5.3(b). In this simulation, the same power and noise profiles were used for all the channels, for simplicity. The additional noise from an EDFA implemented in the experimental recirculation loop setup was ignored in the simulation, as we would like to focus on the impact of pumping schemes on the transmission performance only. At the receiver, after coherent detection, the channel under test was filtered using an 8th order Butterworth low pass filter. The main advantage of Butterworth filter was that it maximised the flatness of the frequency response within the passband. Even order of 8th was chosen as it guaranteed the stability. The DSP adopted in the simulation was similar to the one used in the experiment.

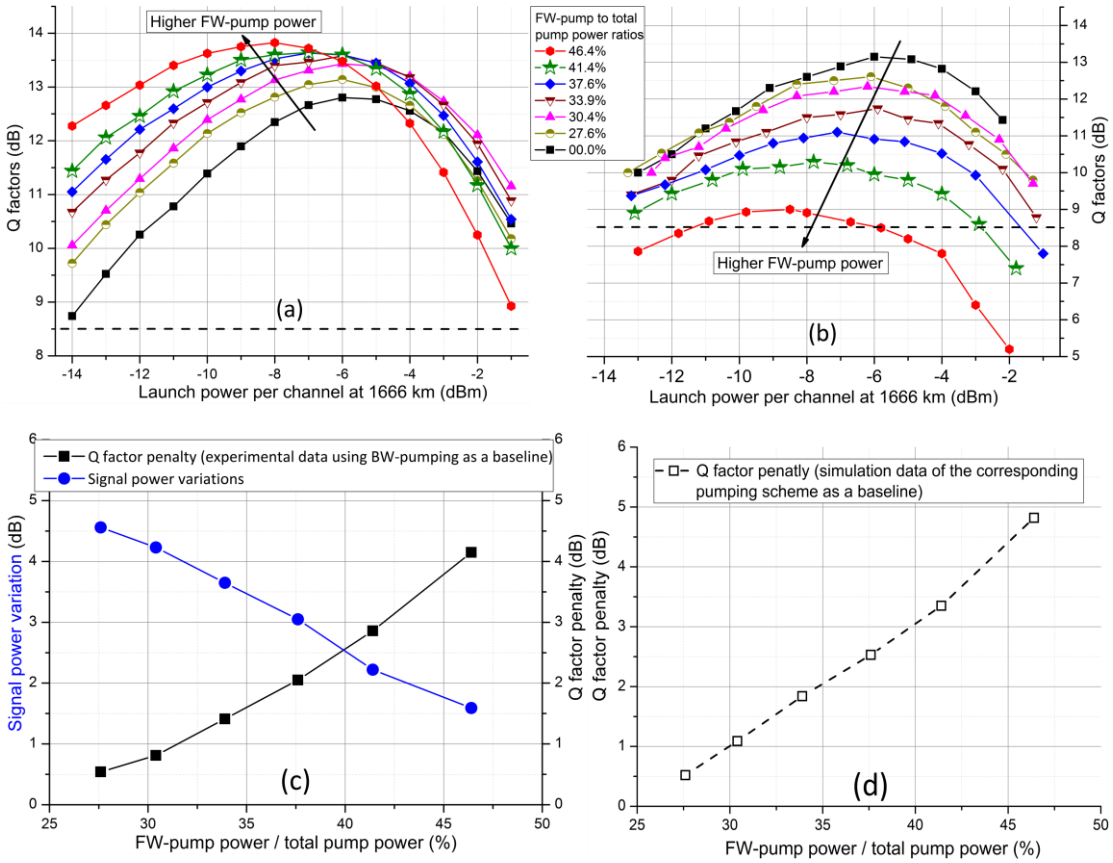

Figure 5.4(a). Simulated Q factors versus launch power per channel at 1666 km using 1545.32 nm channel assuming that the system performance is limited by ASE noise and fibre nonlinearity only. (b). Measured Q factors versus launch power per channel at 1666 km using 1545.32 nm channel. (c). Signal power variations and Q factor penalties (based on experimental results using BW-pump only) versus FW-pump power ratios. (d). Q factor penalties (based on the simulation data of each corresponding scheme) versus FW-pump power ratios [42].

The simulation result is presented in Figure 5.4(a) where the Q factor is plotted versus launch power for each pumping scheme using the 1545.32 nm channel. Note that no RIN-induced impact was considered in this case. As expected, the Q factor was improved with increasing FW-pump power, because the best transmission performance could be found due to more uniform gain distribution. The Q factor was improved from 12.8 dB using BW-pumping only to 13.9 dB using symmetric bidirectional pumping. However, in the experimental results shown in Figure 5.4(b), the measured Q factor was decreased from 13.1 dB to 9 dB as the FW-pumping power was increased. This result clearly demonstrated that using higher FW-pumping power introduced an overall Q factor penalty, despite the reduction in amplifier noise figure due to the use of FW-pump. On the other hand, there was also a reduction in the optimum launch power in both cases as the FW-pump power was increased. This is due to the more uniform power level – for the same launch power there is more nonlinear penalty as FW-pump power is increased hence optimum launch power is decreased. It also indicates that the nonlinear threshold changed as the integral of SPV traces due to the increase of effective nonlinear length. Here, it should be noted that using higher FW-pump power degraded the system performance even with relatively low launch power per channel (i.e. -13 dBm), when the impact of fibre nonlinearity was negligible, which means that the increase of nonlinearity was not responsible for the performance degradation, as the FW-pump power was increased. The associated Q factor penalties and the SPV versus FW-pump power ratios are shown in Figure 5.4(c). As the FW-pump power was increased, the SPV became smaller. However, the Q factor penalty (solid black line) assuming the optimum Q factor with BW-pumping only at 1666 km as a baseline became very significant after 1666 km, from 0.54 dB with 27.6% FW-pump power ratio, to 4.15 dB with 46.4% FW-pump power ratio. Alternatively, the Q factor penalty (dotted black line) assuming the simulated optimum Q factor for each corresponding pumping scheme is shown in Figure 5.4(d). It shows that the Q factor penalty was even larger, as the simulations excluded the RIN-induced impact and only considered the noise reduction due to higher FW-pump power.

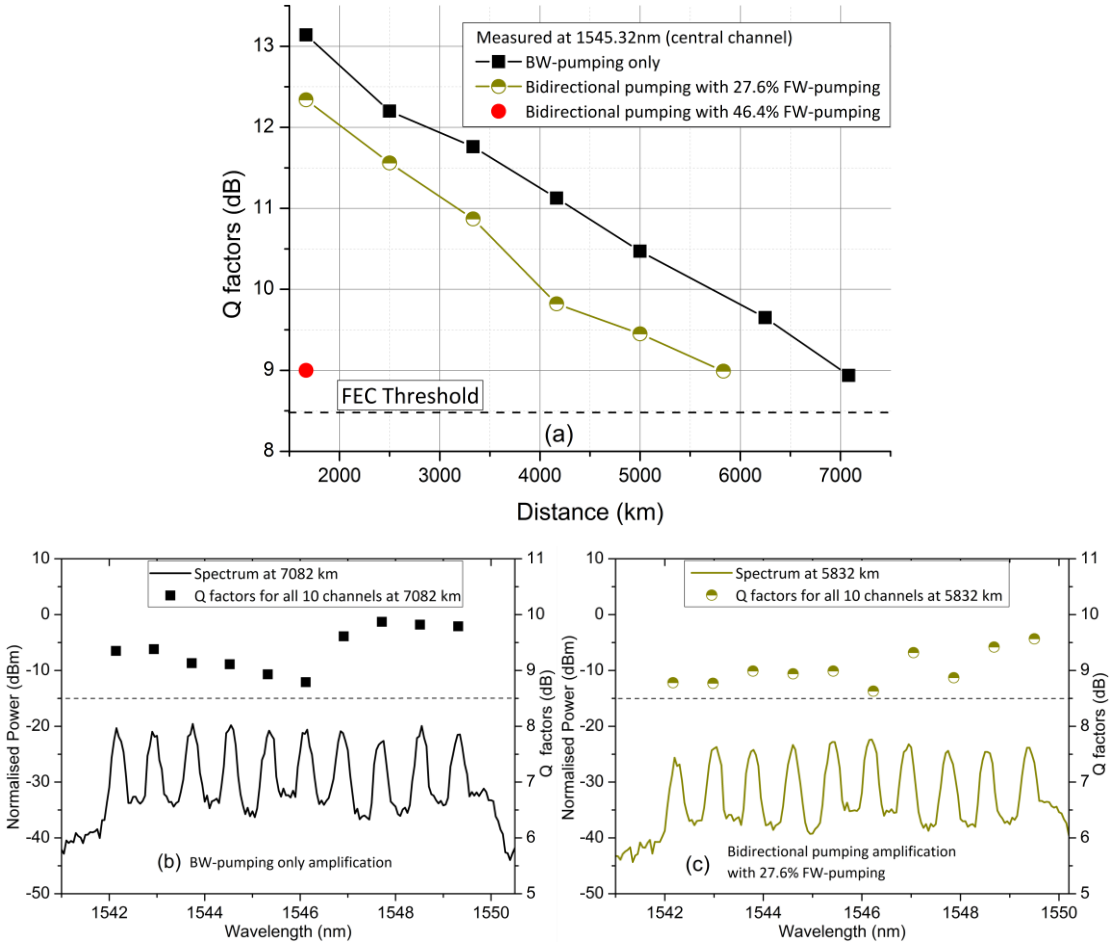

Figure 5.5(a). Q factors of the central channel at 1545.32 nm versus transmission distances using different pump powers. (b). Q factors for all ten channels and received spectra measured at 7082 km with BW-pump only. (c). Q factors for all ten channels and received spectra measured at 5832 km with 27.6% FW-pump power ratio.

Figure 5.5(a) shows Q factors versus transmission distances of the 1545.32 nm channel using 0%, 27.6%, and 46.4% FW-pump power ratios. Figures 5.5(b) and (c) show the spectra and Q factors for all ten channels at maximum transmission distances. The results show that the maximum transmission distance of 7082 km, assuming 8.5 dB Q factor threshold (equivalent to 3.8×10^{-3} in BER, 7% overhead hard decision forward error correction) was achieved with a BW-pumping only configuration [119]. This was reduced to 5832 km with FW-pump power ratio of 27.6%. As for 46.4% FW-pump power ratio, the reach was decreased significantly to only 1666 km.

5.1.3 RIN and mode structures of Raman fibre laser

In order to understand the performance degradation, the characterisations of Raman fibre laser and the output signal for different pump powers were performed in Chapter 4. The RIN of the

output signal after one span was measured at 1545.32 nm from a low RIN (~-140 dB/Hz) tuneable laser source which was used in the transmission experiments.

The reason why we focused on the low frequency range is because high frequency components of RIN from the pump are averaged along the fibre and there is little effect in FW-pumping scheme because of the "walk off" between propagating velocities of signal and pump [40]. The results in Figure 5.6(a) show that there was an increase of up to ~18 dB in output signal RIN as the FW-pump power ratio was increased from 0% to 46.4%. Figure 5.6(b) shows the measured intra-cavity mode structure of the fibre laser at 1455 nm for various FW-pump powers, respectively. There was a clear difference in the intra-cavity electrical spectra for the bidirectional and the BW-pumping only schemes. The spectra shown in Figure 5.6(b) indicate that there were two regimes of fibre lasing, that was a Fabry-Perot fibre laser with bidirectional pumping and a random distributed feedback laser with BW-pumping.

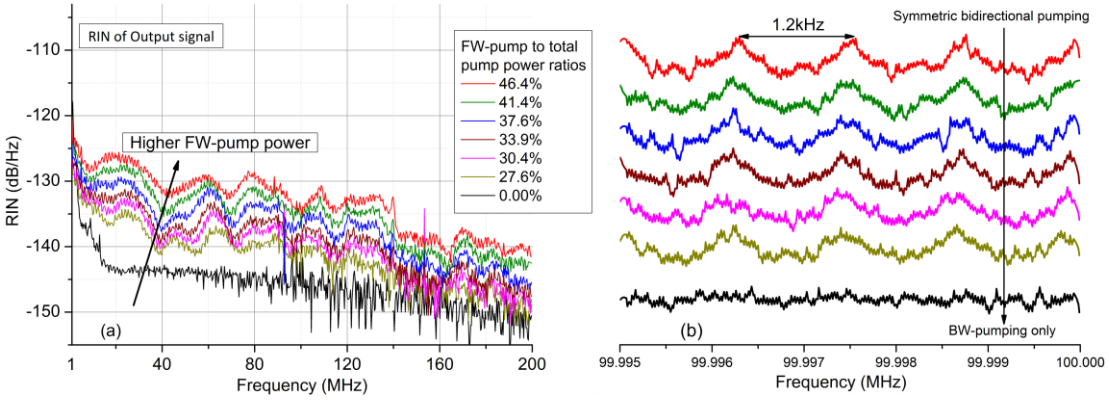

Figure 5.6(a). Measured RIN of the Raman fibre laser and the output signal after 83 km span. (b). Measured mode spacing of the Raman fibre laser.

The transmission degradation can be explained as follows. Among the schemes including the use of the FW-pump, the RIN was transferred to the signal from both the first order Fabry-Perot fibre laser and the second order FW-pump, which causes various penalties like relative phase noise and polarisation crosstalk [15,43,51]. The RIN-induced penalties increased with increasing FW-pump power. Additionally, an ultra-long Fabry-Perot fibre laser based scheme further increased the RIN being transferred to the signal [88,94]. For BW-pumping only scheme, the absence of FW-pump decreased the RIN transferred to the signal significantly. In addition, the induced Raman fibre laser was actually a modeless random DFB fibre laser with much shorter cavity length (30-40 km) than Fabry-Perot cavity laser (83 km) [7,79]. The RIN of the fibre laser

would also get transferred to the output signal more severely for Fabry-Perot fibre laser based amplification with the longer cavity [88].

5.1.4 Summary

Based on long-haul 100G DP-QPSK WDM transmission using F-P laser based amplification scheme, an experimental evaluation of the impact on the transmission performance is performed with different FW-propagated second order pump power, from BW-pumping only to symmetric bidirectional pumping. Using the experimental and simulations results, the relationship between signal power variation and Q factor are analysed considering the situation with and without the RIN-induced penalty from the FW-pump. While using second order FW-pump indeed minimises variation in signal power and hence the amplifier noise figure, the introduced Q factor penalty associated with RIN is too high for any overall performance improvement. The Q factor penalty can be 4.15 dB after 1666 km using symmetric bidirectional pumping, in comparison with BW-pumping only. We attribute the Q factor penalty to increased RIN of the output signal which was transferred from first order Raman fibre laser and increased second order FW-pump power. Two types of lasing regimes are observed, a random DFB fibre lasing for BW-pumping only and conventional Fabry-Perot cavity fibre lasing for bidirectional pumping schemes. For bidirectional pumping schemes, the transmission performances are degraded significantly, because more RIN from the fibre laser and the FW-pump are transferred to the signal due to higher FW-pump power. The RIN of signal with BW-pumping only is significantly lower all over the measurement frequency range, because the RIN transfer to the output signal is lower due to the absence of second order FW-pump as well as the amplification via a short length random fibre laser.

5.2 Transmission performance enhancement using random DFB fibre laser based amplification with bidirectional pumping

To minimise the generation of noise the distributed Raman amplification would exactly counteract the fibre attenuation along the length of the transmission path, maintaining the signal power level at a near constant value [7]. In addition to minimising the noise, recent work has shown that a constant and/or symmetric power level is advantageous for some techniques used

to compensate nonlinear transmission effects [29,69,93,99,100].

As demonstrated in section 5.1, an ultra-long Raman fibre laser based amplification technique with second-order Raman pump and FBG based Fabry-Perot cavity, can achieve very low variation in signal power along the transmission path. Unfortunately, in transmission experiment the use of forward pumping was problematic, as the penalty associated with RIN being transferred to the signal was much greater than the performance improvement from low SPV and noise [42,43]. Using only backward pumping improved the performance but at the expense of an increase in SPV and noise.

Here new Raman amplification schemes based on random distributed feedback fibre laser are reported and compared with conventional Raman amplification schemes. For 10 x 116G DP-QPSK WDM transmission, we demonstrate a bidirectional, second order Raman pumped random DFB fibre laser based amplification scheme, which simultaneously achieves low SPV and improves the transmission performance. More importantly, this scheme enables bidirectional second order pumping without increasing the RIN of the signal. An extended reach of 7915 km is achieved using the proposed random laser based scheme with an SPV of 4 dB, compared to 4999 km and 9 dB using backward first-order Raman pumping, and 7082 km using other amplification schemes. On the other hand, due to the mitigation of RIN, the scheme can be modified to satisfy the link requirement for different nonlinearity compensation techniques [29,69,93,99,100]]. A random DFB fibre laser with backward pumping configuration is illustrated which uses only one pump but has performance comparable to conventional, dual order backward pumping scheme.

5.2.1 Experimental setup and characterisations of different Raman amplification schemes

To evaluate the transmission performance, a recirculating loop experiment was conducted using the setup shown in Figure 5.7. The 10×116 Gb/s DP-QPSK WDM transmitter was exactly the same as illustrated in section 5.1.1. The transmission span in the recirculating loop was 83.32 km standard SMF-28 fibre. The total loss was ~17.6 dB, including ~16.5 dB from the fibre and ~1.1 dB from 1366/1455/1550 filter WDMs. The 1455 path of the WDM wasn't used and the end

was angle-cleaved in order to prevent back reflections. To equalise channel powers, a GFF was used after the Raman link. The ~12 dB loss from the GFF, 50/50 coupler, acousto-optic modulator (AOM), and Raman components was compensated using a single stage EDFA at the end of the loop. The output signal was de-multiplexed by a tuneable filter and amplified by an EDFA before the receiver. The receiver was the same as the one in section 5.1.1. DSP was used offline with standard algorithms for signal recovery and linear impairments compensation. Q factors were calculated from bit-wise error counting, and averaged over two million bits.

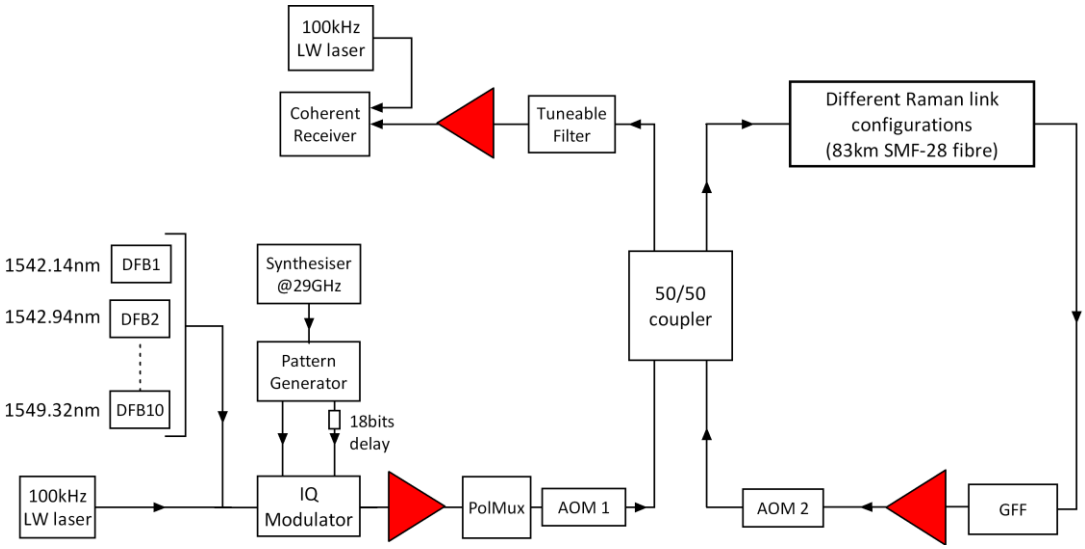

Figure 5.7. Experimental set-up of transmitter, recirculating loop, and coherent receiver.

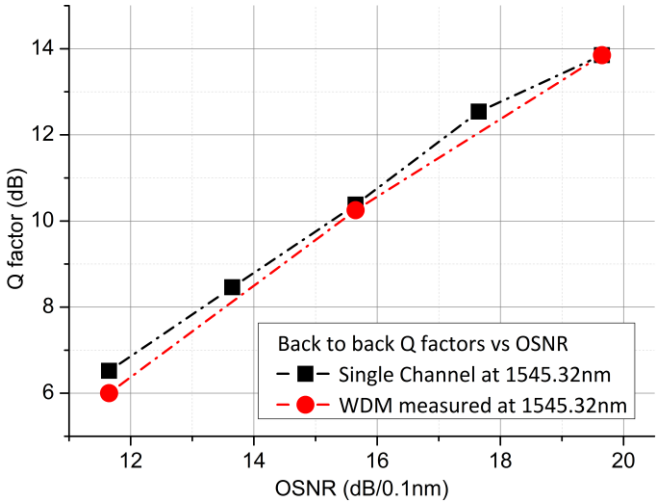

Figure 5.8. Back to back Q factors versus OSNR of the central channel at 1545.32 nm

The noise loaded back-to-back transmitter performances (both single channel and WDM) are shown in Figure 5.8. The Q factor is plotted as a function of OSNR (0.1 nm noise bandwidth, both polarisations) for the central channel at 1545.32 nm. Using hard decision- forward error correction (HD-FEC) threshold corresponding to 3.8×10^{-3} in bit error rate, the FEC threshold is

Q of 8.5 dB. The required OSNR at the FEC threshold is about ~13.7 dB.

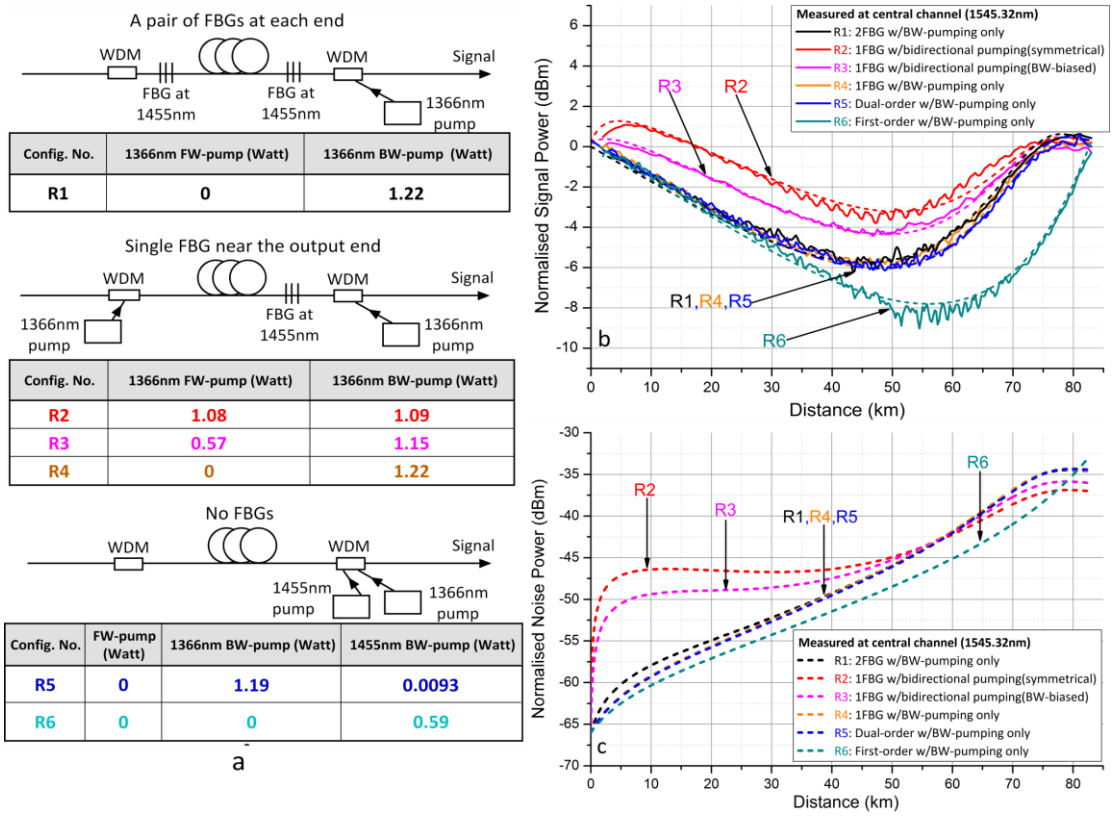

Config. No.	1366nm FW-pump (Watt)	1366nm BW-pump (Watt)
R1	0	1.22

Config. No.	1366nm FW-pump (Watt)	1366nm BW-pump (Watt)
R2	1.08	1.09
R3	0.57	1.15
R4	0	1.22

Config. No.	FW-pump (Watt)	1366nm BW-pump (Watt)	1455nm BW-pump (Watt)
R5	0	1.19	0.0093
R6	0	0	0.59

Figure 5.9(a). Schematic diagrams and pump powers of different Raman configurations; (b). Experimental data (solid lines) and simulations (dotted lines) of signal power distributions using different Raman configurations. (c). Simulations of noise power distributions (dotted lines) using different Raman configurations [97].

Schematic diagrams and pump powers for the Raman configurations tested are shown in Figure 5.9(a). For all the configurations the Raman gain was set to counterbalance the ~16.5 dB attenuation of the fibre. The 1366 nm backward pumping configuration with a Fabry-Perot cavity (a pair of FBG at each end of the span) was used (scheme R1). The FBGs used were centred at 1455 nm with 0.5 nm 3dB bandwidth and 95% reflectivities. As demonstrated in [42], in this configuration with a pair of FBGs, backward pumping only gave the best transmission performance. In random DFB fibre laser based amplifiers (R2, R3 & R4), a single FBG was used at the output end of the span. The first order random laser at 1455 nm was generated by the resonant mode reaching the lasing threshold in a distributed cavity formed by a distributed feedback (Rayleigh scattering) and an FBG [79,87]. Three pump power combinations were used in this configuration, as forward pumping at 1366 nm could amplify the signal near the input section of the fibre by amplifying the forward-propagated random DFB lasing. For comparison,

backward first order and dual order pumping with no FBGs (R5 & R6) were also tested. For all the configurations, the 1366nm second order and 1455 nm first order pumps were highly depolarised and coupled into the span through WDM couplers.

Signal power distributions along the transmission fibre measured at 1545.32 nm using a modified OTDR are shown in Figures 5.32(b) and (c), and confirmed with simulations (dotted lines) [7,30]. For scheme R1, the SPV was ~6 dB. Using a bi-directionally pumped random DFB fibre laser, the SPVs were reduced to ~4 dB in the configurations R2 (symmetrical pumping) and R3 (BW-biased pumping). The performance of backward only pumped random laser based scheme (R4) was identical to the baseline Fabry-Perot backward only pumping (R1). This indicates, for this configuration the FBG at the input end of the span didn't actually contribute to the fibre laser generation, showing that the FBG at the input end for R1 was superfluous. As shown in Figures. 5.9(c), the noise became less as more FW-pump power was applied, because the use of FW-pump can increase the signal power [33,42].

With no FBG, backward dual order pumping scheme R5 (1366 nm and 1455 nm) can be used to give the same SPV as R1 and R4 only if using similar second order pump power and very small first order pump power (only ~9.3 mW) [7,50]. This did however require two pump wavelengths and careful control of first order pump power (otherwise the SPV similar to BW-pumped random DFB fibre laser scheme cannot be achieved), which makes the simplicity of R4 attractive [7]. Scheme R6 used only backward first order pumping and gave the highest SPV of ~9 dB and the highest noise at the output end.

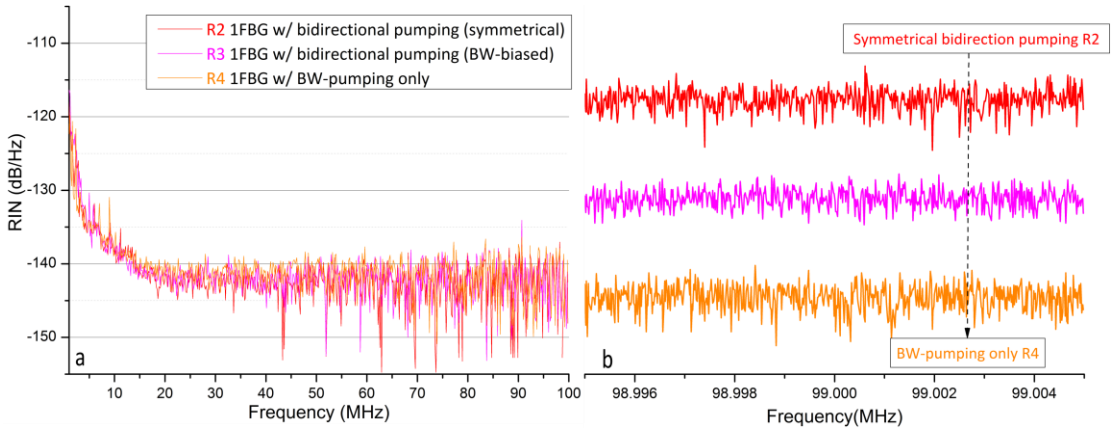

Figure 5.10(a).RIN of output signal using three random fibre laser based scheme. (b). Mode structures of forward-propagated random fibre lasers

As discussed in Chapter 4, in ultra-long Fabry-Perot laser configuration, it has been shown that the RIN of the signal could have significant impact on the long-haul transmission performance resulting in the Q factor penalty of up to 4.15 dB [42]. In random DFB fibre laser configuration, similarly, the relative intensity noise (RIN) of the output signal after one span was measured using random laser schemes R2, R3, and R4 [42]. In Figure 5.10(a), the RIN of the output signal stayed the same over the whole measurement range for all the pumping schemes, which indicates there might be no RIN-induced impact on the transmission using this amplification scheme [43,48]. In Figure 5.10(b), the mode structures of fibre lasers at 1455 nm for different pump powers were demonstrated. There was no mode spacing, which confirms that the fibre laser was random DFB lasing [56,79,87]. The RIN of the signal didn't increase with FW-pump power, because the minimised reflectivity at the input end led to the reduced efficiency of the Stokes generation (from 1366 nm pump to 1455 nm fibre laser) in forward-propagated direction [97]. This was due to the lack of the reflector near the input. Consequently, the main amplification was provided by the backward-propagated short-cavity random DFB laser [96]. This indicated that the RIN transfer was significantly reduced, compared to the Fabry-Perot fibre laser with two high reflectivity reflectors on both sides [42].

5.2.2 Transmission results and discussions

Figure 5.11(a) shows simulated and experimental Q factors versus launch power at 3333 km for all the Raman configurations, showing a good agreement. The simulation setup was similar to the experimental one, where 10×29 Gbaud DP-QPSK channels with 100 GHz spacing were transmitted over 40 fibre recirculations. Due to large number of simulated channels, the length of the random sequence was reduced to 2^{17}-1, compared with PRBS length of 2^{31}-1 adopted in the experiment. Independent and uncorrelated data were transmitted among all channels. The generated signal was oversampled 4 times providing a total simulation bandwidth of ~4 THz. The OSNR at the transmitter was set to 25 dB. The linewidths of both transmitter laser and local oscillator were set to 100 kHz. The propagation of the signal in the fibre link was simulated by solving numerically the Manakov system using the split-step Fourier method, with the simulated signal power profiles (shown in Figure 5.9(b)) providing a step size of 1km. The Raman noise

was modelled as Gaussian noise, which was added to the signal after each step (1 km), following the simulated noise profiles (shown in Figure 5.9(c)). In this simulation, the same power and noise profiles was used for all the channels. In addition, for simplicity, polarisation mode dispersion and other polarisation effects were ignored in simulation. At the receiver, after coherent detection, the channel under test was filtered using an 8th order Butterworth low pass filter with a 3 dB bandwidth of 18 GHz. The DSP in the simulation was similar to the one used in the experiment.

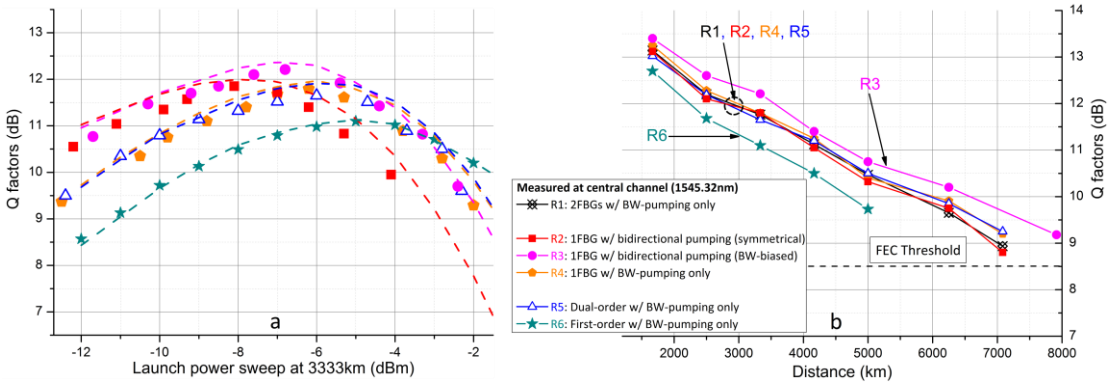

Figure 5.11(a). Experimental (solid points) and simulated (dashed lines) Q factors versus launch power per channel at 3333km [97]. (b). Q factors versus transmission distances.

As RIN-induced impact was not considered in the simulation, there was no RIN-induced penalty on the transmission using random DFB laser configuration with bidirectional pumping. This is particularly important, as the system performance is only limited by ASE noise and nonlinearity without suffering from RIN-induced penalty, signal power profiles can be modified to meet different requirements for the transmission link [48,81,100].

Figure 5.11(b) shows Q factors versus transmission distances. The random DFB laser scheme R3 (bidirectional pumping with less FW-pump power) achieved the best performance at 3333 km and consequently gave the longest transmission distance of 7915 km. As expected from signal/noise distributions shown in Figures 5.9(b) and 9(c), the impact of nonlinearities in R2 (bidirectional symmetrical pumping) degraded the transmission performance - the SPVs of R3 and R2 were the same (~4 dB), but for R2 there was a sharp increase of signal power near the input section. This led to a lower optimum launch power and a reduced maximum reach of 7082 km. The random laser scheme R4 (BW-pumping only) had a higher SPV value of ~6 dB which led to a higher optimum launch power and a reduction in reach to 7082 km. Figs. 9(b) and 9(c)

show that dual-order pumping scheme R5 with no FBG gave the same signal and noise profiles as R1&R4. Consequently all three schemes show the same transmission performance in Fig. 11. With first order BW-pumping R6, the optimum launch power of -5 dBm was achieved, but the maximum reach was decreased to 4999 km because of the most accumulated noise.

Figure 5.12 shows OSNR, Q factors, and received spectra at maximum transmission distances for three random fibre laser based schemes R2 (symmetrical bidirectional pumping), R3 (BW-biased bidirectional pumping), and R4 (BW-pumping only) as comparison with R6 (first order BW-pumping). The variations in the OSNRs and Q factors were due to the mutual effects of Raman gain spectra and the gain flattening filter applied in the recirculating loop. All the measured channels were below the FEC threshold.

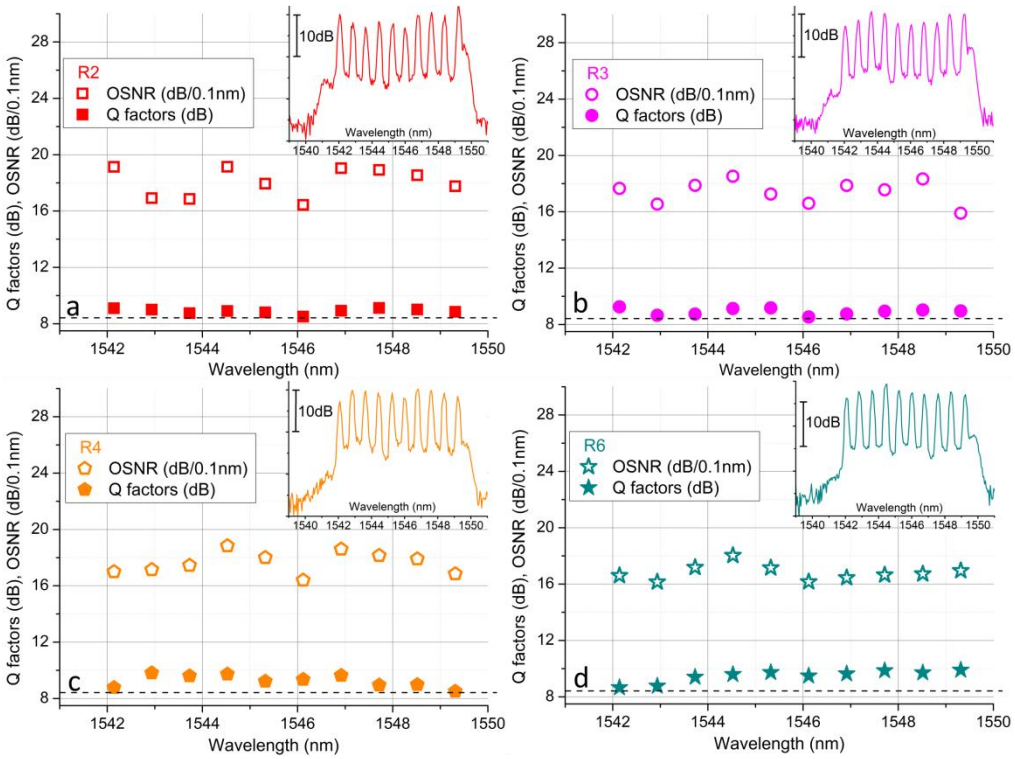

Figure 5.12. OSNRs, Q factors, and received spectra measured at its maximum reach: (a). Bi-directionally pumped random laser scheme R2 (symmetrical pumping) at 7082km; (b). Bi-directionally pumped random laser scheme R3 (BW-biased pumping) at 7915km; (c).BW-pumped random laser scheme R4 at 7082km; (d). BW-pumped first order scheme R6 at 4999km.

5.2.3 Summary

The advantages of using a novel Raman amplification scheme based on random DFB fibre laser has been demonstrated, which enables bidirectional second-order pumping without RIN-induced

penalty. A detailed investigation/comparison of 10×116 Gbit/s DP-QPSK long-haul coherent transmission using different Raman amplification techniques is presented. The best performance (7915 km) was achieved with a random DFB fibre laser based configuration which included bidirectional second order Raman pumping. Further studies showed that there was no increase of signal RIN with symmetric bidirectional pumping [48,97]. This scheme offered the best transmission distance and maintained a low signal power variation simultaneously [47], although the Raman gain efficiency (the ratio between the signal gain and the pump power) was decreased. In addition, on one hand, the proposed scheme with bidirectional pumping had the potential of providing a very symmetric link which maximised the nonlinearity compensation benefit in mid-link OPC based system [29,69,92,93]. On the other hand, it could be highly compatible with nonlinear Fourier transform (NFT) based transmitter [99,100].

5.3 Long-haul coherent transmission using Raman fibre laser based amplification and optical phase conjugation

5.3.1 Optical phase conjugation

Optical phase conjugation is an effective technique to compensate both linear and nonlinear impairments in long-haul transmissions [69,101]. In terms of nonlinear Schrodinger equation (NLSE), by reversing the phase of the signal in the middle of the link, the linear (the chromatic dispersion term β_2) and nonlinear impairments (nonlinear coefficient γ) generated in the first half part of transmissions can be compensated by these from the second half of the link [69,77]. With the rapid development of advanced modulation formats and coherent detection allowing DSP to compensate linear impairments, OPC might not be usually used for the compensation of linear impairments [77]. However, OPC still shows a great potential of efficiently compensating nonlinear impairments in long-haul transmission systems, which is still rather complicated to compensate in DSP by digital back propagation (DBP) [102].

In general, there are three techniques based on the process of three or four wave mixing to achieve the optical phase conjugation: FWM in a semiconductor optical amplifier, three wave mixing using periodically poled lithium niobate (PPLN), and FWM in a highly nonlinear fibre

(HNLF) [69,77,138,139]. For SOA-based OPC device, the intrinsic noise from the amplified spontaneous emission (ASE) is present and potentially decreases the conversion efficiency [69]. Although the PPLN waveguide OPC has a very broad conversion bandwidth (>50 nm) and is able to conjugate a number of WDM channels, the major drawback is that the OPC has to be operated above 180^{o} C in order to avoid the photorefractive effect [69]. This potentially increases the operation complexity using this device in telecoms. In comparison, HNLF, as a passive medium, is easy to be spliced to single mode fibre which is widely used in telecoms, although its conversion bandwidth is rather limited compared with PPLN based OPC.

In order to maximise the benefit of compensating nonlinearity with mid-link OPC, an important requirement is that the signal power profile of the transmission span has to be symmetric for the optimum performance [69,92,93]. This nearly symmetrical power profile can be achieved by RFL based amplification technique, and transmission performance improvement using mid-link OPC will be discussed in the following sections. But first, the OPC device needs to be characterised to confirm its potential capability in a long-haul transmission system.

In practice, OPC should be operated over a broad bandwidth to be cost-effective [103]. So far, for a HNLF based OPC device, only PM-OFDM "superchannel" signal with very narrow frequency bandwidth (150 GHz) has been demonstrated in [104]. Here an OPC device with a bandwidth of more than 1 THz (~9 nm) is demonstrated for the phase conjugation of polarisation multiplexed WDM signal, and a back-to-back transmission performance evaluation is performed using 10×114 Gb/s DP-QPSK WDM signals.

5.3.1.1 Experimental setup of optical phase conjugator characterisations

The schematic diagrams of optical phase conjugator and characterisations of OPC are shown in Figure 5.13. The OPC is constructed based on four wave mixing (FWM) in a diverse polarisation configuration [103]. The pump was from a laser (~500 kHz linewidth) at 193.4 THz (1550.12 nm) followed by an amplifier EDFA 2 with an output power of 40 dBm. The output pump was filtered by a bandpass filter (BPF 1, 2 dB insertion loss, 3dB bandwidth of 1 nm) in order to remove unwanted ASE. The PC 1 was used to control pump polarisation at 45º in order to equalise the power on both arms of PBS which were monitored by PM 2 and PM 3 [77]. The

pump and signal were combined using a 2×2 polarisations beam splitter (PBS) into a loop including 188 m highly nonlinear fibre (HNLF), which were split into two orthogonal "TE" and "TM" polarisations. The PC 2 was used to adjust the loop polarisation and optimise the spectral shape of the conjugated signal [103]. Optical phase conjugation occurred when the pump and the signal had the same polarisation and the direction in the loop, and therefore two orthogonal parts of conjugated signal were recombined near the output of the PBS. Figure 5.14 shows a sample spectrum measured at the output of PBS before the BPF 2.

The HNLF was commercially available, and the total loss was ~2.6 dB. The nonlinear coefficient was 6.9 $(W.\ km)^{-1}$., Because the fibre was aluminium-doped and linearly strained from 100g to 1000g to generate an SBS threshold of 1W, the zero dispersion wavelength (ZDW) was from 1552 nm with 100g strain to 1564 nm with 1000g strain [77]. In average, the dispersion at 1550 nm was -0.19 ps/(nm.km) and the slope of the dispersion was 0.024 ps/(nm^2.km) [77].

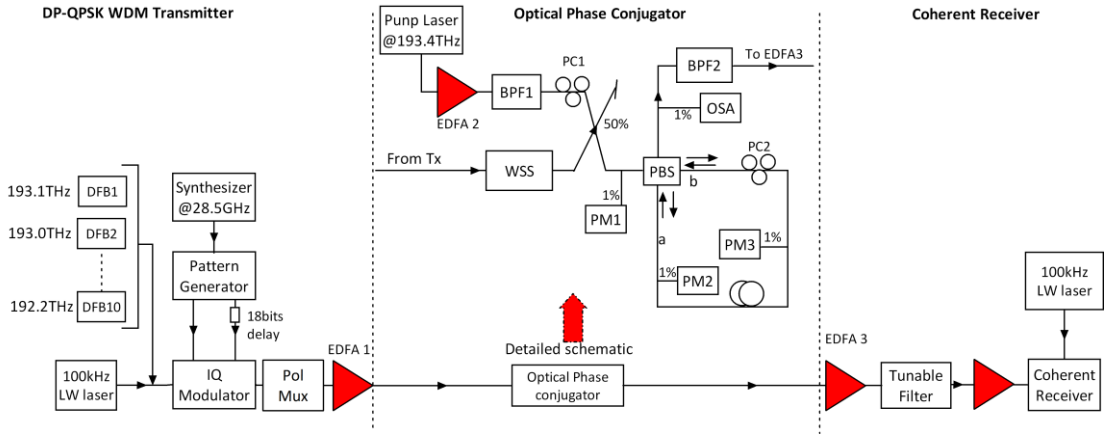

Figure 5.13. The schematic diagrams of OPC and the characterisations system [103]

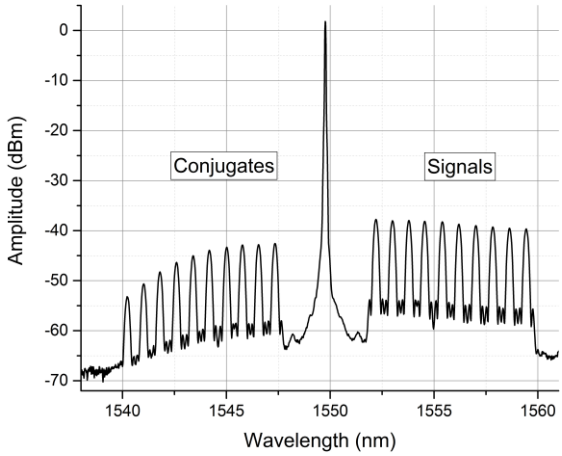

Figure 5.14. A sample spectrum measured at the output of PBS [103]

At the DP-QPSK transmitter, 10 DFB lasers with 100 GHz spacing from 1552.5 nm (193.1 THz)

to 1559.8 nm (192.2 THz) were multiplexed and a 100 kHz linewidth tuneable laser was used as "channel under test" during the measurement cycle [29,77]. The signal was modulated by a Mach-Zehnder I/Q modulator driven by a normal and inverted PRBS pattern (18 bits delay in between) from a pattern generator with 28.5 Gbit/s and 2^{31}-1 word length. The output signal was multiplexed by a polarisation emulator with 10 ns delay on one arm. The output power from EDFA 1 was 20 dBm, and there was 6 km SMF in the middle stage of EDFA 1 to give a decorrelation of 15 bits [77]. The additional ASE noise outside the WDM signal spectrum was removed by a WSS (wavelength selective switch). From the output of the OPC, ten conjugated channels from 1540.6 nm (194.6 THz) and 1547.7 nm (193.7 THz) were filtered by BPF 2. EDFA 3 contained another 6 km SSMF to compensate the dispersion generated by 6 km SMF at EDFA 1. The measured channel was selected using a tuneable filter and amplified into a coherent receiver. The local oscillator with 10 dBm output power was combined with the conjugated signal into 90º optical hybrids followed by balanced detectors and real-time scope with 80 GS/s and 36 GHz bandwidth. Data was processed offline and Q factors were estimated from the constellation diagrams and averaged over 570k symbols.

5.3.1.2 Experiments results of OPC characterisations

The transmission performances of OPC were characterised in two ways. The first one was that the ASE noise source was injected after OPC (at the output of OPC) and the Q factors were recorded. These results were compared with 10×114 Gb/s DP-QPSK transmitter back-to-back performances. In this way, the back-to-back Q penalty of the OPC could be measured. The second one was that the ASE noise was injected at the input of the OPC to examine the OSNR degradation after OPC. This would tell how the OSNR was changed before and after the OPC, and whether the OPC device were highly suitable for advanced modulation format which usually requires higher OSNR [4]. Figures 5.15(a) and (b) show back-to-back Q factors at different OSNR levels on the noise-loaded DP-QPSK transmitter and conjugated channels after OPC, respectively. The violet triangle points were drifted, because at the time of measurement de-multiplexing filter was set slightly offset from the designated centre wavelength. Figure 5.16 shows the direct comparisons of Q factors versus OSNRs after averaged all the 10 channels.

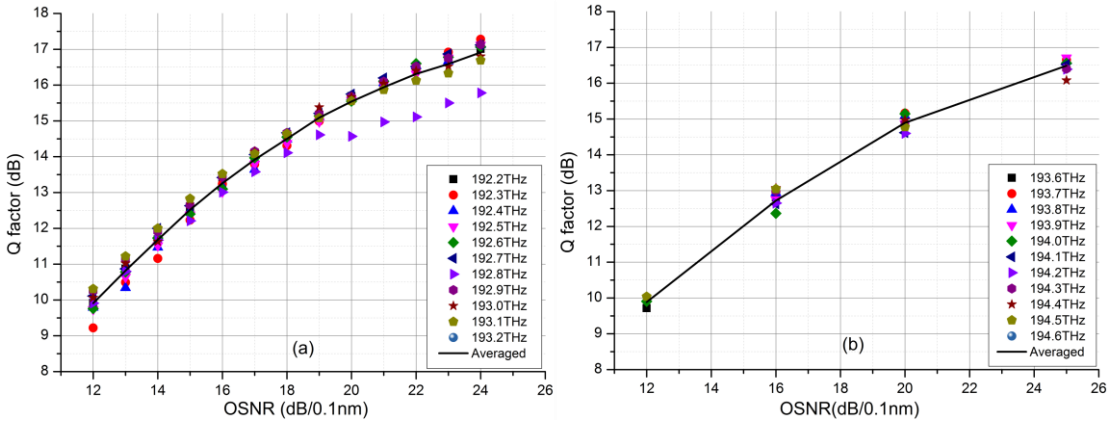

Figure 5.15. Q factor versus OSNR (dB/0.1nm) of DP-QPSK transmitter (a) and conjugated signals (b)

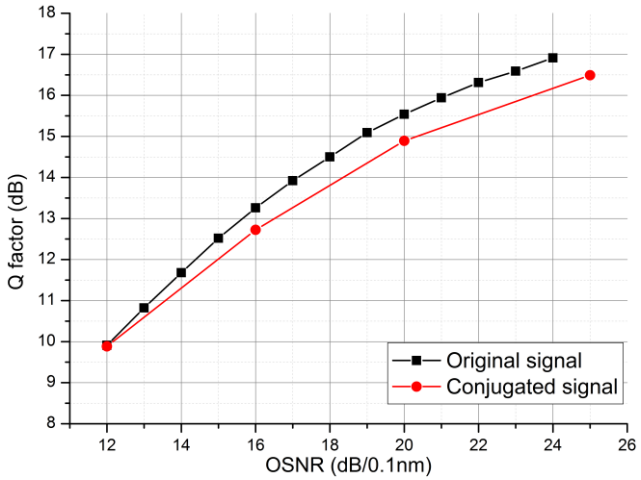

Figure 5.16. Comparisons of Q factor versus OSNR between original and conjugated signals after averaged over 10 channels

As shown in Figure 5.16, the averaged Q penalty was from 0.1 dB at 12 dB OSNR to 0.65 dB at 20 dB OSNR. This was possibly from the unwanted FWM products at conjugated signals, pump noise, and residual ASE noise [77]. For the channel with the worst performance, its Q factor penalty was between 0.6 dB at 12 dB OSNR and 0.9 dB at 20 dB OSNR. The Q factor penalty after the OPC was always within 1 dB. In particular, when the OSNR was low as this was likely to happen in a real mid-link OPC system, the Q factor penalty was very small, indicating that the proposed polarisation-diverse OPC was potentially capable to be used for long-haul 100G DP-QPSK WDM transmission with mid-link OPC.

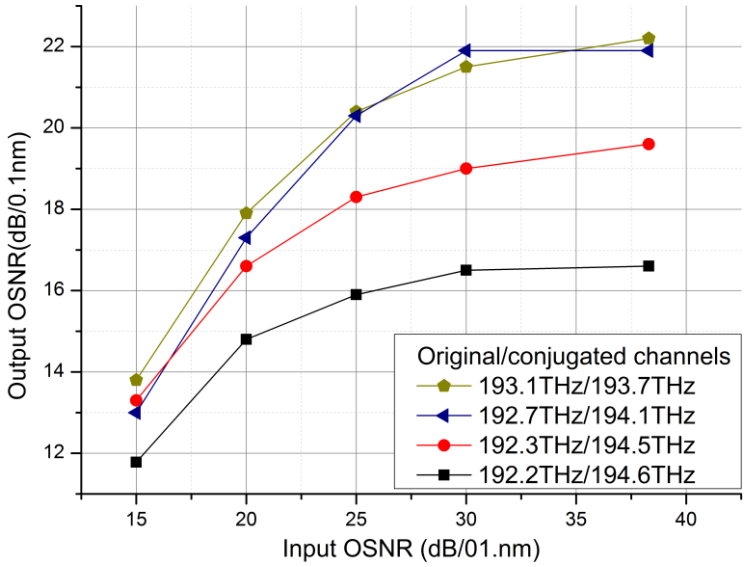

Figure 5.17. Output OSNR versus Input OSNR

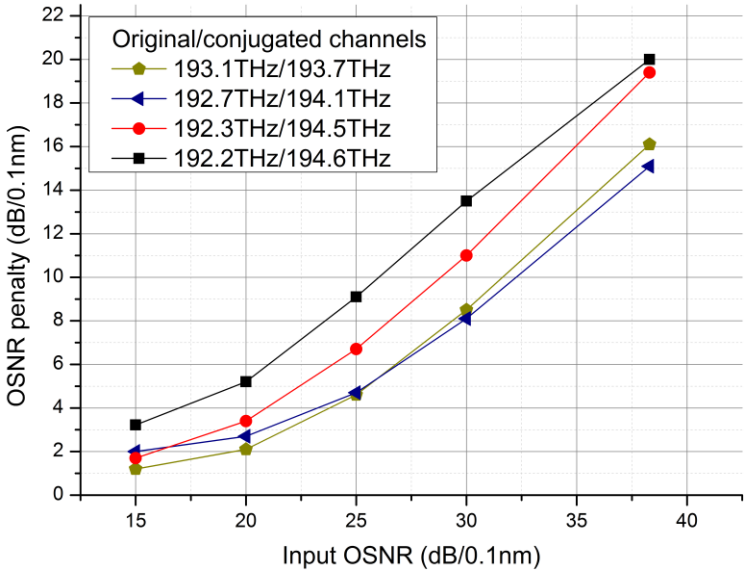

Figure 5.18. OSNR penalty versus input OSNR

The OSNR degradation performances are shown in Figures 5.17 and 5.18. In Figure 5.17, OSNR after OPC was limited to 22 dB approximately no matter what the input OSNR was. In Figure 5.18, the OSNR penalty was defined as the OSNR difference between the input OSNR of signal and the output OSNR of conjugated signal, which can be seen as a "conversion efficiency" of this OPC device. The OSNR penalty at 15 dB input OSNR was 1.2 dB at 193.7 THz, 1.7 dB at 194.1 THz, 2 dB at 194.5 THz, and 3.2 dB at 194.6 THz. This indicates that the conjugated channel (i.e. 193.7 THz) near the pump (193.4 THz) had the lowest OSNR penalty, and the OSNR penalty was increased as the channel was further from the pump. This was likely because the ZDW of HNLF changed with the strain [77], and could be further optimised using a HNLF

with more uniform ZDW which is closer to the pump wavelength. However, the penalty would become less significant for the lower input OSNR which was likely the case after the transmission in the first half link.

Above all, polarisation-diverse OPC characterisation with 10×114 Gb/s DP-QPSK WDM transmitter was demonstrated for the first time [77]. The proposed OPC scheme provided the capability for dual-polarisation signal conjugation, very broad bandwidth (~1 THz/9nm), and very strong potential for mid-link OPC applications to compensate both linear and nonlinear impairments in long-haul transmission systems [29]. It can be also expected that further improvement on the bandwidth can be achieved by using alternative HNLF with optimised fibre characteristics (i.e. ZDW, dispersion slope).

5.3.2 Long-haul transmissions with single band OPC

In long-haul optical transmission systems, generally speaking, the best transmission performance can be obtained by the best trade-off between the ASE noise and fibre nonlinearity [81]. Therefore, the fibre nonlinearity is one of the major impairments which limit the transmission performance. Nowadays, there are several ways to combat the nonlinearity, such as digital back propagation (DBP) in DSP algorithm, mid-link OPC, and so on [106-108]. As for DBP, the main limitation is that there is effective increase in reach for single channel/superchannel transmission, but the benefit would be limited for WDM transmission [98]. In the last section, a 1 THz bandwidth and polarisation-diverse optical phase conjugator is presented and shows its potential to compensate the nonlinearity and chromatic dispersion. One of the reasons that mid-link OPC is not used widely is because it requires very symmetrical signal power profiles along the transmission span, and obviously conventional EDFA was not able to achieve [93,96]. However, as demonstrated in Chapters 4, RFL based amplification with second order Raman pumping is able to provide an easily modified way with better transmission performance to satisfy different requirements for the transmission span, compared with EDFA system. In this section, experimental demonstration of 100G DP-QPSK WDM transmission system using different amplification techniques (EDFA, backward pumped/bidirectional pumped RFL based amplifiers with two FBGs) without and with single band OPC are demonstrated. Note that single band

OPC here means there is only one conjugated waveband at one time. Dual band OPC means both wavebands are conjugated at the same time, which will be demonstrated in next section 5.3.3.

5.3.2.1 Experimental setup

A schematic diagram of the experimental setup is shown in Figure 5.19. The WDM grid consisted of 8 DFB lasers spaced at 100 GHz from 1551.72 nm (193.2 THz) to 1557.36 nm (192.5 THz) which were multiplexed by an AWG (array waveguide grating), and its output was combined with narrow linewidth (~100 kHz) tuneable laser. The setup for Mach-Zehnder I-Q modulator and optical phase conjugator has been described in previous sections. A dual input configuration was used at the input of the loop for both signals and conjugated signals. As a benchmark of Q factor performance without OPC, the conjugated signals were present but only original channels were measured. In order to achieve this, a 50/50 coupler was used at the mid stage of EDFA 9, which allowed the signal to enter the OPC. The WSS at the OPC path was used to block out the conjugated signal from the previous recirculation, and let only original signals pass the OPC. In the recirculating loop, a GFF was to equalise the channels after each recirculation, and an additional EDFA was to compensate the loop specific loss from the couplers, AOMs and so forth. The original signal performance could be measured at the conventional recirculating loop output during the measurement window, as illustrated in Chapter 3. To measure the conjugated signal, the filling time needs to be set to one round trip time, and coherent receiver needed to be connected to the WSS (wavelength selective switch). For the first half of the transmission, the signal was propagated N times within the loop and its output entered into the OPC via the WSS. Then for the second half of the transmission, the signal was phase-conjugated by the OPC and the conjugates signal was fed into the loop entrance through the 50/50 coupler. Therefore, the conjugated signals filled up in the loop during this second filling time (also equals to one round trip time), and propagated in the loop for the other N times. The conjugated signals after propagated 2N times can be measured via the output from the WSS.

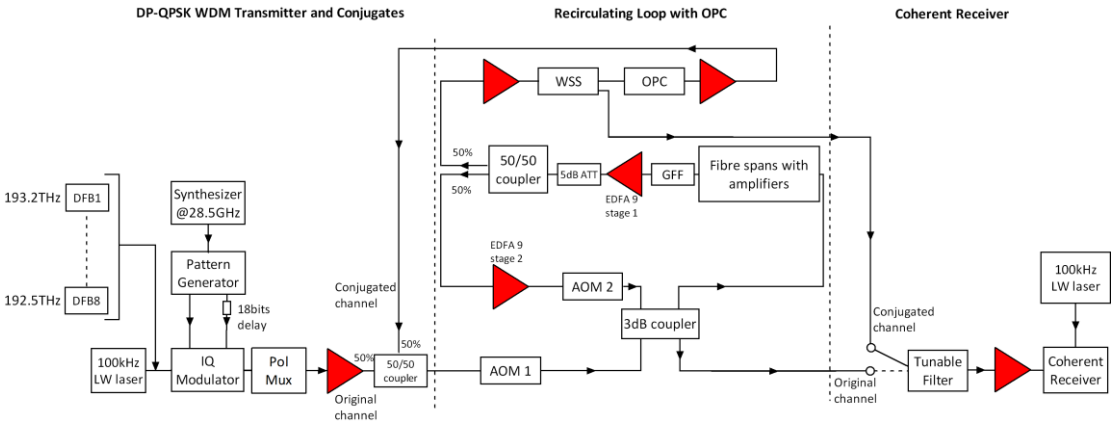

Figure 5.19. Schematic diagram of the experimental setup

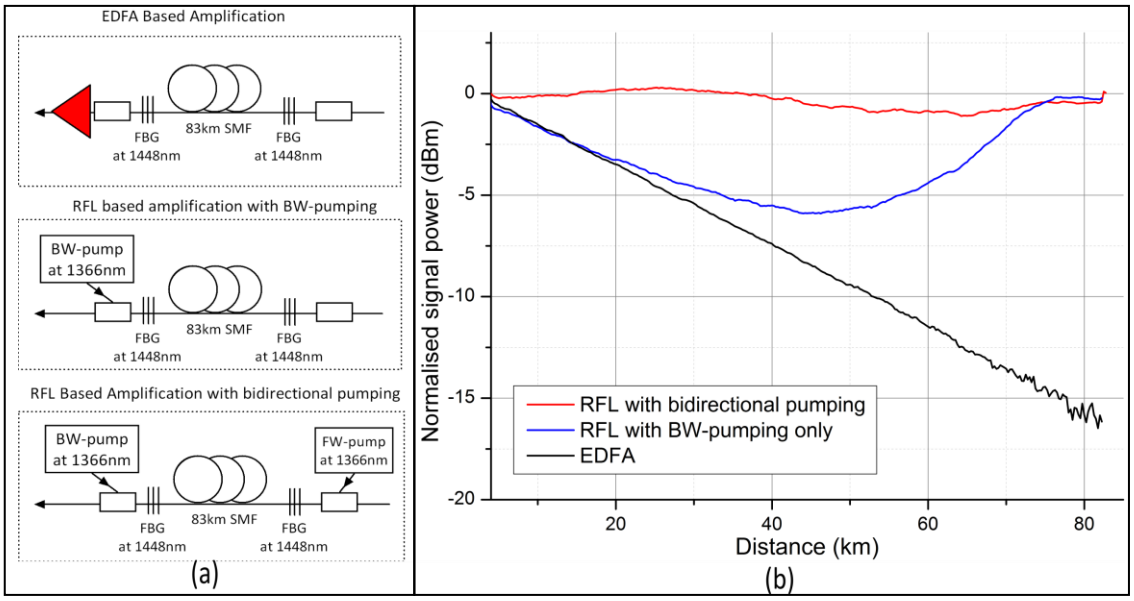

Figure 5.20(a). Schematic diagrams of three amplification schemes. (b). Signal power profiles along the fibre with different amplification schemes.

As presented in Figure 5.20(a), there were three amplification techniques used in the experiments, including EDFA, backward pumped RFL, and bidirectional pumped RFL based amplification with two FBGs. For EDFA only based systems, there were four SMF spans (19 dB loss, 83 km for each) amplified by four EDFAs in the recirculation loop. For RFL based amplification systems, as illustrated in previous sections, a matched pair of ~95% reflectivity fibre Bragg gratings (FBGs) with a centre peak at 1448 nm and a 3 dB bandwidth of ~0.5 nm were used with one located at each end of an 83 km SMF span. Second order pumps at 1366 nm with RIN of approximately -120 dB/Hz were used to create a Raman fibre laser at the wavelength of 1448 nm. As discussed previously, the fibre laser was random DFB laser using BW-pumping only and Fabry-Perot fibre laser using bidirectional pumping. The resultant fibre lasing at 1448 nm and the

pump at 1366 nm amplified the signals in the C band [78]. Signals power profiles measured at 192.8 THz using three amplification techniques were shown in Figure 5.20(b). For EDFA amplified span, the signal power profile was linearly reduced due to the fibre attenuation. For RFL based amplification techniques with two FBGs, BW-pumping gave ~5.8 dB SPV and bidirectional pumping scheme (43% FW-pump power ratio) minimised the variation to only ~1.9 dB It has been shown that the use of second order FW-pumping gave a significant reduction in SPV, and also reduced the amplifier noise figure [33].

For the coherent receiver, the received signal was filtered by a 100 GHz tuneable filter before amplified by an EDFA. The amplified signal was combined with a narrow linewidth (~100 kHz) LO in a polarisation-diverse 90º optical hybrid. The output signals from the optical hybrid were detected by balanced receivers, recovering the in-phase (I) and quadrature (Q) signals in both X and Y polarisations. These four signals were sampled and digitised using an 80 Gs/s real time oscilloscope with a 36 GHz analogue bandwidth. The data was processed using off-line DSP. Q factors were estimated from the constellation diagrams and averaged over 570 k symbols.

5.3.2.2 EDFA only system without and with OPC

For EDFA based system, Figure 5.21(a) demonstrates Q factor versus launch power at their maximum reach, and Figure 5.21(b) shows Q factor versus transmission distance at 193.1 THz and its conjugated signal at 193.7 THz. From Figure 5.21(a), it can be seen that there was no improvement in Q factor, although the optimum launch power with OPC was increased slightly from 2 dBm to 4 dBm. As indicated in the launch power sweep, the maximum transmission distance for the conjugates was the same as for the original channels. It is crucial that signal power profiles has to be as symmetrical as possible in order to maximise the benefit [92,93]. Obviously, the signal power profile using EDFA was not symmetrical, which reduced the amount of Kerr effect compensation [69].

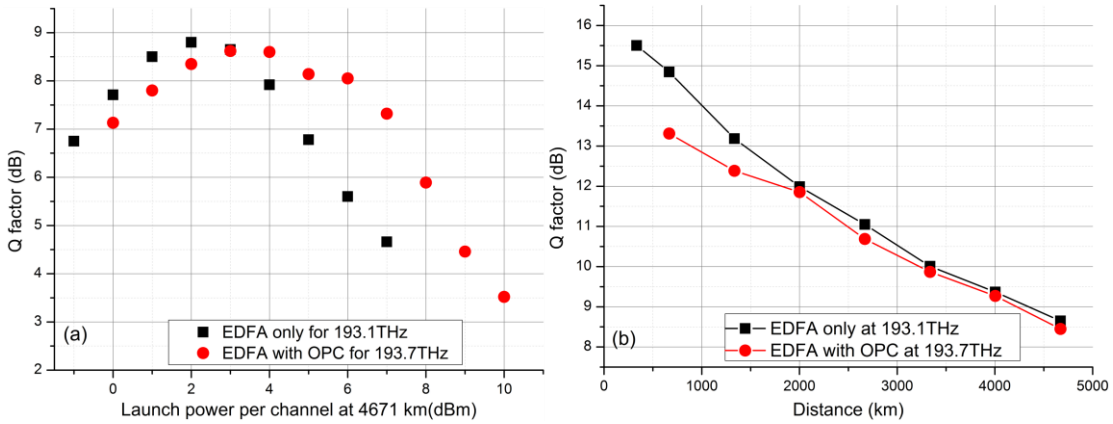

Figure 5.21(a). Q factor versus launch power without and with OPC. (b). Q factor versus transmission distance without and with OPC.

Figure 5.22(a) shows the measured spectrum at maximum reach of 4671 km, and Figure 5.22(b) confirms all the measured channels were above the Q factor threshold of 8 dB at the same maximum reach. Therefore, there was no transmission performance improvement that could be found with EDFA based system using mid-link OPC.

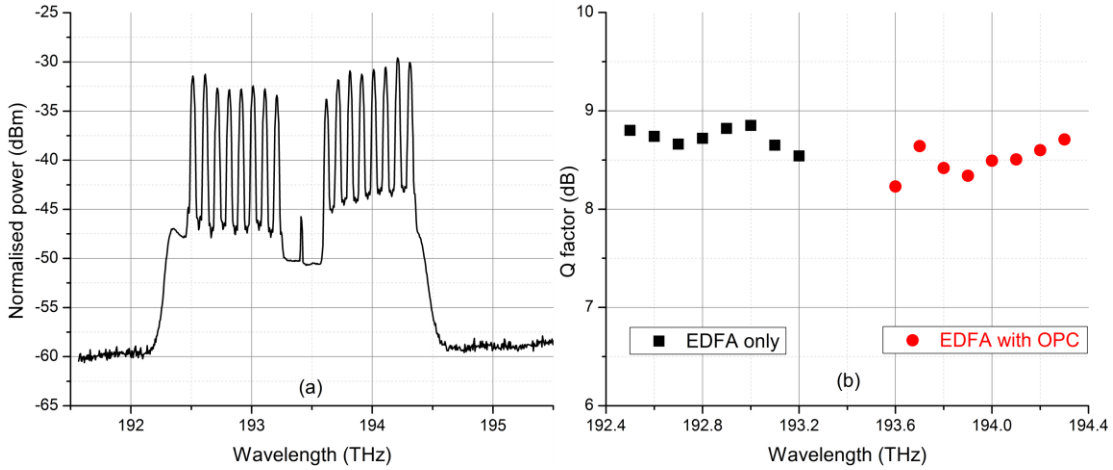

Figure 5.22(a). Received spectrum at maximum transmission distance. (b). Q factors for all the channels without and with OPC using EDFA

5.3.2.3 BW-pumped RFL based amplification without and with OPC

Similar experiments were implemented using second order BW-pumped RFL based amplification. As show in Figure 5.23(a), the optimum launch power was increased by 3 dB from -3.5 dBm without OPC to -0.5 dBm with OPC. There was an obvious Q factor improvement, even if the launch power sweep was done at 5359 km without OPC and 6760 km with OPC. Q factor versus transmission distance at 192.8 THz and its conjugated channels 194 THz were shown in Figure

5.23(b). The maximum reach was 7833 km with no OPC and 10059 km with OPC, so there was more than 28% increase in reach using mid-link OPC. Compared with EDFA-OPC transmission system, the maximum reach for BW-pumped RFL based system was more than doubled, although one 83 km span was in the loop indicating more loop specific loss.

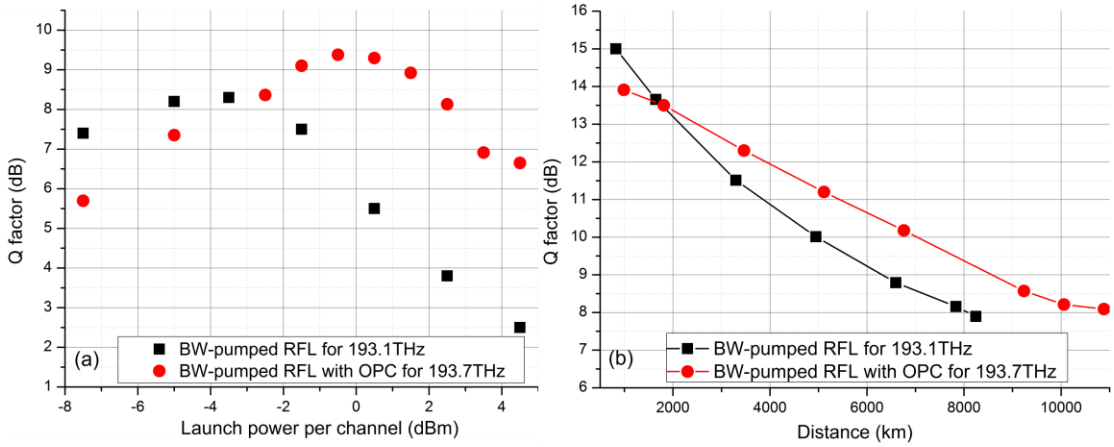

Figure 5.23(a). Q factor versus launch power without and with OPC. (b). Q factor versus transmission distance without and with OPC.

The received spectrum at 65 recirculations (5340 km) is shown in Figure 5.24(a). Q factors for all the original and conjugated channels at their maximum reach are presented in Figure 5.24(b). It can be seen that there were seven channels above the threshold, but the channel furthest from the OPC pump failed. Possible reasons are that there was a larger OSNR degradation further from the pump when the conversion efficiency was decreased as demonstrated in 5.3.1.2. In addition, the filter bandwidth of BPF near the OPC output was too narrow, which caused a significant decrease on the Q factor of this channel. The channel was expected to have similar performance as demonstrated in EDFA-OPC and bi-directionally pumped RFL-OPC based system when the BPF was set wide enough.

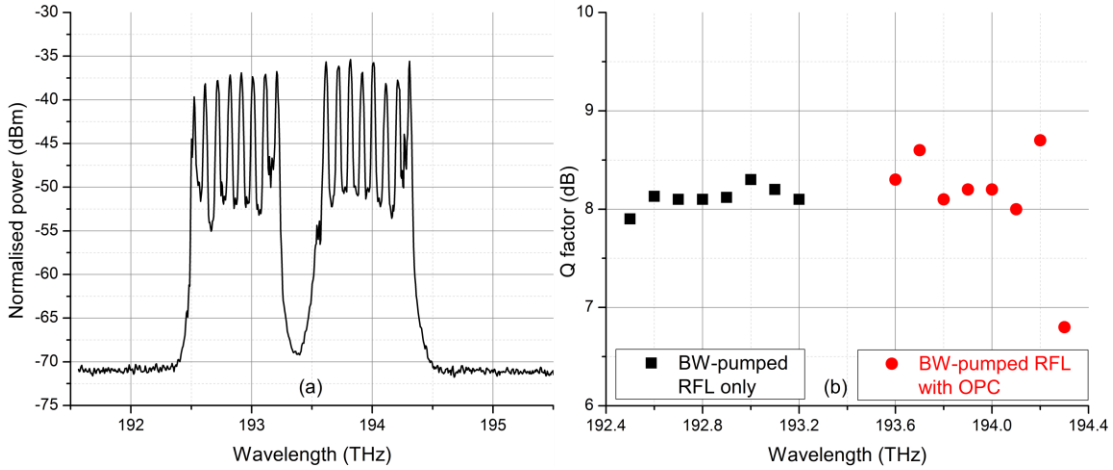

Figure 5.24(a). Received spectrum at 65 recirculations. (b). Q factors for all the channels without and with OPC using BW-pumped RFL based amplification

5.3.2.4 Bidirectional pumped RFL based amplification without and with OPC

The same experiments were also implemented on the bidirectional pumped RFL based amplifier. The launch power versus Q factor at 3299 km was demonstrated in Figure 5.25(a). The optimum launch power was changed from -1.5 dBm with no phase conjugation to 1.5 or 2.5 dBm with phase conjugation. However, the Q factor improvement was only 1 dB. It can be also seen from Figure 5.25(b) that the transmission performance improvement was rather limited, only from 4287 km to 5112 km, which indicated an increase of 19% in reach, compared to 28% using BW-pumped RFL based scheme.

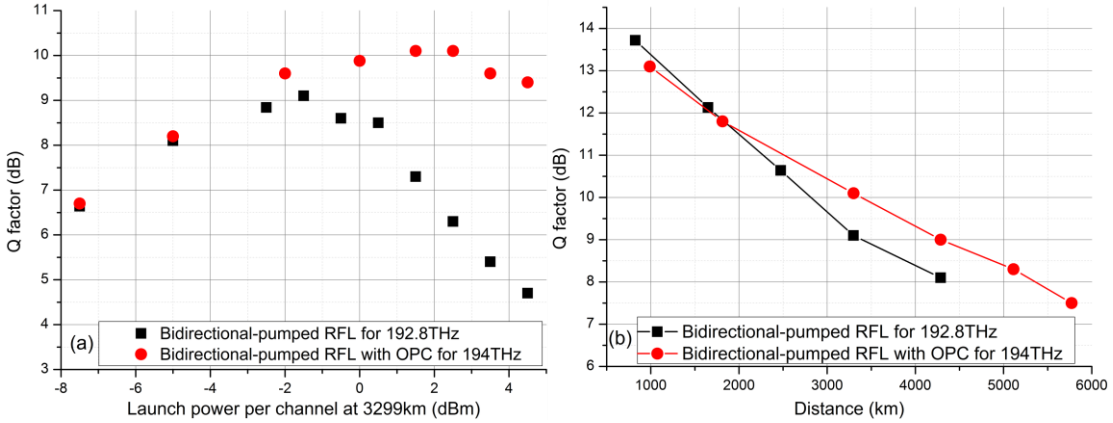

Figure 5.25(a). Q factor versus launch power without and with OPC. (b). Q factor versus transmission distance without and with OPC

The received spectrum at 62 recirculations (5112 km) is shown in Figure 5.26(a), and Q factors including all the measured 16 channels are shown in Figure 5.26(b). For the transmission results

without OPC, the maximum reach was 4287 km, compared with 7833 km using BW-pumped RFL based amplifier and 4671 km using EDFA. As discussed in Chapter 4, the lower signal power variation with more FW-pump power should lead to a reduction in noise and higher OSNR [33,36], indicating better transmission performance. However, the worse transmission performance was due to the RIN-induced penalty from the use of the 1366nm FW-pump [42]. Due to the lack of signal power symmetry, the transmission improvement using mid-link OPC was worse than BW-pumped RFL based amplifier [92].

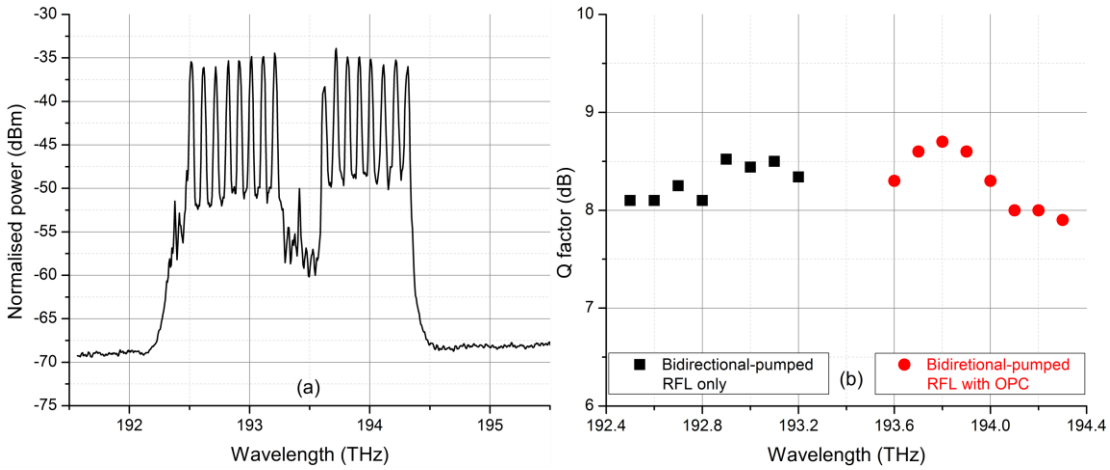

Figure 5.26(a). Received spectrum at 62 recirculations. (b). Q factors for all the channels without and with OPC using bidirectional-pumped RFL based amplification

5.3.2.5 Summary

7×114 Gbit/s DP-QPSK WDM transmissions using three different amplification techniques without and with OPC have been experimentally presented. It has been shown as for EDFA based transmission, the maximum reach was 4671 km, and there was no improvement using mid-link OPC. As for BW-pumped RFL based amplification, the maximum transmission distance was 7833 km with no OPC, and there was more than 28% increase in reach which is up to 10059 km. As for bidirectional pumping RFL based amplification, the maximum reach was 4287 km without OPC, and there was 19% enhancement in reach up to 5112 km. Therefore, BW-pumped RFL based gave the best transmission performance for both non-OPC and mid-link OPC system. For non-OPC system, compared with EDFA, RFL based amplification with BW-pumping only reduced signal power variation, leading to a reduction in ASE noise which consequently enhanced the transmission performance with no OPC. Compared with bidirectional-pumped

RFL based amplifier, no RIN-induced penalty was introduced due to the lack of FW-pump [42]. For mid-link OPC system, BW-pumped RFL based amplification system provided the best symmetry level among three amplification techniques [92,93], which compensated the most nonlinear impairment and maximised the benefit from using mid-link OPC.

5.3.3 Long-haul transmission using dual band OPC

In order to achieve the highest capacity, it is crucial to minimise the ASE noise by using RIN-induced penalty free distributed Raman amplification [42], and to fully compensate the nonlinear impairment [109], as well as to increase spectral efficiency by using super-channels at the same time [110]. 7×114 Gb/s DP-QPSK transmission experiment using three different amplification techniques without and with mid-link single band OPC were demonstrated [29]. However, in single band OPC, although there was nearly 30% increase in transmission reach, only half of the spectrum was used and the other half was "wasted" (not used for transmission) [111]. In order to solve the problem and further maximise the capacity, it is very important to conjugate both wavebands at the same time, which is called "dual band OPC".

In this section, a dual band optical phase conjugation transmission experiment is presented for the first time. The subsystems include DP-16QAM multi-superchannels transmitter, random DFB fibre laser based amplification with second order BW-pumping, and dual band OPC configuration. A record total capacity of 2.4 Tb/s was achieved at the maximum transmission distance of 2700 km using multiple six superchannels transmitter [111,112].

5.3.3.1 Experimental setup

Figures 5.27, 5.28 and 5.29 show the experimental configuration, including 400 Gbit/s Nyquist WDM superchannel transmitter, dual band OPC, Raman fibre laser based amplified span, and the recirculating loop configuration. For Nyquist WDM transmitter, a combination of DFB/external cavity lasers, and fibre lasers formed two groups of lasers (up to 5 lasers each band) centred at 193 THz and 194.6 THz with 100 GHz spacing. During the measurement cycle, the DFB laser for that superchannel was replaced with an external cavity laser [111]. The 10 independent lasers were multiplexed together and subsequently modulated with Nyquist shaped 10 Gbaud (2

samples per symbol) 16QAM in-phase (I) and quadrature (Q) electrical signals (with 215 bits sequences) using an IQ modulator [112]. The roll off factor for the digital Nyquist filter was 0.01 for the output of the arbitrary waveform generator (AWG). The resultant optical Nyquist signals were amplified and fed into a Mach Zehnder modulator (MZM) driven at 20.2 GHz and biased to provide a 3-line comb [111]. The output signals were split and one copy was frequency shifted by 10.1 GHz using a single side band modulation scheme with over 30 dB extinction ratio. The other copy was delayed by 5 symbols before recombining to form a superchannel with a spectral width of approximately 60 GHz. After EDFA, the signals were polarisation multiplexed with a 400 ps relative delay [111]. The total gross data rate for one superchannel was 480 Gbit/s, so a net data rate was 400 Gbit/s assuming 20% overhead for the FEC.

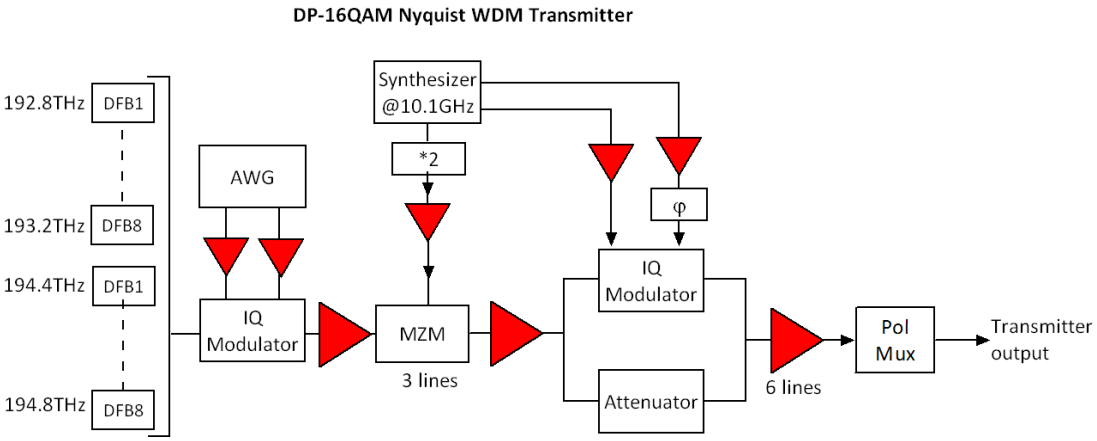

Figure 5.27. Schematic of Nyquist DP-16QAM WDM transmitter [111]

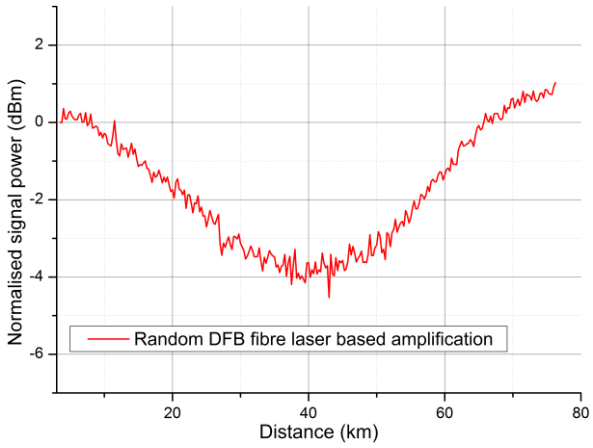

Figure 5.28. Signal power profiles of random DFB fibre based amplifier over 75.6 km Sterlite SMF [111]

The signals from the transmitter were launched into a multi-path recirculating loop which includes three Random DFB fibre laser based spans. Each span has 75.6 km Sterlite OH-LITE™(E) fibre [133], the FBG centred at 1452/1455 nm, and backward -propagated

pump at 1366 nm [111]. The mechanism of random DFB fibre laser based amplifier is explained in detail in Chapter 4, that is, a distributed feedback lasing was generated by Rayleigh backscattering between the fibre and the reflection from the FBG, consequently resulting in the amplification of C band signals. The spread of wavelengths of FBGs was to enhance the gain flatness. The pump power at 1366 nm was about 1.1 W for each span. As signal power profiles of the second span was illustrated in Figure 5.28, the amplification scheme gave relatively symmetric power profile to improve the efficiency of mid-link OPC based nonlinearity compensation [47,92,93]. A signal power variation of ~5 dB is presented, and the power asymmetry level analysis can be found in [92,93].

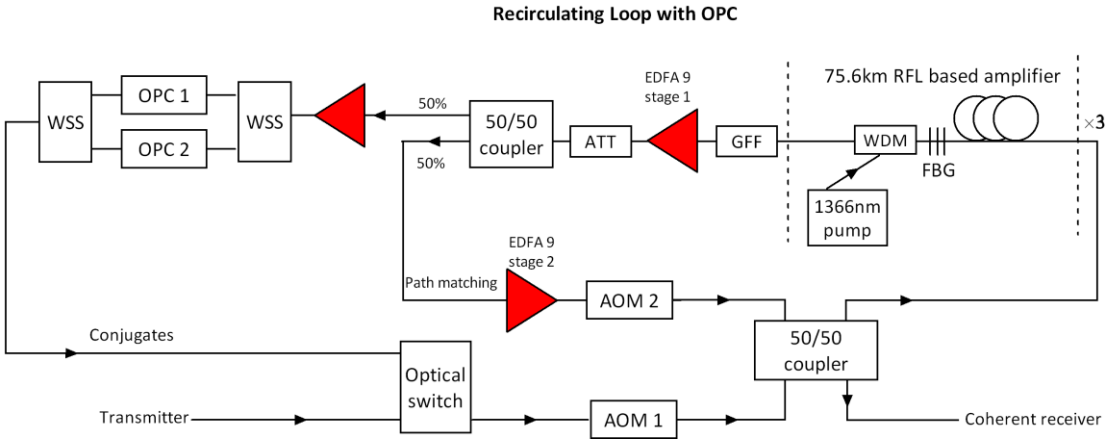

Figure 5.29. Schematic diagram of recirculating loop configuration [112]

The recirculating loop setup was based on the one shown in section 5.3.2.1. However, in order to enable the phase conjugation of both bands simultaneously, an additional fast response optical switch was used together with AOM 1 at the input and AOM 2 in the loop. In the filling time, the optical switch was set to let the signal pass and block out the conjugates, and AOM 1 was set to pass. AOM 2 was disconnected to block the signals. In the first half of the transmission, the optical switch kept the same setting, but AOM 1 was set to block the signal and AOM 2 was set to let the signal transmit. Therefore, after N recirculations, the signal came out from the 50/50 coupler in the loop and consequently the conjugates were obtained via the WSS and OPC path just before the optical switch. In the WSS and OPC path, the two groups of 5 x 400Gbit/s superchannels were amplified before split into two parallel paths using a WSS, giving 12 dBm total power per waveband [112,] and conjugated by two nearly identical single pump polarisation-diverse OPCs as illustrated in section 5.3.1 [77]. The OPCs used independent pump

lasers and aluminium doped highly-nonlinear fibres with lengths, fibre loss and nonlinear coefficients of 100 m, 6.3 dB/km and 6.9 /(W.km), respectively [77,112]. The ZDW ranged from 1552 nm to 1564 nm due to different fibre strain. At the output of each OPC, the residual pumps were blocked by thin-film notch filters. Two conjugated bands were gain-equalised and combined using another WSS at the output. Unlike previous experiments [29,102,113], this ensured that all the channels on both bands were launched simultaneously, and intra-band nonlinearity compensation was also performed on both bands at the same time [111]. In the second filling time, the optical switch was set to block out the signal and let only the conjugates pass. AOMs were set to be the same as the first filling time in order to fill the loop with the conjugated signal. In the second half of the transmission, the settings for AOMs were set to be the same as the first half of the transmission, and the conjugated signal was transmitted for the same number of recirculations. The measurement window was set to be at the last recirculation time, meaning that the transmission distance was N+N multiplied by the span length. Therefore, the output conjugated signal under test was filtered by a 20 GHz tuneable filter, and detected by a conventional coherent receiver. Captured data was processed offline using standard digital signal processing, and BER was derived from bit-wise error counting.

5.3.3.2 Transmission results and discussions

At the beginning, a two-superchannel transmitter was used (one on each band). The BER threshold was assumed to be equal to 1.9×10^{-2}. In Figure 5.30(a), the launch power versus an averaged BER performance over the central sub channel of each superchannel without and with OPC is demonstrated. The optimum launch power was increased from 1 dBm without OPC to 3 dBm with OPC, and the BER performances at 1350 km were significantly improved when using OPC. The same experiment was also performed on the six-superchannel configuration. As shown in Figure 5.30(b), the results were similar to two-superchannel configuration, except that the BER improvement was less significant.

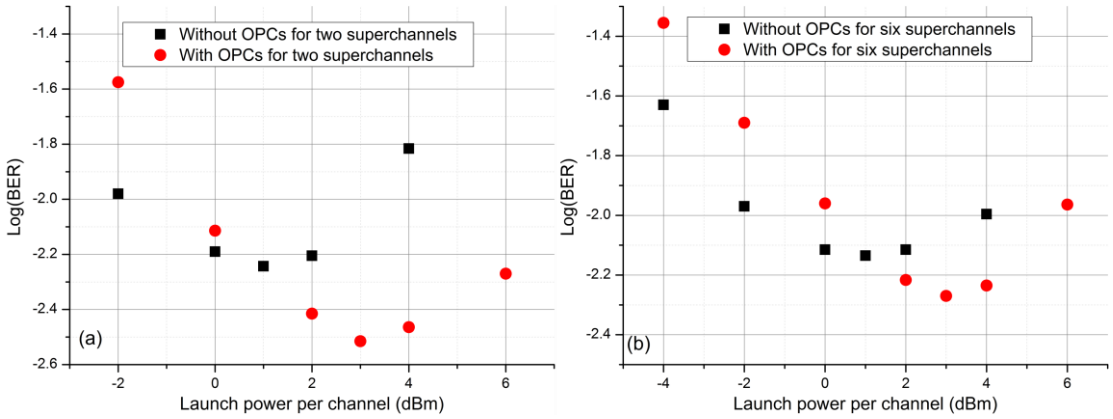

Figure 5.30. Averaged BER versus launch power over the central subchannel of the central superchannel of both upper and lower bands without OPC (black) and with OPC (red) at 1350km. (a). Two superchannels transmitter. (b). Six superchannels transmitter.

The transmission distance versus averaged BER at the optimum launch power was demonstrated for both two and six superchannels configuration. For two superchannels configuration, the maximum reach was improved from 2250 km with no OPC to 3600 km with OPC, achieving 60% improvement in reach. The received spectra were measured at 3600 km with phase conjugation on both bands as shown in Figure 5.31(b).

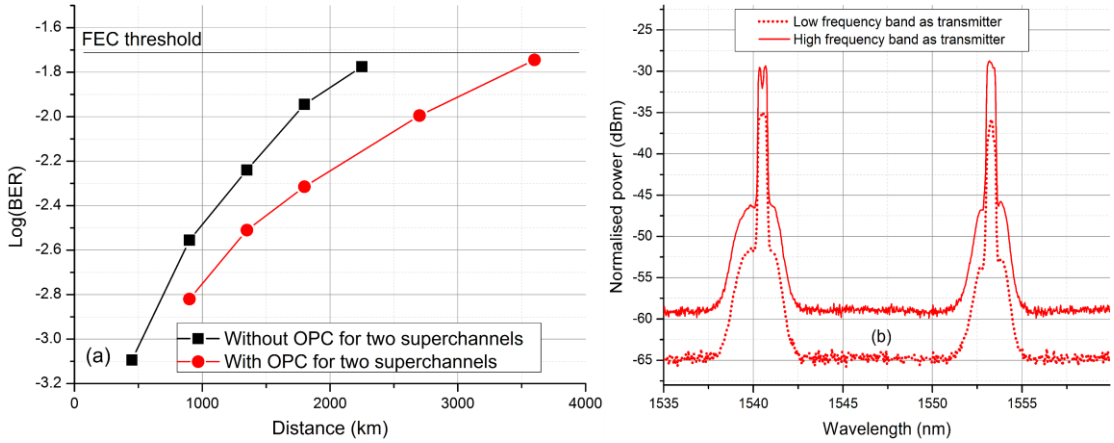

Figure 5.31(a). Averaged BER versus launch power over the central subchannel of each superchannel from both upper and lower bands without OPC (black) and with OPC (red) in two superchannels configuration.(b). Received spectra at 3600km with dual band OPC.

The results for six superchannels configuration were shown in Figures 5.32(a) and (b). The transmission distances were increased from 2025 km without OPC to 2700 km with OPC, which means there was a 33% enhancement in reach. The dip was due to the bias voltage error [111]. In Figure 5.33, all the subchannels of each superchannel without OPC and with OPC for both bands (18 subchannels on each band) were measured at their maximum reach, indicating that a

total record capacity of 2.4 Tb/s was transmitted over 2700 km by using dual band OPC configuration.

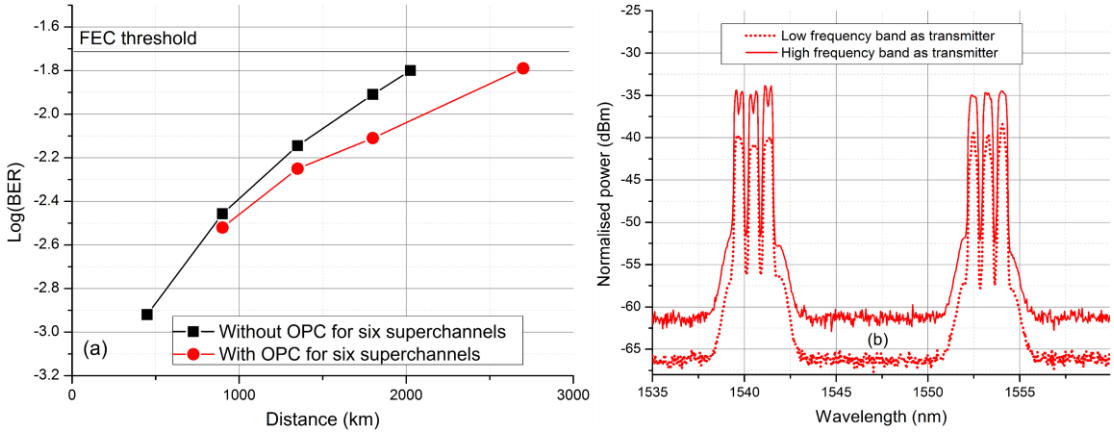

Figure 5.32(a). Averaged BER versus transmission distance over the central subchannel of central superchannel from both upper and lower bands without OPC (black) and with OPC (red) in six superchannels configuration.(b). Received spectra at 2700km with dual band OPC.

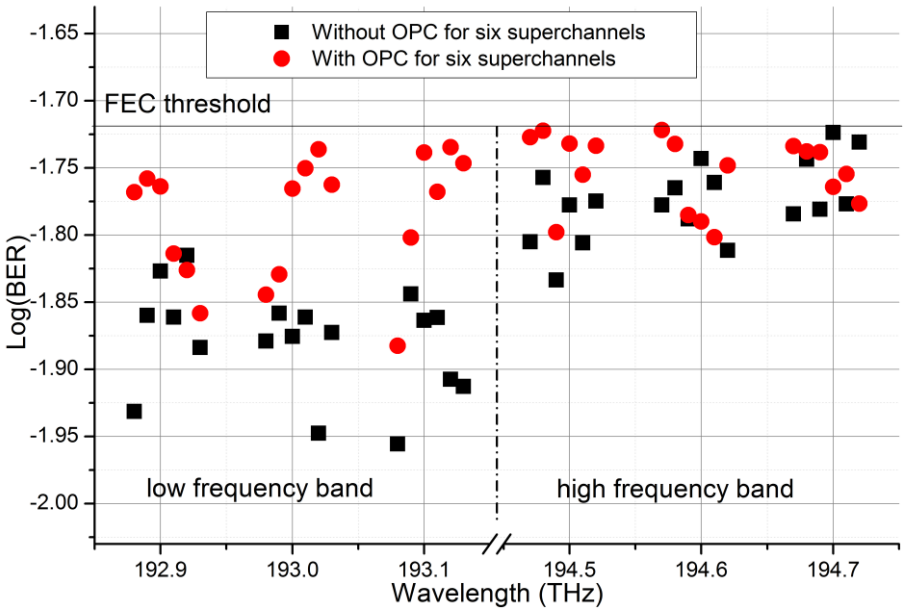

Figure 5.33. BERs of all the subchannels at their maximum reach with six superchannels configuration. (Black points) without dual band OPC at both low and high frequencies bands at 2025km; (Red points) with dual band OPC at both low and high frequencies bands at 2700km.

In Figure 5.34, their transmission distances versus the number of superchannels without and with OPC was demonstrated. It was clearly shown that the maximum reach enhancement using OPC was decreased, as the number of superchannels was increased. As demonstrated in section 5.3.1, the OSNR degradation of the OPC was observed, and this became more severe when more superchannels were added.

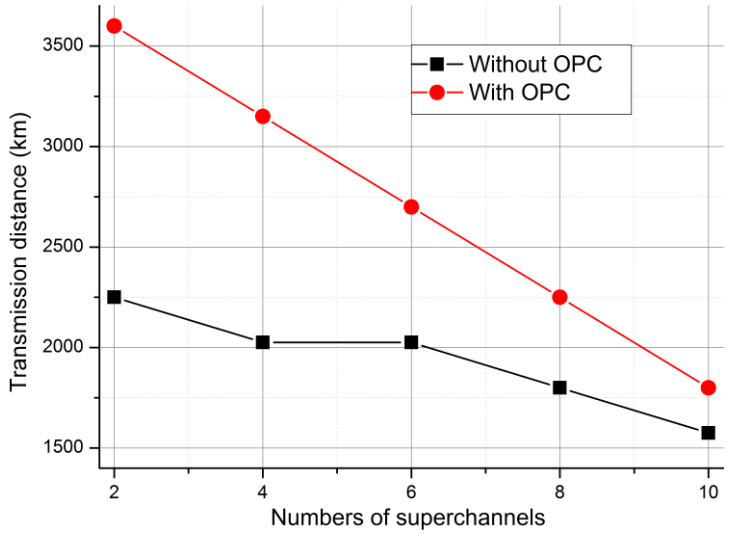

Figure 5.34. Transmission distances versus number of superchannels at the transmitter without and with dual band OPC [111].

Figure 5.35 shows the BER performances of the central subchannel of each central superchannel without and with OPC at their maximum reach. All BERs were below the FEC threshold.

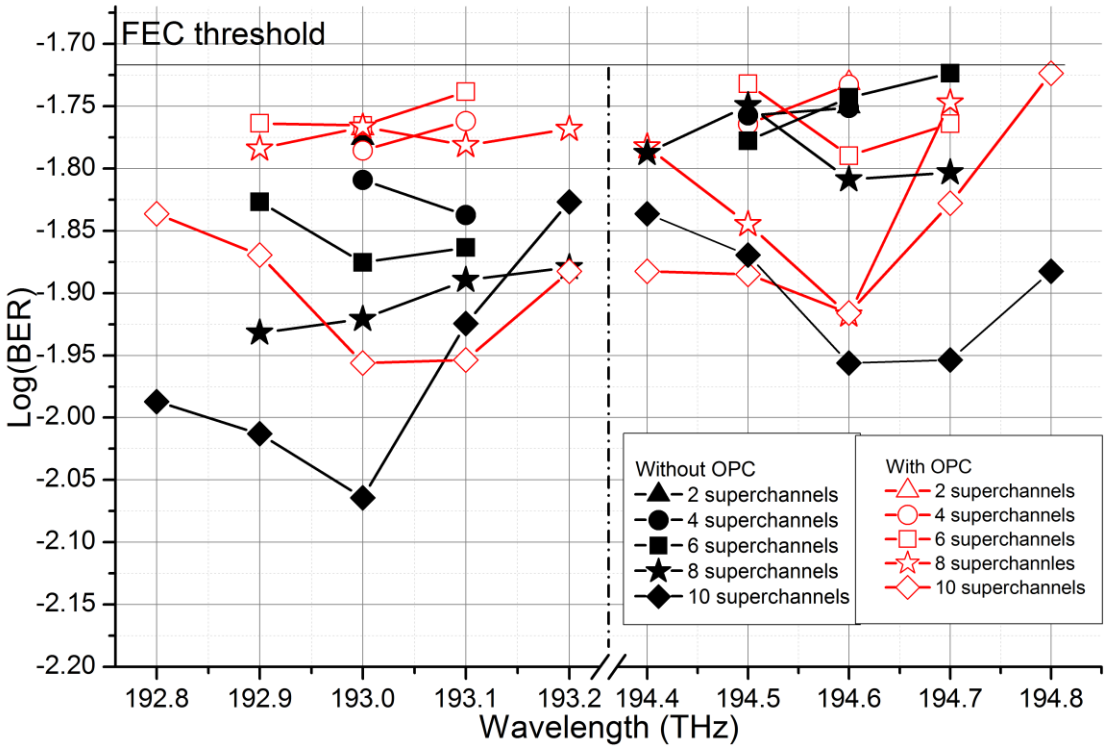

Figure 5.35. Measured BER for the central subchannel of each central superchannel at their maximum reach. (Black points). Without OPC for 2, 4, 6, 8, and 10 superchannels configuration; (Red points). With OPC for 2, 4, 6, 8, and 10 superchannels configuration;

5.3.3.3 Summary

In this section, we demonstrated, for the first time, dual band optical phase conjugation of Nyquist WDM superchannel using Raman amplified 75km SMF spans. The results showed 60% increase in reach (up to 3600 km) for two simultaneously transmitted 400 Gb/s superchannels, and 33% improvement in reach (up to 2700 km) for six superchannels. Therefore, a record total bit rate of 2.4 Tbit/s was achieved by using dual band OPC and RFL based amplification with BW-pumping only. Through both single band and dual band OPC experiments, RFL based amplification technique was proved to be very effective in the transmission performance improvement for mid-link OPC systems.

5.4 Summary and conclusions

In this chapter, the RFL based amplification techniques in long-haul coherent transmission systems are demonstrated in detail. First, in order to evaluate the transmission performance using Raman fibre laser based amplification with two FBGs, a long-haul transmission experiment with 10×100G DP-QPSK WDM signals was implemented. While using second order FW-pump indeed minimised variation in signal power and hence the amplifier noise figure, the introduced Q factor penalty associated with RIN is too high for any overall performance improvement. The Q factor penalty was at least 4.15 dB at 1666 km using symmetric bidirectional pumping. Indeed, backward pumping only gave the best transmission performance in two FBGs based configuration. We attribute the Q factor penalty to increased RIN of the output signal which was transferred from first order Fabry-Perot fibre laser and increased second order FW-pump power. Two types of lasing regimes were observed, a random DFB lasing for BW-pumping only and conventional Fabry-Perot cavity lasing for bidirectional pumping schemes. Second, the similar transmission performances using only random DFB fibre laser were evaluated and also compared this with other conventional distributed Raman schemes (first order and dual order). The best performance was achieved using BW-biased bidirectional pumped random DFB laser based amplification, as it also mitigated the RIN transferred to the signal. Therefore, this scheme is easily modified to meet different link requirement by varying the FW-pump power. In particular, it allows the span profiles to be very symmetric without suffering RIN-induced penalty, which

maximises the benefit of nonlinearity compensation using mid-link OPC. Therefore, the mid-link single band OPC transmission with different amplification techniques is demonstrated. The transmission performances without and with OPC using EDFA, RFL based amplifier with BW-pumping only, and RFL based amplifier with bidirectional pumping are compared. Consequently, RFL based amplification with BW-pumping exceeded dramatically in transmission distance due to relatively high power profile symmetry level and no RIN-induced penalty. Furthermore, long-haul transmission performance using BW-pumping only RFL based amplifier and dual band mid-link OPC is also demonstrated. The results showed 60% increase in reach (up to 3600 km) for two 400 Gb/s superchannels and 33% improvement in reach (up to 2700 km) for six superchannels. This clearly shows that RFL based amplification technique is very effective to combat the nonlinear impairments in mid-link OPC system.

6. Unrepeatered Coherent Transmission Using Raman Fibre Laser Based Amplification

In Chapter 5, the applications of different RFL based amplification techniques in long-haul repeatered transmission systems are reviewed. Due to the number of amplifiers required in the long-haul transmission system (the recirculating loop), the RIN-induced penalty from the FW-pump would be accumulated after each recirculation [15,64], indicating that a way to suppress the RIN of the signal is required to achieve the optimum transmission performance. As demonstrated in Chapter 4 and 5, it has been verified that random DFB fibre laser with bidirectional pumping is able to mitigate the RIN of the signal and improve the transmission performance. However, in an unrepeatered single span transmission system, this RIN-induced penalty is reduced dramatically, because the signal passes through the transmission link only once. In this chapter, the RFL based amplification technique in unrepeatered transmission is demonstrated experimentally.

6.1 Review of unrepeatered transmission in recent years

Unlike long-haul repeatered system, unrepeatered transmission is a cost-effective solution that enables the transmission of very high capacity over relatively short distances (several tens or hundreds of kilometres) with no in-line amplifier or leveller [114]. Alternatively, unrepeatered systems can be deployed for low capacity systems and over much longer distances. There are a number of applications that require unrepetered transmission systems, such as in some remote and hostile areas , or under the sea [114]. As the demand of high capacity increases rapidly, the transmission data rate has been increased from 10 Gb/s, 40 Gb/s to 100 Gb/s. In recent years, there have been a number of 100G or above transmission experiments. As below, table 6.1 shows the experiments summary of unrepeatered transmission systems using advanced modulation format (QPSK and 16QAM), including total capacity, spectral efficiency, modulation format, amplification techniques, transmission distance, and defined FEC threshold.

Capacity/ Spectral Efficiency	**Modulation Format**	**Amplification Techniques**	**Type of Fibre/ Transmission Distance**	**Defined FEC Threshold**
4×120 Gb/s WDM (100GHz spacing) 1.2 b/s/Hz	RZ-DP-QPSK	Bidirectional first order Raman pumping Two ROPAs	Vascade® EX2000 fibre 557km (one channel) 90.2dB loss 523km (4 channels) 84.8dB loss [114]	15% overhead SD-FEC (1.9×10^{-2})
9×40Gb/s (10.7 GHz spacing) 3.73 b/s/Hz	Nyquist-DP-QPSK	Bidirectional-pumped second order random DFB fibre laser based amplification	320 km SMF 65dB loss [115]	7% overhead HD-FEC (3.8×10^{-3})
8×120Gb/s (100GHz spacing) 1.2 b/s/Hz	NRZ-DP-QPSK	Bidirectional first order Raman pumping One ROPA	480.4km (20km pure silica core fibre (PSCF) and 460km Vascade EX2000) 76.6dB loss[116]	15% overhead SD-FEC (1.9×10^{-2})
12×120Gb/s (100G spacing) 1.2 b/s/Hz	NRZ-DP-QPSK	Bidirectional first order Raman pumping	383.5km PSCF Or 342.7km SMF 66.8dB loss[117]	15% overhead SD-FEC (1.9×10^{-2})
26×100Gb/s (50GHz spacing) 2b/s/Hz	RZ-DP-QPSK	Backward third order Raman pumping One ROPA	401km Enhanced PSCF (E-PSCF) 66.9 dB loss [118]	7% overhead HD-FEC (3.8×10^{-3})
40*112Gb/s (50GHz spacing) 2.24b/s/Hz	DP-QPSK	Backward first order Raman pumping	365km (40km with 128μm², 165km with 112μm², 160km with 76μm² A_{eff}) 59.6dB loss[119]	7% overhead HD-FEC (3.8×10^{-3})
60×100Gb/s (40GHz and 50GHz spacing)	RZ-DP-QPSK	Backward third order Raman pumping One ROPA	437km ULL fiber including E-PSCF with 115μm² A_{eff} and ultra large	20% overhead SD-FEC (1.9×10^{-2})

2-2.5 b/s/Hz			A_{eff}-PSCF (ULA-PSCF) with 135μm² A_{eff}) 71dB loss[120]	
32×120Gb/s (100GHz spacing) 1.2 b/s/Hz	DP-QPSK	Bidirectional second order Raman pumping One ROPA	445km A_{eff} managed span using three kinds of OFS ULA low loss fibre 79 dB loss[121]	20% overhead SD-FEC (1.9×10^{-2})
34*120Gb/s (50GHz spacing) 2.4 b/s/Hz	NRZ-DP-QPSK	Bidirectional first order Raman pumping One ROPA.	432.8km standard PSCF 74.4dB loss[122]	15% overhead SD-FEC (1.9×10^{-2})
63×128Gb/s (50GHz spacing) C&L band 2.56b/s/Hz	DP-QPSK	Backward second order Raman pumping One ROPA, L band EDFA	402km (ULAF (ultra-large-area fibre), Tearwave SLA+, Allwave ZWP) 71.1dB loss [123]	20% overhead SD-FEC (1.9×10^{-2})
150×120Gb/s (100GHz spacing) C&L band 1 b/s/Hz	NRZ-DP-QPSK	Bidirectional first order Raman pumping, One ROPA	389.6km ultra-low-loss (ULL) fibre 64.3 dB loss [124]	15% overhead SD-FEC (1.9×10^{-2})
22×115.6 Gb/s or 14×115.6 Gb/s (100GHz spacing) 1b/s/Hz	DP-QPSK	Bidirectional-pumped second order random DFB fibre laser based amplification	327.6km SSMF fibre 64dB loss 352.8km SSMF fibre 68.6 dB loss [89,125]	7% overhead HD-FEC (3.8×10^{-3}) for 327.6km, 15% overhead SD-FEC (1.9×10^{-2}) for 352.8km
7×80Gb/s (10.01 GHz spacing) 7.99 b/s/Hz Net SE 6.95	Nyquist DP-16QAM	EDFA only	253.4 km ULL fibre 41.8 dB loss [126]	15% overhead SD-FEC (1.9×10^{-2})
7×80Gb/s (10.01 GHz	Nyquist DP-16QAM	Bidirectional-pumped second order random	364km Corning ULL fibre	20% overhead SD-FEC

spacing) 7.99 b/s/Hz (Net SE 6.6)		DFB fibre laser based amplification DBP for nonlinear compensation	61.3dB loss [127]	(2.7×10^{-2})
80×224Gb/s (50GHz spacing) 4.48 b/s/Hz	RZ-DP-16 QAM	Backward first order Raman pumping	240km of large A_{eff} (133μm²) fibre 39.1dB loss [128]	7% overhead HD-FEC (3.8×10^{-3})
40×200Gb/s (50 Gb/s spacing) 4 b/s/Hz	DP-16QAM	Backward third order Raman pumping Forward first order Raman pumping One ROPA	363km (E-PSCF and ULA-PSCF) 59.1 dB loss [129]	23% overhead SD-FEC (2.3×10^{-2})
80×200Gb/s (50GHz spacing) 4.4 b/s/Hz	DP-16QAM	Backward third order Raman pumping	321km ULA-PSCF 49.2 dB loss [130]	23% overhead SD-FEC (2.3×10^{-2})
40×256Gb/s (50GHz spacing) 5.12 b/s/Hz Net SE 3.12	DP-16QAM	Backward first order Raman pumping DBP for nonlinear compensation	304km (242km EX3000+62km EX2000) with DBP 44.5 dB loss [131].	28% overhead SD-FEC (1.9×10^{-2})

Table 6.1. Summary of recent unrepeatered transmission work with advanced modulation.

In table 6.1, it can be found that most of current transmission experiments were assisted by remote optical pumped amplifier (ROPA) which consists of a piece of erbium doped fibre located at tens of kilometres away from the transmitter/receiver end [52,132]. However, using in-line ROPA requires accurate calculation of where the ROPA is exactly placed and how much the pump power is required, which increases the complexity of unrepeatered system from both the cost and implementation aspects. As shown in the red shaded row in the table, enabled by random DFB fibre laser with second order bidirectional pumping, the highest capacity over this length of SMF fibre without using ROPA was achieved [89]. This will be demonstrated in detail in the section 6.2. Alternatively, in the blue shaded row, random DFB fibre laser based Raman amplification technique with Nyquist DP-16QAM transmitter with very high net spectra efficiency (SE) of 6.6 b/s/Hz is demonstrated [126,127]. The results show that we successfully

transmitted over 327 km ultra-low-loss (ULL) fibre with the highest SE at this distance. Furthermore, second order bi-directionally pumped RFL based amplifier with multi-channel digital back propagation (MC-DBP) was combined for the first time [127], leading to nonlinearity compensation and transmission performance improvement. This will be discussed in section 6.3.

6.2 Unrepeatered DP-QPSK transmission using random DFB fibre laser based amplification

In unrepeatered transmissions, distributed Raman amplifications offer better noise performance resulting in higher OSNR, compared with EDFA [15]. By using higher order distributed Raman amplifications, the signal power variation can be further reduced leading to highly uniform signal power distribution and better transmission performance [30]. Here, based on the RFL based amplification techniques, the transmission performance using 100G DP-QPSK WDM signals over up to 352.8 km SMF has been investigated without using ROPA or any specialty fibre.

6.2.1 Experimental setup

The experimental setup is illustrated in Figure 6.1. The 100G DP-QPSK WDM transmitter is similar to the one in previous experiments described in Chapter 5. The 100 GHz spaced WDM signal was modulated by an IQ modulator driven at 28.9 Gbit/s, 2^{31}-1 word length with normal and inverted PRBS patterns (with 18 bits relative delay). Then the QPSK modulated signal was polarisation multiplexed to generate 115.6 Gbit/s DP-QPSK WDM signals.

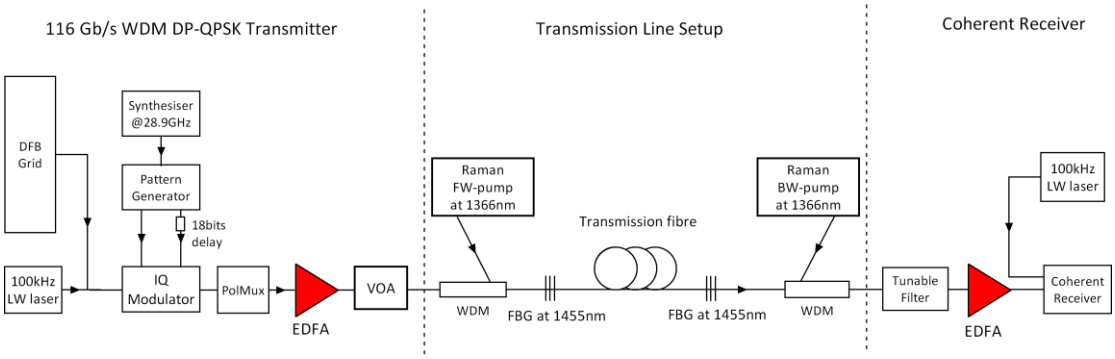

Figure 6.1. Experimental setup of transmitter, transmission link, and coherent receiver

A RFL based amplification technique with bidirectional second order pumping was deployed in the transmission link. The experimental setup was exactly the same as the one shown in Figure

5.24 in Chapter 5 except the fact that the length of the fibre was much longer (327.6 km or 352.8 km in this case). This resulted in the change of the fibre laser generation mechanism. With short length of fibre below 270 km [86], the fibre laser with bidirectional pumping was ultra-long Fabry-Perot fibre laser as explained in section 4.1.4. However, with longer fibre using bidirectional pumping, there were actually two independent random DFB fibre laser (generated by the Rayleigh backscattering of the fibre and one FBG) near both the input and output sections [89]. This was similar to the situation in section 5.2.1 which presented the random DFB fibre laser near the output end only.

The transmission fibre used in the experiments was Sterlite OH-LITE(E) single mode fibre, and the attenuation was ~0.19 dB/km [133]. The measured loss at 1550 nm was ~64 dB for 327.6 km and ~68.6 dB for 352.8 km after splicing the fibre reels together. The measured loss was ~0.6 dB from the input WDM and an FBG, and ~0.8 dB from the output WDM and an FBG.

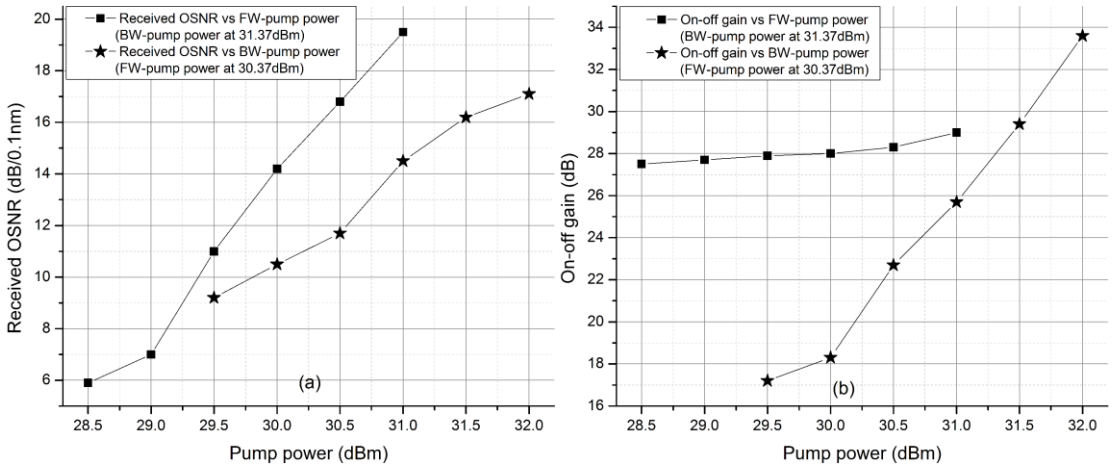

Figure 6.2(a). Received OSNR versus FW-pump power or BW-pump power. (b). On-off gain versus FW-pump power or BW-pump power.

In random DFB fibre laser based amplification over very long span, the OSNR of the output signal can be improved by using more FW-pump power. However, the Raman on-off gain was dominated by the BW-pump [89,134]. Figure 6.2(a) shows the OSNR with the FW-pump when the BW-pump power was fixed at 31.37 dBm, and the OSNR with the BW-pump when the FW-pump power was fixed at 30.37 dBm. It can be seen that the OSNR was improved more rapidly when using more FW-pump power. Figure 6.2(b) illustrates the on-off gain with the FW-pump when the BW-pump power at 31.37 dBm, and the on-off gain with the BW-pump when the FW-pump power was fixed at 30.37 dBm. The on-off gain increased significantly with

the increase of BW-pump power, but remained almost the same when increasing the FW-pump power. The length of the fibre was 327.6 km in this case.

The pump powers were listed in table 6.2. In the optimisation process of pump powers, the target was to achieve as many as channels below the FEC threshold. First, the BW-pump was modified to give enough gain which enabled the signal above the sensitivity of EDFA at the receiver. Second, the FW-pump power was adjusted to give an acceptable OSNR level, and then varied with the signal launch power to find the best Q factors.

Distance (km)	FW-pump power (dBm)	BW-pump power (dBm)
327.6	31.2	32.1
352.8	32.0	32.2

Table 6.2. FW-pump power and BW-pump powers in the experiments

The receiver setup was the same as the one in section 5.2.1. DSP was used offline with standard algorithms for signal recovery and linear transmission impairments compensation. Q factors were calculated from bit-wise error counting, and averaged over 1 million samples.

6.2.2 Transmission results and discussions

The optimum launch power of the central channel over 327.6 km and 352.8 km fibre link was found to be 3 dBm and -4 dBm, respectively. In 327.6 km fibre link, the OSNR was not the major problem, as relatively low FW-pump power was enough to achieve an acceptable OSNR level. Therefore, higher signal launch power was allowed to achieve the balance between ASE noise and nonlinearity. However, for 352.8 km fibre link, due to longer fibre length, the on-off gain had to be increased by increasing the BW-pump power so that the EDFA at the receiver was able to detect the signal. This also led to the increase of ASE noise introduced by the BW-pump. Therefore, in order to maintain the OSNR, the FW-pump power had to be increased, resulting in the lower signal launch power to achieve the balance. Q factors versus launch power sweep can be found in Figure 6.3.

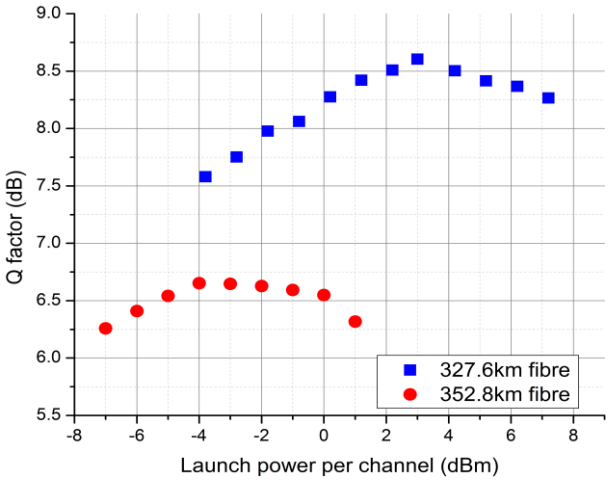

Figure 6.3. Q factors versus launch power over 327.6 km and 352.8km link

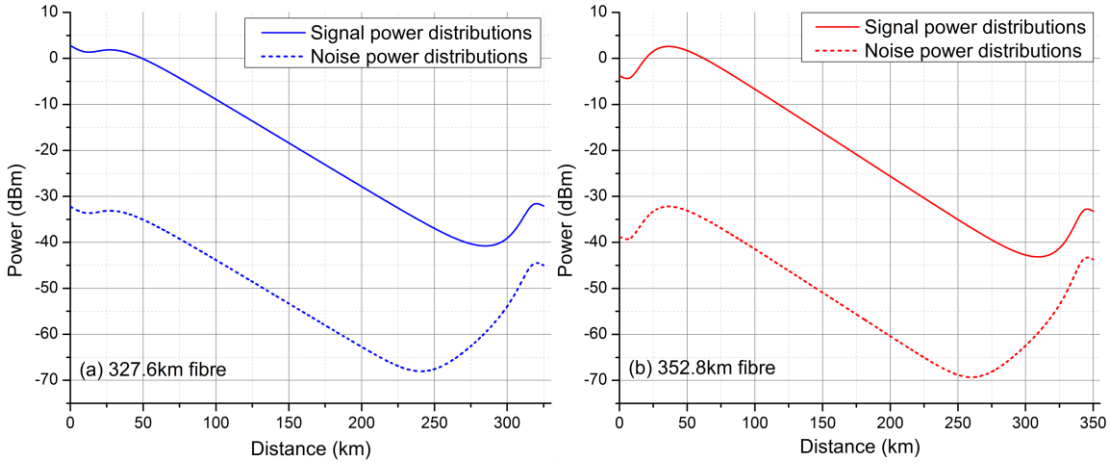

Figure 6.4. Signal and noise power distributions in (a) 327.6km and (b) 352.8km fibre link [89]

The signal and noise power distributions shown in Figure 6.4 were simulated numerically at the optimum launch power of the central channel at 1557 nm [89]. As illustrated in Figure 6.4, the peak-to-peak variations were 43.5 dB for 327.6 km link, and 45.7 dB for 352.8 km fibre link. Compared with signal power distributions in 352.8km, the signal power distribution using less FW-pump power for 327.6 km fibre link significantly distributed the signal power near the input section more uniformly, which caused less nonlinear impairment and consequently led to higher signal launch power.

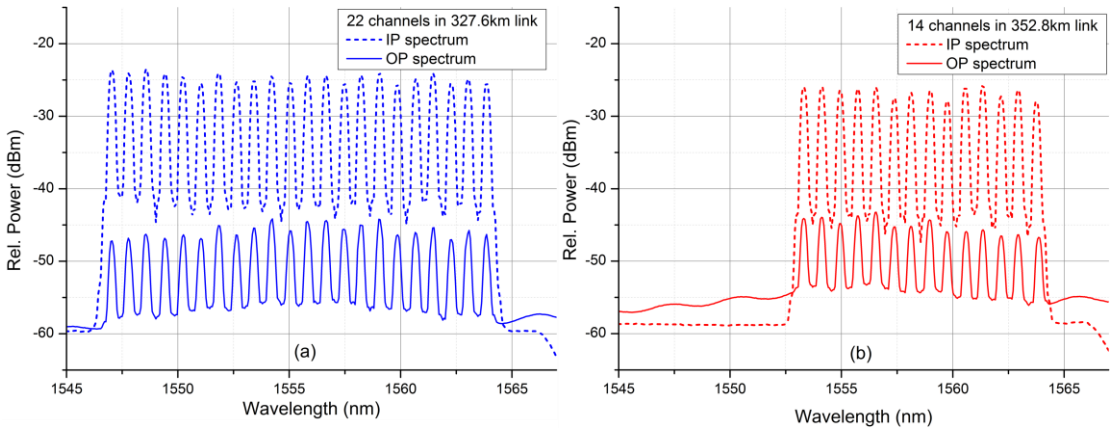

Figure 6.5. Transmitted (Dashed) and received (Solid) spectra (0.1 nm resolution bandwidth) in (a) 327.6km and (b) 352.8km fibre link

The input and output spectra from the transmission span are shown in Figures 6.5(a) and (b). The amplitude is relative power and deliberately differentiated in order to see the differences. No gain flattening filter or pre-emphasis in the transmitter was applied. The gain flatness of the RFL based amplifier (the difference between the output spectra and the input spectra) was within 1 dB for both fibre links, the 327.6 km fibre (17 nm bandwidth) and the 352.8 km fibre (11 nm bandwidth). This gain variation was very low considering only single wavelength pumps were used, and could be further optimised by using additional FBGs or first order pump seed at different wavelengths [90,91].

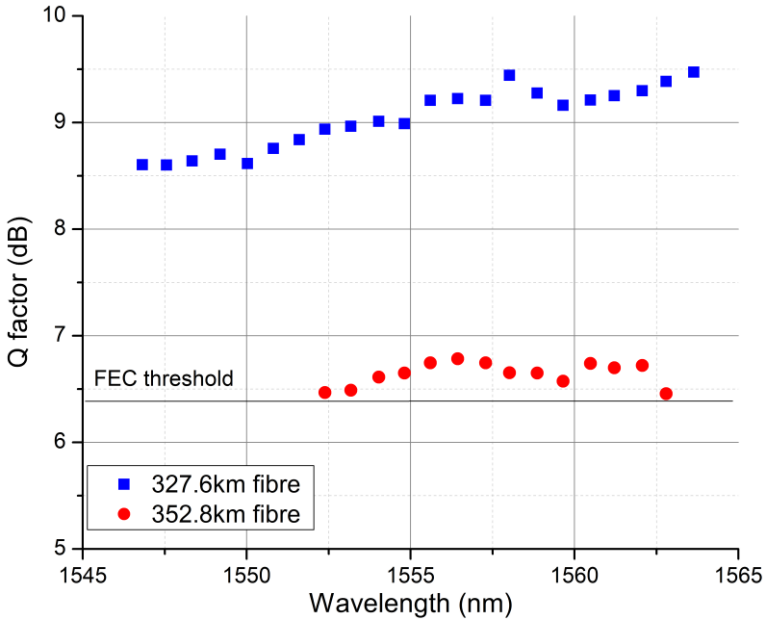

Figure 6.6. Q factors of all the channels measured in (a) 327.6km and (b) 352.8km fibre link

The Q factors for all the channels measured in both fibre links are shown in Figures 6.6. 22

channels at 327.6 km and 14 channels at 352.8 km was able to be transmitted using 15% OH SD-FEC (equivalent to 1.9×10^{-2} in bit error rate). It can be noticed that there were large Q factor margins of more than 2 dB in the 327.6 km fibre link, which could allow for the transmission of additional channels. However, because of the limited number of lasers sources, only 22 channels were able to be transmitted. Alternatively, 7% HD-FEC (equivalent to 3.8×10^{-3}) could be applied, leading to higher net data rate per channel.

6.2.3 Summary

The transmission of 2.2 Tb/s over 327.6 km SMF and 1.4 Tb/s over 352.8 km SMF using 100G DP-QPSK WDM transmitter is experimentally demonstrated. Compared to other transmission experiments summarised in table 6.1, this is the highest capacity achieved in unrepeated transmission at this distance (352.8 km SMF), without using ROPA and any speciality fibre. In [117], with first order bidirectional pumping, 1.2 Tb/s over 342.7 km was transmitted, which was lower capacity and shorter distances. On the other hand, our amplification technique can be also compatible with ROPA when a small amount of pump power at 1480 nm was applied, which would extend the Raman gain bandwidth, improve the gain flatness, and increase the data capacity [91].

It has been proved that random DFB fibre lase based amplifier with second order Raman pumping was compatible with direct detection system using ASK and DP-QPSK transmitter [134]. Its superior performance with 100G DP-QPSK coherent transmission systems has been also demonstrated. Therefore, random DFB fibre laser based amplifier provides a great potential to be used to upgrade the existing installed SSMF link [89].

6.3 Unrepeatered Nyquist DP-16QAM transmission using random DFB fibre laser based amplification and DBP

As we know, the data capacity can be increased by using more advanced modulation format, extending the amplification bandwidth, or reducing the frequency spacing between WDM channels [99]. There has been enormous progress in unrepeatered transmission with 100G DP-QPSK modulation format, as discussed in the last two sections. In order to increase the

capacity, research focus has been shifted to higher modulation format, like DP-16QAM. In the previous experiments with DP-16QAM [128-131], the channel spacing was 50 GHz spacing, indicating that the spectral efficiency was ~4 b/s/Hz. The first and only Nyquist DP-16QAM system was reported in [126], but this was EDFA-only amplified system, and the performances were unimpressive (220 km with no DBP and 254 km with DBP) in comparison with Raman system. Here, unrepeatered transmission of 7×80 Gb/s Nyquist DP-16QAM superchannels (net SE of 6.6 b/s/Hz) over 364 km ultra-low-loss (ULL) fibre is reported, using bi-directionally pumped random DFB fibre laser based amplification technique and multi-channel DBP. This is the first time that multi-channel digital back-propagation (MC-DBP) was applied with higher order bi-directionally pumped Raman fibre laser amplification systems [127].

6.3.1 Experiment setup

The experimental setup of the transmission system is shown in Figure 6.7(a). A 100 kHz linewidth external cavity laser (ECL) at 1550 nm was fed into optical comb generator (OCG) consisted of a MZM driven by 10.01 GHz sinusoidal signal, which generated 7 even-spaced frequency-locked comb lines [126]. The comb was subsequently injected into an interleaver separating odd and even carriers. IQ modulators were to modulate these carriers. Four bit sequences with the length 2^{15} were corresponded to 16 QAM symbols. Then the signals were filtered by root-raised-cosine filters with 0.1% roll-off factor [127]. I and Q signals were loaded into digital-to-analogue convertors (DAC) at 20 GSa/s. The output from each DAC was linked to two cascaded electrical low pass filters (7.5 GHz bandwidth) for the remove of the signal images. The odd and even channels were optically de-correlated with a 3.4 m fibre and passed through a polarisation multiplexing (PM) emulator with 50 ns delay between X and Y polarisations [135]. This formed 7 Nyquist-spaced 10 G Baud DP-16QAM sub-channels, with 7.99 bit/s/Hz gross spectral efficiency. The signal was amplified by an EDFA and followed by a VOA (variable optical attenuator) to control the launch power into the amplified span.

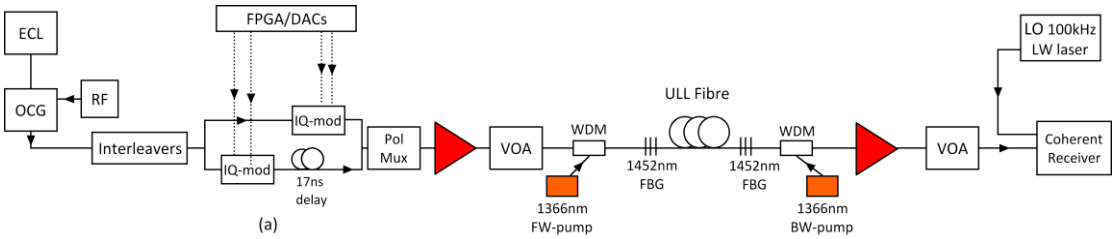

Figure 6.7. Experimental configuration of transmission system [127].

The transmission link was comprised of SMF-28 ULL fibre with an attenuation of 0.165 dB/km. Random DFB fibre laser based amplification wit bidirectional pumping was applied at each end of the fibre span. High depolarised pumps at 1366 nm were used to generate two independent random DFB fibre laser by Rayleigh backscattering and FBGs centred at 1452 nm near the input and output sections [89]. The insertion loss from WDMs couplers and FBGs were ~1.8 dB. The simulated signal and noise power distributions over 327 km and 364 km spans can be found in [127]. The optimisation process of pump powers was similar to the one described in section 6.2.1. The optimum forward and backward pump powers were 30.7 dBm and 31.6 dBm at 327 km, 31.1 dBm and 31.4 dBm at 364 km, providing 36.3 dB and 41.6 dB on-off gain, respectively [127]. The total loss of the link was 54.8 dB for 327 km fibre and 61.3 dB for 364 km fibre.

The received signal was amplified by an EDFA before detected by coherent receiver. The output electrical signal from the photodetectors was sampled at 160 GSa/s using real time oscilloscopes with 63 GHz analogue electrical bandwidth [127]. The DSP and DBP algorithm was used offline and Q factors were derived from bit-wise-error counting. The BER threshold was 20% overhead SD-FEC (equivalent to 2.7×10^{-2} in bit error rate). In comparison with EDFA-based system which the signal power profiles was simply attenuated linearly with the distance, the signal power profiles in random DFB fibre laser based amplification system required more complicated calculation to obtain the correct power evolution at each step of DBP algorithm [7,135].

6.3.2 Transmission results and discussions

Q factor versus launch power based on the central subchannel is illustrated in Figures 6.8(a) and (b) for 327 km and 364 km fibre link, respectively. Also, the launch power versus Q factor was also compared after using multi-channel DBP (70 GHz bandwidth). Without DBP, the optimum performance was found to be 6.6 dB Q factor at -4 dBm power per channel. With DBP, the Q

factor was improved by 2.15 dB up to 8.75 dB and the optimum launch power was also increased from ~-4 dBm to 0 dBm. The similar improvement occurred in 364 km fibre link. The Q factor was also improved by 2 dB, from 4.1 dB to 6.1 dB, and the optimum launch power was improved by 3 dB.

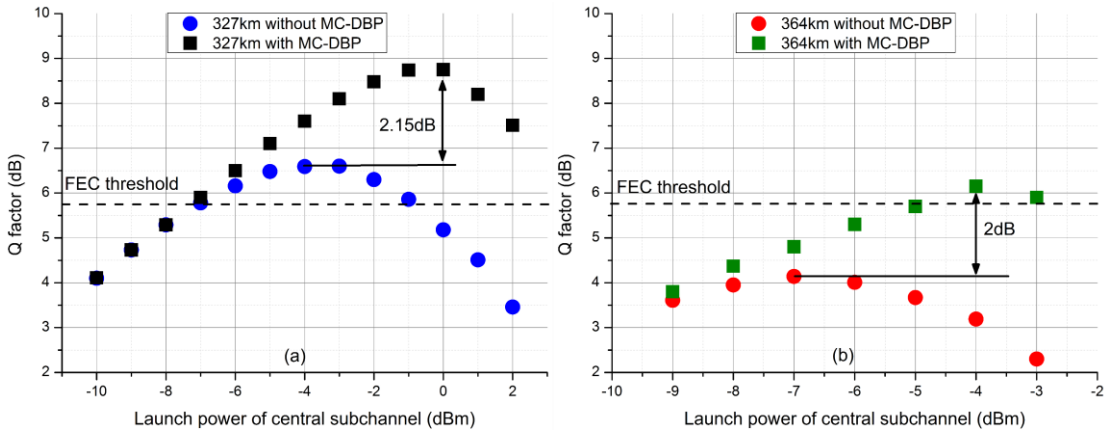

Figure 6.8(a). Q factor versus launch power in 327 km link without and with DBP. (b). Q factor versus launch power in 364km link without and with DBP [127].

The Q factors for all the subchannels were measured at 327 km and 364 km without and with MC-DBP, as demonstrated in Figure 6.9. For 327 km fibre link, we can see that without DBP, all the subchannels exceeded the assumed FEC threshold. After MC-DBP, there was about 2 dB Q factor margin. For 364km fibre link, all the measured subchannels were below the FEC threshold, with an averaged Q factor of 4.1 dB. However, after using MC-DBP, all the subchannels were above the threshold giving an averaged Q factor of 6.1 dB.

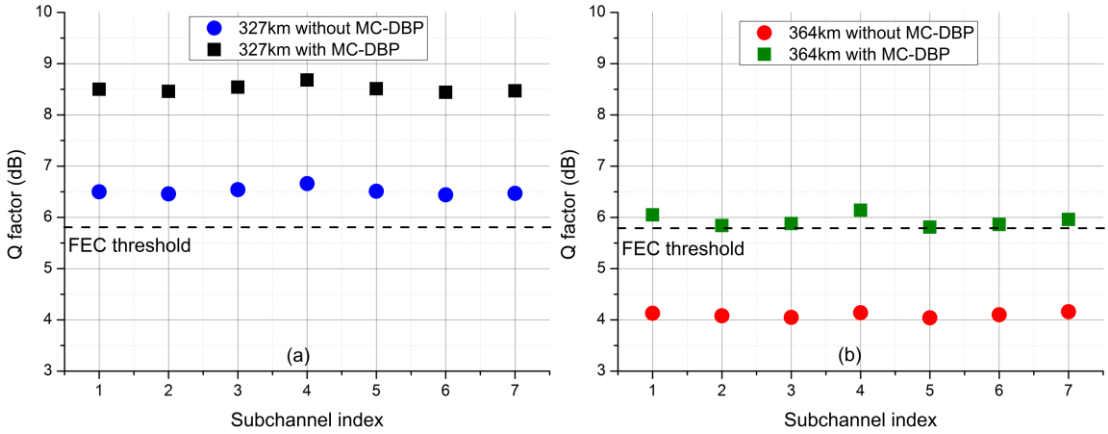

Figure 6.9(a).Q factors of all the subchannels in 327 km link without and with DBP. (b). Q factors of all the subchannels in 364km link without and with DBP [127].

Figure 6.10 shows the transmitted spectra (black) and received spectra at 364 km with the launch

power of -7 dBm (red) and -4 dBm (green). It can be seen that the ASE noise level with -4 dBm launch power was decreased by 2 dB, compared with that at -7 dBm launch power.

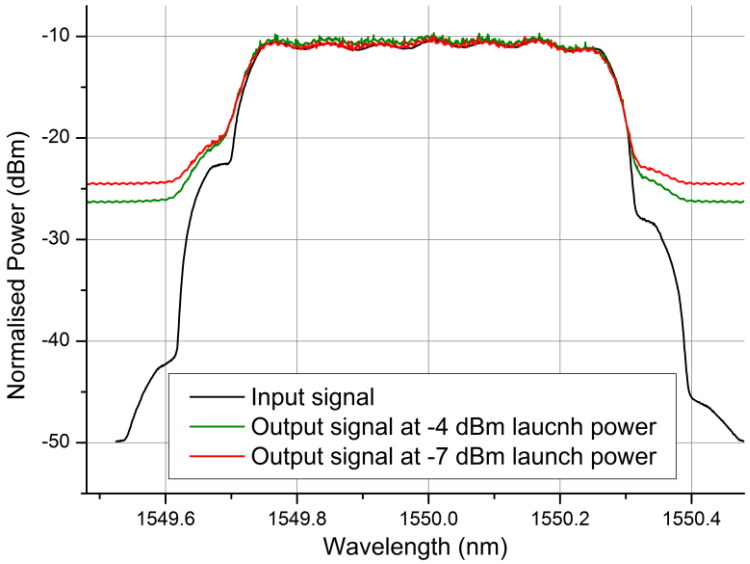

Figure 6.10. Input (black), received spectra at -7dBm (red) and -4dBm (green) using 0.1nm resolution bandwidth in 364km fibre link

6.3.3 Summary

To sum up, transmission with a net SE of 6.6 bit/s/Hz is demonstrated in unrepeatered systems over 364 km of SMF-28 ULL fibre, using bidirectional-pumped second order random DFB fibre laser based amplification and MC-DBP. This result was achieved without using ROPA, but in principle the DBP could be used to further extend the reach of Raman systems by compensating nonlinear impairment. The use of MC-DBP improved the performance in Q factor by 2 dB, enabling an increase of 37 km in the transmission distance.

6.4 Summary and conclusion

In this chapter, the applications of random DFB fibre laser based amplification technique on the unrepeatered transmission system are demonstrated. First, by reviewing and summarising the unrepeatered transmission experiments in recent years, no one has done any unrepeatered coherent transmission experiment with this RFL based amplification technique. In order to fill the research gap, unreapetered transmission of 1.4 Tb/s DP-QPSK WDM signals over 352.8 km SSMF was demonstrated, which turned out to be the highest capacity over this length of fibre without using ROPA or speciality fibre. In addition, this Raman amplification technique is also

compatible with in-line ROPA, which can further improve the transmission performance. Then, as more advanced modulation format (DP-16QAM) has drawn a lot of interest, in co-operation with UCL optical network group, unrepeatered transmission experiment was conducted using Nyquist DP-16QAM superchannel signal with random DFB fibre laser based amplification technique and multi-channel DBP. 7× 10G baud Nyquist DP-16QAM signals with high net spectral efficiency of 6.6 bit/s/Hz (the highest net SE at this transmission distance) was successfully transmitted over 364 km ULL fibre. It was also the first time to combine the second order RFL based amplification and MC-DBP, which significantly improved the transmission performance. In conclusion, it has been demonstrated that random DFB fibre laser based amplification worked well, not only in ASK, DPSK direct detection system [9], but also in DP-QPSK and DP-16QAM coherent detection systems. Therefore, the proposed amplification scheme can be potentially deployed to upgrade the existing installed single mode fibre links [89].

7. Conclusion and future work

7.1 Conclusion

In this thesis, different Raman fibre laser based amplification techniques and their applications in both long-haul and unrepeatered coherent transmission systems are demonstrated in detail.

The insight of different Raman fibre laser based amplifications techniques were characterised from different perspectives, including signal/noise power distributions, RIN, mode structures of induced Raman fibre lasers, and so forth. In terms of the fibre laser regime, it was found for the first time that Raman fibre laser based amplification techniques could be divided into several categories. For an 83 km SMF-28 span which was typical length for repeatered system, they were Fabry-Perot fibre laser based amplification with two FBGs, weak Fabry-Perot fibre laser based amplification with one FBG, and random DFB fibre laser based amplification with one FBG. It was also discovered for the first time that random DFB fibre laser could be achieved even in a closed cavity with two FBGs (or a half-opened cavity with one FBG) when using backward pumping only, as opposed to Fabry-Perot lasing when using bidirectional pumping. In addition to this, for very long spans (>270 km) [86], it was actually two independent random DFB fibre lasers located at both ends when using bidirectional pumping with two FBGs. Table 7.1 shows the summary of different Raman fibre laser based amplification techniques. This classification of Raman fibre laser based amplification formed the crucial basis of the following work.

Raman fibre laser based amplification techniques				
	83 km SMF span			>270 km SMF span
	Two FBGs	One FBG and 3% reflection	One FBG	Two FBGs
BW-pumping only	Random DFB laser	Random DFB laser	Random DFB laser	Random DFB laser
Bidirectional pumping	Fabry-Perot laser	Weak Fabry-Peot laser	Random DFB laser	Random DFB laser

Table 7.1. Different Raman fibre laser based amplification techniques

The characterisations of different Raman fibre laser based amplifications showed that BW-pumping only gave the largest signal power variation, the lowest signal power level, and

consequently the worst noise performance. On the contrary, bidirectional pumping reduced signal power variation, enabled the gain to occur near the input section, and improved the noise performance. However, depending on the configuration of Raman fibre laser based amplification, the RIN might be transferred to the signal from the use of the FW-pump. The results showed that for two FBGs, the RIN transferred to the signal was the most. However, the RIN increase was significantly suppressed with one FBG near the output end and 3.4% reflection near the input end. The RIN did not increase at all when using only single FBG. This was because the lowered reflectivity at the input end led to the reduced efficiency of the Stokes shift from the FW-pump in forward-propagated direction, as no reflector was located near the input. This means that the main amplification was provided by the backward-propagated weak F-P laser/short-cavity random DFB laser. Consequently, the RIN transfer was dramatically reduced, compared to the Fabry-Perot fibre laser with two high reflectivity reflectors on both sides. This is very important for long-haul coherent transmission, because the transmission performance is only limited by ASE noise and nonlinearity without suffering from RIN-induced penalty. Therefore, by further optimising the FBG reflectivity near the input end, there might be a "sweet spot" to achieve the best transmission performance among the RIN-induced penalty, ASE noise, and nonlinear impairment.

In order to evaluate the long-haul transmission performance of these Raman amplifiers, recirculating loop experiments using 10×100G DP-QPSK signals were conducted. For Fabry-Perot laser based amplification with two FBGs, it was found for the first time that the Q factor penalty can be at least 4.15 dB with symmetrical bidirectional pumping, compared with backward pumping only. On the contrary, for random DFB laser based amplification with single FBG, the RIN of the signal was mitigated to the same level as BW-pumping only, so bidirectional pumping with a proper amount of forward pump power offered the best transmission up to 7915 km among all the amplification schemes, exceeding the backward pumping only scheme by 0.6 dB. Compared to bi-directionally pumped Fabry-Perot laser based amplifier, the enhancement on the long-haul transmission distance using this scheme was very significant from 1666 km and 7915 km due to the mitigation of RIN-induced penalty. Furthermore, this scheme was easily modified to meet different link requirement by varying the FW-pump power. In particular, it allowed the signal power profiles to be very symmetric without suffering the RIN-induced penalty,

which potentially maximised the benefit of nonlinearity compensation using mid-link OPC. Raman fibre laser based amplification techniques with BW-pumping only could also provide relatively symmetrical signal power profiles, and achieved effective improvement in maximum reach in both single and dual band mid-link OPC transmission systems by compensating the nonlinear impairments. Using single band OPC, 7×100G DP-QPSK conjugated signal could be transmitted more than 10000 km, compared with only 4000 km using EDFA and 7800 km using BW-pumped Raman fibre laser amplifier without OPC. When using dual band OPC, it showed 60% increase in reach (from 2250 km to 3600 km) for two simultaneously transmitted 400 Gb/s superchannels and 33% improvement in reach (from 2025 km to 2700 km) for six superchannels. The result clearly showed that RFL based amplification technique was very effective to combat the nonlinear impairments in mid-link OPC system.

Additionally, in unrepeatered transmission experiments, random DFB fibre laser based amplification technique achieved excellent transmission performances due to more uniform signal power profiles and improved noise performances. First, the unrepeatered transmission experiments with advanced modulation format in recent years were reviewed, and it was found that no one had done any unrepeatered coherent transmission experiment with this amplification technique. To fill the research gap, unreapetered transmission of 1.4 Tb/s DP-QPSK WDM signals over 352.8 km SMF was demonstrated using bidirectional pumped random DFB laser based amplification technique, which turned out to be the highest capacity over this length of fibre without using ROPA or speciality fibre. Furthermore, unrepeatered transmission experiment was also conducted using Nyquist DP-16QAM superchannel signal with similar random DFB laser amplifier and multi-channel DBP. 7×10G baud Nyquist DP-16QAM signals with net spectral efficiency of 6.6 bit/s/Hz (the highest net SE at this distance) was successfully transmitted over 364 km ULL fibre. It showed that random DFB fibre laser based amplification worked well with DP-QPSK and DP-16QAM coherent transmission systems. Therefore, the proposed scheme can be potentially deployed to upgrade the existing installed SMF links.

In conclusion, different Raman fibre laser based amplification techniques have been characterised and evaluated in both long-haul repeatered and unrepeatered coherent transmission systems over standard single mode fibre. The results shows that random DFB fibre laser based Raman amplification, enables bidirectional second order pumping and offered better transmission

performance, due to the mitigation of the signal RIN (thanks to the reduced efficiency second order Stokes generation) and reduces ASE noise, and is proved to be highly effective to compensate the nonlinear impairment and enhance the transmission distance in mid-link single band and dual band OPC transmission system. In addition, the scheme is also highly flexible and adjustable to meet different requirement on the transmission links.

7.2 Future work

Future works are recommended as a follow up to the research of the PhD study.

For Raman fibre laser based amplification technique used in long-haul transmission system, the bandwidth can be further extended to cover both C and L bands by adding low seed pump power or FBGs at other wavelengths. The application of such technique together with RFL based amplification can be implemented in long-haul transmission system in order to increase the total capacity. In addition, the RIN on the signal might be also further suppressed by varying the reflectivity, the bandwidth, the reflection shape, and the wavelength of the reflector, which might achieve a better trade-off between RIN-induced penalty, ASE noise and nonlinearity to improve the transmission distance.

Raman fibre laser based amplification has been proved to be highly compatible with mid-link OPC transmission system, but the combination of this amplification scheme and digital back propagation or nonlinear Fourier transform in long-haul transmission system has not been demonstrated. Further work can be performed on the combination with the nonlinearity compensation techniques.

In an unrepeatered transmission, it has been demonstrated that in principle Raman fibre laser based amplification technique should be compatible with widely used remote optical pumped amplifier (ROPA). Further work can be also focused on the design and implementation of Raman fibre laser based amplification with in-line ROPA, which can significantly increase the maximum reach and further extend the signal bandwidth. In addition, there have been a lot of unrepeatered transmission systems using the PSCF instead of conventional SMF, which can enhance the OSNR but might degrade the Raman amplifier performance. Further investigations can be focused on RFL based amplification using PSCF with large effective area.

References

1. C. Headley, and G. P. Agrawal, "Raman amplification in fiber optic communication systems," Academic press, 1st edition, 2005.
2. G. P. Agrawal, "Fiber-optic communication systems," Wiley, 4th edition, 2010.
3. C. J. Koester, and E. Snitzer, "Amplification in a Fiber Laser," Applied Optics, 3, 1182-1186, 1964.
4. E. Ip, A. P. T. Lau, D. J. F. Barros, and J. M. Kahn. "Coherent detection in optical fiber systems," Optics Express, 16(2), 753-791, 2008.
5. P. Rosa, "Quasi-lossless data tranmission with ultra-long Raman fibre laser based amplification," PhD thesis, Aston University, 2013.
6. M. N. Islam, "Raman amplifiers for telecommunications," IEEE Journal of Selected Topics Quantum Electronics, 8(3), 548-559, 2002.
7. J. D. Ania-Castañón, "Quasi-lossless transmission using second-order Raman amplification and fiber Bragg gratings," Optics Express 12(19), 4372-4377, 2004.
8. P. Wan and J. Conradi, "Impact of double Rayleigh backscatter noise on digital and analog systems," Journal of Lightwave Technology, 14(3), 288-297, 1996.
9. K. Borzycki, "Fusion splicing and testing of photonic crystal fibers," Journal of Telecommunications and Information Technology, 72-74, 01/2009.
10. ITU, https://www.itu.int/rec/T-REC-G.652/en
11. S. Radic, "Parametric amplification and processing in optical fibers," Laser & Photonics Revews, 2(6), 498-513, 2008.
12. M. E. Marhic, P. A. Andrekson, P. Petropoulos, S. Radic, C. Peucheret, and M. Jazayerifar, "Fiber Optical Parametric Amplifiers in Optical Communication," Laser & Photonics Reviews, 9(1), 50-74, 2015.
13. J. A. Levenson, I. Abram, and Th. Rivera. "Reduction of quantum noise in optical parametric amplification." Journal of Optical Society of America B, 10(11), 2233-2238, 1993.
14. M.F.C. Stephens, I. D. Phillips, M. Tan, and N. J. Doran, "Towards a 'blackbox' FOPA-QPSK amplification, parametric amplifier workshop, 2014.
15. W. S. Pelouch, "Raman Amplification: an Enabling Technology for High-Capacity, Long-Haul Transmission," in Optical Fiber Communication Conference, OSA Technical Digest (online) (Optical Society of America, 2015), paper. W1C.1.
16. M. Shimizu, M. Yamada, M. Horiguchi, T. Takeshita, and M. Okayasu. "Erbium-Doped Fibre Amplifiers With An Extremely High Gain Coefficient of 11dB/mW," Electronics Letters, 26(20), 1641-1643, 1990.
17. C. R. Giles, and E. Desurvire, "Modeling erbium-doped fiber amplifiers," Journal of Lightwave technology, 9(2), 271-283, 1991.
18. R. I. Laming, J. E. Townsend, D. N. Payne, F. Meli, G. Grasso, and E. J. Tarbox, "High-power erbium-doped-fiber amplifiers operating in the saturated regime," IEEE Photonics Technology Letters, 3(3), 1141-1135, 1997.
19. P. C. Becker, N. A. Olson, and J. R. Simpson, "Erbium-doped fibre amplifiers: fundamental and technology," Academic Press, 1st edition, 1999.

20. S. Namiki, and Y. Emori, "Ultrabroad-band Raman amplifiers pumped and gain-equalized by wavelength-division-multiplexed high-power laser diodes," IEEE on Selected Topics in Quantum Electronics, 7(1), 3-16, 2001.
21. C. V. Raman, "A new class of spectra due to secondary radiation," Indian Journal of Physics, 2, 399-419, 1928.
22. OFS, http://fiber-optic-catalog.ofsoptics.com/Asset/TrueWaveRSLWP-120-web.pdf
23. Corning, https://www.corning.com/media/worldwide/coc/documents/Fiber/LEAF%20optical%20fiber.pdf
24. M. A. Camas, "Applications of ultralong Raman fiber lasers in photonics," PhD thesis, Aston University, 2011.
25. R. H. Stolen, J. P. Gordon, W. J. Tomlinson, and H. A. Haus, "Raman response function of silica-core fibers," Journal of Optical Society of America B, 6(6), 1159–1166, 1989.
26. R. H. Stolen, "Polarization effects in fiber Raman and Brillouin lasers," IEEE Journal of Quantum Electronics, 15(10), 1157–1160, 1979.
27. J. Bromage, "Raman Amplification for Fiber Communications Systems," Journal of Lightwave Technology, 22(1), 79-93, 2004.
28. K. Böhm, K. Petermann, and E. Weidel, "Performance of Lyot depolarizers with birefringent single-mode fibers," Journal of Lightwave Technology, 1(1), 71–74, 1983.
29. I. D. Phillips, M. Tan, M.F.C. Stephens, M. McCarthy, E. Giacoumidis, S. Sygletos, P. Rosa, S. Fabbri, S. T. Le, T. Kanesan, S. K. Turitsyn, N. J. Doran, and A. D. Ellis, "Exceeding the nonlinear Shannon limit using Raman fibre based amplification and optical phase conjugation," in Optical Fiber Communication Conference (Optical Society of America, San Francisco, California, 2014), paper. M3C.1.
30. J. D. Ania-Castañón, V. Karalekas, P. Harper, and S. K. Turitsyn, "Simultaneous spatial and spectral transparency in ultralong fiber lasers," Physics Review Letters, 101, 123903, 2014.
31. Md. A. Iqbal, First order Raman amplifier, private email, 2015.
32. Y. Emori, and S. Namiki, "100nm bandwidth flat gain Raman amplifiers pumped and gain equalized by 12 wavelength channel WDM high power laser diodes," OFC 1999, paper. PD19.
33. B. Bristiel, S. Jiang, P. Gallion, and E. Pincemin, "New model of noise figure and RIN transfer in fiber Raman amplifiers," IEEE Photonics Technology Letters, 18(8), 980-982, 2006.
34. J.-C. Bouteiller, K. Brar, S. Radic, J. Bromage, Z. Wang, and C. Headley, "Dual-order Raman pump providing improved noise figure and large gain bandwidth," OFC 2002, PDP FB3-1.
35. P. Harper, A. E. El-Taher, L. Barker, P. Rosa, S. K. Turitsyn, J. Nuno, J. D. Castanon, S. Savory, "Ultra-long Ranam lasers and applications," Presentation, 2011..
36. V. Karalekas, J. D. Ania-Castanon, J. Perez-Gonzalez, X. Chen, L. Zhang, and P. Harper, "Performance optimization of ultra-long Raman laser cavities for quasi-lossless transmission links," Optics Communications, 277(1), 214-218, 2007.
37. C. H. Kim, J. Bromage, and R. M. Jopson, "Reflection-induced penalty in Raman amplified systems," IEEE Photonics Technology Letters, 14(4), 573–575, 2002.
38. R. Hui, M. O'Sullivan, "Fiber optic measurement techniques," Academic Press, 1st edition, 2009.

39. M. Tan, P. Rosa, I. D. Phillips, and P. Harper, "Long-haul Transmission Performance Evaluation of Ultra-long Raman Fiber Laser Based Amplification Influenced by Second Order Co-pumping," in Asia Communications and Photonics Conference(Shanghai, China, 2014), paper. ATh1E. 4.
40. Y. Ohki, N. Hayamizu, S. Irino, H. Shimizu, J. Yoshida, and N. Tsukiji, "Pump laser module for co-propagating Raman amplifier," Furukawa Review 24, 6-12, 2003.
41. M. D. Mermelstein, K. Brar, and C. Headley, "RIN transfer measurement and modelling in dual-order Raman fiber amplifiers," Journal of Lightwave Technology, 21(6), 1518-1523, 2003.
42. M. Tan, P. Rosa, S. T. Le, I. D. Phillips, and P. Harper, "Evaluation of 100G DP-QPSK long-haul transmission performance using second order co-pumped Raman laser based amplification," Optics Express 23(17), 22181-22189, 2015.
43. J. Cheng, M. Tang, A. P. T. Lau, C. Lu, L. Wang, Z. Dong, S. M. Bilal, S. Fu, P. P. Shum, and D. Liu, "Pump RIN-induced impairments in unrepeatered transmission systems using distributed Raman amplifier," Optics Express 23(9), 11838-11854, 2015.
44. A. El-Taher, X. Pang, R. Schatz, G. Jacobsen, S. Popov, and S. Sergeyev, "Noise Characterization and Transmission Evaluation of Unrepeated Raman Amplified DP-16QAM Link," OFC 2015, paper. Th2A.31.
45. J. D. Ania-Castanon, private email, 2015.
46. J. –C. Bouteiller, K. Brar, and C. Headley, "Quasi-constant signal power transmission," ECOC 2002, 3, 1-2.
47. M. Tan, P. Rosa, I. D. Phillips, and P. Harper, "Extended Reach of 116 Gb/s DP-QPSK Transmission Using Random DFB Fiber Laser Based Raman Amplification and Bidirectional Second-order Pumping," in Optical Fiber Communication Conference, OSA Technical Digest (online)(Optical Society of America, 2015), paper. W4E.1.
48. M. Tan, P. Rosa, Md. A. Iqbal, I. D. Phillips, J. Nuno, J. D. Ania-Castanon, and P. Harper, "RIN mitigation in second-order pumped Raman fibre laser based amplification," ACP 2015, paper. AM2E.6.
49. J. Cheng, M. Tang, S. Fu, P. P. Shum, D. Liu, M. Xiang, Z. Feng, and D. Yu, "Relative phase noise estimation and mitigation in Raman amplified coherent optical communication system," Optics Express 22(2), 1257-1266, 2014.
50. J.-C. Bouteiller, K. Brar, J. Bromage, S. Radic, and C. Headley, "Dual-order Raman pump," IEEE Photonics Technology Letters, 15(2), 212-214, 2003.
51. D. Chang, W. S. Pelouch, S. Burtesv, P. Perrier, and H. Fevrier, "Unrepeatered High-speed Transmission Systems," in Optical Fiber Communication Conference, OSA Technical Digest (online) (Optical Society of America, 2015), paper. W4E.3.
52. H. Bissessur, "State of the art in non repeatered optical transmission," in 37th European Conference and Exposition on Optical Communications, OSA Technical Digest (CD) (Optical Society of America, 2011), paper. Tu.3.B.1.
53. S. B. Papernyi, V. I. Karpov, and W. R. L. Clements, "Third-Order Cascaded Raman Amplification," OFC 2002, paper. FB4.
54. S. Papernyi, V. Ivanov, Y. Koyano, and H. Yamamoto, "Six-Order Cascaded Raman Amplification," OFC 2005, paper. OThF4.
55. P. Rosa, G. Rizzelli, M. Tan, P. Harper, and J. D. Ania-Castañón, "Characterisation of

random DFB Raman laser amplifier for WDM transmission," Optics Express 23(22), 28634-28639, 2015.

56. X. H. Jia, Y. J. Rao, F. Peng, Z. N. Wang, W. L. Zhang, H. J. Wu, and Y. Jiang, "Random-lasing-based distributed fiber-optic amplification," Optics Express, 21(5), 6572-6577, 2013.
57. S. Makovejs, "High speed optical fibre transmission using advanced modulation formats," PhD thesis, UCL, 2011.
58. G. P. Agrawal, Lightwave Technology: Components and Devices, Wiley, Hoboken, NJ, 2004.
59. M. Haji, "Optical code division multiple access systems in AlGaInAs/InP," PhD thesis, University of Glasgow, 2012.
60. L. Hou, M. Tan, M. Haji, I. Eddie, J. H. Marsh, "EML based side-wall grating and identical epitaxial layer," IEEE. Photonics Technology Letters, 25(12), 1169-1172, 2013.
61. S. Watson, M. Tan, S. P. Najda, P. Perlin, M. Leszczynski, G. Targowski, S. Grzanka, and A. E. Kelly, "Visible light communications using a directly modulated 422 nm GaN laser diode," Optics Letters, 38(19), 3792-3794, 2013.
62. S. Kumar, and M. J. Deen, "Fiber optic communications: fundamentals and applications," Wiley, 1st edition, 2014.
63. E. Pincemin, J. Karaki, M. Selmi, D. Grot, T. Guillossou, C. Gosset, Y. Jaouen, and P. Ciblat, "100Gbs DP-QPSK Performance over DCF-free legacy system infrastructure." ECOC 2012, paper. Tu.E.2.
64. N. S. Bergano, and C. R. Davidson, "Circulating loop transmission experiments for the study of long-haul transmission systems using erbium-doped fiber amplifiers," Journal of Lightwave Technology, 13(5), 879-888, 1995.
65. P. Harper, Recirculating loop Presentation, Private email, 2013.
66. Y. Jiang, "High-speed electronics signal processing for pre-compensation in optical communications," PhD thesis, Queen's University, Canada, October, 2011.
67. I. Fatadin, D. Ives, and S. J. Savory, "Blind equalization and carrier phase recovery in a 16-QAM optical coherent system," Journal of Lightwave Technology, 27(15), 3042-3049, 2009.
68. E. Valencia, "Digital coherent transceiver for optical communications. From design to implementation," Master thesis, Universitat Politecinca de Catalunya, 2012.
69. S. L. Jansen, D. Borne, P. M. Krummirch, S. Spalter, G.D. Khoen, AND H. Waardt, "Long haul DWDM transmission systems employing optical phase conjugation," IEEE Journal of Selected topics in quantum electronics, 12(4), 505-520, 2006.
70. R. H. Stolen and A. Ashkin, "Optical Kerr effect in glass waveguide", Applied Physics Letters, 8(6), 294-296, 1973.
71. M. Blazek, S. Hartmann, A. Molitor, and W. Elsaesser, "Unifying intensity noise and second-order coherence properties of amplified spontaneous emission sources", Optics Letters, 36 (17), 3455-3457, 2011.
72. R. Paschotta, tutorial on "Fiber Amplifiers", part 4 on amplified spontaneous emission.
73. S. J. Savory, "Digital coherent receivers: key concepts and subsystems," IEEE Journal of Selected Topics in Quantum Electronics, 16(5), 1164-1179, 2011.
74. A. D. Ellis, M. E. McCarthy, M. A. Z. Al-Khateeb, and S. Sygletos, "Capacity limits of systems employing multiple optical phase conjugators," Optics Express 23(16), 20381-20393

2015.

75. D. S. Millar, S. Makoevjs, C. Behrens, S. Hellerbrand, R. I. Killley, P. Bayvel, and S. J. Savory, "Mitigation of Fiber Nonlinearity Using a Digital Coherent Receiver," IEEE Selected Topics in Quantum Electronics, 16(5), 1217-1226, 2010.
76. D. Rafique, J. Zhao, and A. D. Ellis, "Fundamental limitations of digital back-propagation in coherent transmission systems," ICTON 2011.
77. M.F.C. Stephens, M. Tan, I. D. Phillips, S. Sygletos, P. Harper, and N. J. Doran, "1.14 Tb/s DP-QPSK WDM polarization-diverse optical phase conjugation," Optics Express 22(10), 11840-11848, 2014.
78. T. J. Ellingham, J. D. Ania-Castañón, R. Ibbotson, X. Chen, L. Zhang, and S. K. Turitsyn, "Quasi-lossless optical links for broad-band transmission and data processing," IEEE Photonics Technology Letters, 18(1), 268-270, 2006.
79. S. K. Turitsyn, S. A. Babin, D. Churkin , Ilya D. Vatnik, Maxim Nikulin, and E. V. Podivilov, "Random distributed feedback fibre lasers," Physics Reports, 542, 133-193, 2014.
80. D. V. Churkin, S. A. Babin, A. E. El-Taher, P. Harper, S. I. Kablukov, V. Karalekas, J. D. Ania-Castañón, E. V. Podivilov, and S. K. Turitsyn, "Raman fiber lasers with a random distributed feedback based on Rayleigh scattering," Physics Reviews A, 82, 033828, 2010.
81. J. Karaki, E. Giacoumidis, D. Grot, T. Guillossou, C. Gosset, R. Le Bidan, T. Le Gall, Y. Jaouën, and E. Pincemin, "Dual-polarization multi-band OFDM versus single-carrier DP-QPSK for 100 Gb/s long-haul WDM transmission over legacy infrastructure," Optics Express 21(14), 16982-16991, 2013.
82. C. R. S. Fludger, V. Handerek, and R. J. Mears, "Pump to signal RIN transfer in Raman fiber amplifiers," Journal of Lightwave Technology, 19(8), 1140-1148, 2001.
83. J. Bromage, J.-C. Bouteiller, H. J. Thiele, K. Brar, L. E. Nelson, S. Stulz, C. Headley, R. Boneck, J. Kim, A. Klein, G. Baynham, L. V. Jorgensen, L. Gruner-Nielsen, R. L. Lingle, and D. J. DiGiovanni, "WDM transmission over multiple long spans with bidirectional Raman pumping," Journal of Lightwave Technology, 22(1), 225-232, 2004.
84. Agilent technologies, Product note 86100-7, "Digital analyser(DCA), Measure Relative intensity noise (RIN)."
85. C. O'Brien, M. L. Majewski, and A. D. Rakic, "A critical comparison of high speed VCSEL Characterisation techniques," Journal of Lightwave Technology, 25(12), 597-605, 2007.
86. S. K. Turitsyn, J. D. Ania-Castañón, S. A. Babin, V. Karalekas, P. Harper, D. Churkin, S. I. Kablukov, A. E. El-Taher, E. V. Podivilov, and V. K. Mezentsev, "270-km ultralong Raman fiber laser," Physics Review Letters, 103, 13301 1-4, 2009.
87. W. L. Zhang , Y. J. Rao, J. M. Zhu, Z. X. Yang, Z. N. Wang, and X. H. Jia, "Low threshold 2nd-order random lasing of a fiber laser with a half-opened cavity," Optics Express, 20(13), 14400-14405, 2012.
88. M. Alcon-Camas, and J. D. Ania-Castañón, "RIN transfer in 2nd-order distributed amplification with ultralong fiber lasers," Optics Express, 18(23), 23569-23575, 2010.
89. P. Rosa, M. Tan, I. D. Phillips, S. T. Le, J. D. Ania-Castanon, S. Sygletos, and P. Harper, "Unrepeatered DP-QPSK transmission over 352.8km SMF using random DFB fiber laser amplification," IEEE Photonics Technology Letters, 27(11), 1189-1192, 2015.
90. M. Alcon-Camas, A. E. El-Taher, J. D. Ania-Castanon, and P. Harper, "Gain bandwidth optimisation and enhancement in ultra-long Raman fibre laser based amplifiers," in ECOC

2010, P.1.17.

91. A. E. Bednyakova, M. P. Fedoruk, P. Harper, and S. K. Turitsyn, "Hybrid gain-flattened and reduced power excursion scheme for distributed Raman amplification," Optics Express, 21(24), 29140-29144, 2013.
92. P. Rosa, S. T. Le, G. Rizzelli, M. Tan, and J. D. Ania-Castanon, "Signal power asymmetry optimisation for optical phase conjugation using random DFB laser Raman amplifier," ACP 15, paper. AM3D.5.
93. K. Solis-Trapala, T. Inoue, and S. Namiki, "Signal Power Asymmetry Tolerance of an Optical Phase Conjugation-Based Nonlinear Compensation System," in Proc. of ECOC 2014, Cannes, France, Sept. (2014), paper. We. 2.5.4.
94. J. Nuño, M. Alcon-Camas, and J.D. Ania-Castañón, "RIN transfer in random distributed feedback fiber lasers," Optics Express 20(24), 27376-27381, 2012.
95. J. D. Ania-Castanon, V. Karalekas, J. Perez-Gonzalez, P. Harper, X. Chen and L. Zhang, "Signal power excursion and pump efficiency in Quasi-lossless ultra-long Raman laser links," in ECOC 2006, 24-28 Sept. 2006.
96. P. Rosa, S. T. Le, G. Rizzelli, M. Tan, and J. D. Castanon, "Signal power asymmetry optimisation for optical phase conjugation using Raman amplification," Optics Express, 23(25), 31772-31778, 2015.
97. M. Tan, P. Rosa, S. T. Le, Md. A. Iqbal, I. D. Phillips, and P. Harper, "Transmission performance improvement using random DFB laser based Raman amplification and bidirectional second-order pumping," submitted to Optics Express, Oct. 2015.
98. S. J. Savory, G. Gavioli, E. Torrengo, and P. Poggiolini, "Impact of interchannel nonlinearities on a split-step intrachannel nonlinear equalizer," IEEE Photonics Technology Letters, 22(10), 673-675, 2010.
99. J. E. Prilepsky, S. A. Derevyanko, K. J. Blow, I. Gabitov, and S. K. Turitsyn, "Nonlinear Inverse Synthesis and Eigenvalue Division Multiplexing in Optical Fiber Channels," Physics Review Letters, 113, 013901, 2014.
100. S. T. Le, J. E. Prilepsky, M. Kamalian, P. Rosa, M. Tan, J. D. Ania-Castañón, P. Harper, and S. K. Turitsyn, "Modified Nonlinear Inverse Synthesis for Optical Links with Distributed Raman Amplification," ECOC 2015, paper. Tu.1.1.3.
101. S. L. Jansen, D. Borne, B. Spinnler, S. Carabro, H. Suche, P. M. Krummrich, W. Sohler, G.-D. Khone, and H. De. Waardt, "Optical phase conjugation for ultra long haul phase-shift-keyed transmission," Journal of Lightwave Technology, 24(1), 54-64, 2006.
102. I. Sackey, F. D. Ros, J. K. Fischer, T. Richter, M. Jazayerifar, C. Peucheret, K. Petermann, and C. Schubert, "Kerr Nonlinearity Mitigation: Mid-Link Spectral Inversion versus Digital Backpropagation in 5×28-GBd PDM 16-QAM Signal Transmission", Journal of Lightwave Technology, 33(9), 1821-1827, 2015.
103. M. F. C. Stephens, M. Tan, I. D. Phillips, S. Sygletos, P. Harper, and N. J. Doran, "1THz-Bandwidth Polarization-Diverse Optical Phase Conjugation of 10x114Gb/s DP-QPSK WDM Signals," in Optical Fiber Communication Conference, OSA Technical Digest (online) (Optical Society of America, 2014), paper. W3F.6.
104. M. Morshed, L.B. Du, B. Foo, M. D. Pelusi, and A. J. Lowery, "Optical phase conjugation for nonlinearity compensation of 1.21 Tb/s Pol-Mux coherent optical OFDM," OECC/PS 2013.

105. I. D. Phillips and M.F.C Stephens, "OPC results summary presentation", private email, 2013.
106. P. Minzioni, P. Harper, V. Pusino, L. Barker, C. Langrock, M. M. Fejer, J. Ania-Castanon, and V. Degiorgio, "Optical phase conjugation for dispersion and nonlinearity compensation in a 1600km, 42Gb/s quasi-lossless system," in Advance in Optical Science Congress, OSA Technical digest, paper. NThA5.
107. M. D. Pelusi, and B. J. Eggleton, "Optically tunable compensation of nonlinear signal distortion in optical fiber by end span optical phase conjugation," Optics Express, 20(7), 8015-8023, 2012.
108. D. Lavery, C. Behrens, S. Makovejs, D. S. Millar, R. I. Killey, S. Savory, and P. Bayvel, "Long haul transmission of PS-QPSK at 100Gb/s using digital backpropagation," IEEE Photonics Technology Letters, 24(3), 176-178, 2012.
109. D. Rafique, and A.D.Ellis, "Impact of signal-ASE four-wave mixing on the effectiveness of digital back-propagation in 112 Gb/s PM-QPSK systems," Optics Express, 19(4), 3449-3454, 2011.
110. D. Qian, M.-F. Huang, E. Ip, Y.-K. Huang, Y. Shao et al.," 101.7-Tb/s(370×294-Gb/s) PDM-128QAM-OFDM Transmission over 3×55-kmSSMF using Pilot-based Phase Noise Mitigation," in Optical Fiber Communication Conference, Anaheim, California, 2011, paper. PDPB5.
111. A. D. Ellis, I. D. Phillips, M. Tan, M.F.C. Stephens, M. E. McCarthy, M.A.Z. Al Kahteeb, M. A. Iqbal, A . Perentos, S. Fabrri, V. Gordienko, D. Lavery, G. Liga, G. Saaverdra, R. Maher, S. Sygletos, P. Harper, N. J. Doran, P. Bayvel, and S. K. Turitsyn, "Enhanced superchannel transmission using phase conjugation" ECOC 2015, paper. We. 2.6.4.
112. A. D. Ellis, M. Tan, M. A. Iqbal, M.A.Z. Al Khateeb, V. Gordienko, G. Saavedra. M, S. Fabbri, M.F.C. Stephens, M. E. McCarthy, A. Perentors, I. D. Phillips, D. Lavery, G. Liga, R. Maher, P. Harper, N. J. Doran, S. K. Turitsyn, S. Sygletos, P. Bayvel, "4 Tbit/s transmission reach enhancement using 10×400Gbit/s super-channels and polarisation insensitive dual band optical phase conjugation," provisionally accepted by Journal of Lightwave Technology, 2015.
113. K. Solis-Trapala, M. D. Pelusi, H. N. Tan, T. Inoue, and S. Namiki, "Transmission Optimized Impairment Mitigation by 12 Stage Phase Conjugation of WDM 24x48 Gb/s DP-QPSK Signals," OFC 2015, paper. Th3C.2.
114. T. J. Xia, D. L. Peterson, G. A. Wellbrock, D. Chang, P. Perrier, H. Fevrier, S. Ten, C. Tower, and G. Mills, "557-km Unrepeatered 100G Transmission with Commercial Raman DWDM System, Enhanced ROPA, and Cabled Large Aeff Ultra-Low Loss Fiber in OSP Environment," in Optical Fiber Communication Conference: Postdeadline Papers, (Optical Society of America, 2014), paper. Th5A.7.
115. P. Rosa, M. S. Erkilinç, R. Maher, M. Paskov, S. Kilmurray, M. Tan, P Harper, I. D. Philips, A. D. Ellis, J. D. Ania-Castañón, B. C. Thomsen, S. Savory, R. Killey, P. Bayvel, "Nyquist-WDM PDM-QPSK Transmission over SMF-28 Fibre Using URFL Amplification," ICTON 2014.
116. D. Chang, P. Patki, S. Burtsev, and W. Pelouch, "8*120Gb/s transmission over 80.8dB/480.4km unrepeated span," OFC/NFOEC 2013, paper. JTh2A.42.
117. D. Chang, P. Patki, S. Burtsev, and W. Pelouch, "Real-time processed 12×120Gb/s unrepeatered transmission over 383.5km PSC fibre and 342.7km SMF without ROPA," IPC

2012, paper. ThS2.A.

118. D. Mongardien, P. Bousselet, O. Bertran-Pardo, P. Tran, and H. Bissessur, "2.6Tb/s (26*100Gb/s unrepeated transmission over 401km using PDM-QPSK with a coherent receiver," ECOC 2009, paper. 6.4.3.
119. J. D. Downie, J. Hurley, J. Cartledge, S. Ten, S. Bickham, S. Mishra, X. Zhu, and A. Kobyakov, "40*112Gb/s transmission over an unrepeated 365km Effective Area-managed span comprised of ultra-low loss optical fibre," ECOC 2010, paper. We.7.C.5.
120. H. Bissessur, S. Etienne, P. Bousselet, S. Ruggeri, and D. Mongardien, "6Tb/s unrepeated transmission of 60*100Gb/s PDM-RZ-QPSK channels with 40GHz spacing over 437km," ECOC 2012, paper. Mo.1.C.3.
121. B. Zhu, P. Borel, K. Carlson, X. Jiang, D. W. Peckham, and R. Jr. Lingle, "Unrepeated transmission of 3.2Tb/s (32*120Gb/s over 445km fiber link with Aeff managed span," OFC/NFOEC 2013, paper. OTu2B.2.
122. D. Chang, P. Patki, S. Burtsev, and W. Pelouch, "Real-time processed 34*120Gb/s transmission over 432.8km unrepeated link with legacy fiber and span loss of 74.4 dB," ECOC 2012, pape. 4.02.
123. B. Zhu, P. Borel, K. Carlson, X. Jiang, D. W. Peckham, R. Lingle, J. M. Law, J. Rooney, and M. F. Yan, "Unrepeatered transmission of 6.3 Tb/s (63×128Gb/s) over 402km fiber link," IEEE Photonics technology letters, 26(17), 1711-1714, 2014.
124. D. Chang, H. Pedro, P. Perrier, H. Fevrier, S. Ten, C. Towery, I. Davisand S. Makovejs, "150×120 Gb/s unrepeatered transmission over 333.6 km and 389.6 km (with ROPA) G.652 fiber," in Proc. ECOC 2014, paper. Tu.1.5.4.
125. P. Rosa, M. Tan, I. D. Phillips, S. T. Le, J. D. Ania-Castanon, S. Sygletos, and P. Harper, "Unrepeatered DP-QPSK transmission over 350 km standard fibre using URFL based amplification," ACP 2014, paper. ATh4E.5.
126. L. Galdino, G. Liga, D. Lavery, R. Maher, T. Xu, M. Sato, R. I. Killey, S. Savory, B. C. Thomsen, and P. Bavyel, "Unrepeated Transmission over 253.4 km Ultra Low Loss Fiber Achieving 6.95 b/s/Hz SE using EDFA-only Pre-amplification," ECOC 2014, p.5.2.
127. L. Galdino, M. Tan, D. Lavery, P. Rosa, R. Maher, I. D. Phillips, J. D. Ania Castañón, P.Harper, R. I. Killey, B. C. Thomsen, S. Makovejs, and P. Bayvel, "Unrepeatered Nyquist PDM-16QAM transmission over 364 km using Raman amplification and multi-channel digital back-propagation," Optics Letters, 40(13), 3025-3028, 2015.
128. S. Oda, T. Tanimura, Y. Cao, T. Hoshida, Y. Akiyama, H. Nakashima, C. Ohshima, K. Sone, Y. Aoki, M. Yan, Z. Tao, J. C. Rasmussen, Y. Yamamoto, and T. Sasaki, "80*224Gb/s unrepeated transmission over 240km of large Aeff pure slica core fiber without remote optical pre-amplifier." ECOC 2011, paper. Th.13.C.7.
129. H. Bissessur, C. Bastide, S. Dubost, S. Etienne, and D. Mongardienn, "8Tb/s unrepeatered transmission of real-time processed 200Gb/s PDM-16QAM over 363km," ECOC 2014, paper. Tu.1.5.3.
130. H. Bissessur, C. Bastide, S. Dubost, and S. Etienne, "80×200 Gb/s 16-QAM unrepeatered transmission over 321km with third order Raman amplification," OFC 2015, paper. W4E.2.
131. J. Downie, J. Hurley, I. Roudas, D. Pikula, and J. A. Garza-Alanis, "Unrepeatered 256 Gb/s PM-16QAM transmission over up to 304 km with simple system configurations," Optics Express, 22(9), 10256-10261, 2014.

132. D. Chang, W. S. Pelouch, S. Burtsev, B. Clesca, P. Perrier, H. A. Fevrier, "Advanced technologies for unrepeatered transmission systems and their applications," ACP 2014, paper. ATh4G.4..
133. Sterlite Technologies, http://www.sterlitetechnologies.com/.
134. P. Rosa, J. D. Ania-Castanon, and P. Harper "Unrepeatered DPSK transmission over 360 km SMF-28 fibre using URFL based amplification," Opt. Express, 22(8), 9687-9692, 2014.
135. R. Maher, T. Xu, L. Galdino, M. Sato, A. Alvarado, K. Shi, S. J. Savory, B. C. Thomsen, R. I. Killey and P. Bayvel, "Spectrally Shaped DP-16QAM Super-Channel Transmission with Multi-Channel Digital Back-Propagation," Scientific Reports, 5, 2015.
136. M. D. Mermelstein, K. Brar, and C. Headley, "RIN transfer suppression technique for dual-order Raman pumping schemes," IEEE Photonics Technology Letters, 15(10), 1354-1356, 2003.
137. W. Forysiak, D. Govan, I. McClean, B. Nayar, O. Olubodun, and N. J. Doran, "Analysis of extended range variable gain hybrid Raman-EDFAs in systems using Nyquist-WDM 100G/200G PM-QPSK/16QAM." OFC 2014, paper. W2A.8.
138. D. Nesset, MFC. Stephens, AE. Kelly, C. Gillbertas, J. Reed, K. A. Williams, S. Bouchoule, R. Kashyap, A. D. Ellis, and D. G. Moodie, "40 Gbit/s transmission over 186.6 km of installed fibre using mid-span spectral inversion for dispersion compensation," OFC 1999, paper. Vol. 3, 118-120.
139. P. Minzioni, V. Pusino, I. Cristiani, L. Marazzi, M. Martinelli, C. Langrock, M. M. Fejer, and V. Degiorgio, "Optical phase conjugation in phase-modulated transmission systems: experimental comparison of different nonlinearity-compensation methods," Optics Express, 18(17), 18119-18125, 2010.